PROGRAMMING MICROENVIRONMENTAL SIGNALS WITH BIOACTIVE PEPTIDE AMPHIPHILES FOR SKELETAL AND CARDIAC MYOGENESIS

A THESIS

SUBMITTED TO THE MATERIALS SCIENCE AND

NANOTECHNOLOGY PROGRAM

OF THE GRADUATE SCHOOL OF ENGINEERING AND SCIENCE

OF BILKENT UNIVERSITY

IN PARTIAL FULFILLMENT OF THE REQUIREMENTS

FOR THE DEGREE OF

MASTER OF SCIENCE

By

İmmihan Ceren Garip

August, 2014

I certify that I have read this thesis and that in my opinion it is fully adequate, in scope and in quality, as a thesis of the degree of Master of Science.

.....

Assist. Prof. Dr. Ayşe Begüm Tekinay (Advisor)

I certify that I have read this thesis and that in my opinion it is fully adequate, in scope and in quality, as a thesis of the degree of Master of Science.

.....

Assoc. Prof. Dr. Mustafa Özgür Güler

I certify that I have read this thesis and that in my opinion it is fully adequate, in scope and in quality, as a thesis of the degree of Master of Science.

.....

Assoc. Prof. Dr. Çağdaş Devrim Son

Approved for the Graduate School of Engineering and Science:

.....

Prof. Dr. Levent Onural

Director of the Graduate School of Engineering and Science

ABSTRACT

PROGRAMMING MICROENVIRONMENTAL SIGNALS WITH BIOACTIVE PEPTIDE AMPHIPHILES FOR SKELETAL AND CARDIAC MYOGENESIS

İmmihan Ceren Garip
M.S. in Materials Science and Nanotechnology
Supervisor: Assist. Prof. Dr. Ayşe Begüm Tekinay
August, 2014

The extracellular matrix (ECM) is crucial for the coordination and regulation of various cellular processes, including cell adhesion, recruitment, differentiation and death. ECM components structurally support tissue function and regeneration by acting as a substrate for cell migration and differentiation. In addition, by facilitating the fine localization of signals within their structural framework, these components activate receptors on the cell membrane for the initiation of signal transduction cascades. As such, cell-matrix interactions and matrix-associated signals are important for the normal functioning of cells, as well as for natural or artificially assisted tissue regeneration. In keeping with this ECM-centric approach, we designed and synthesized peptide amphiphiles with bioactive epitopes to resemble the native microenvironment of muscle tissue and to examined their potential in the induction of progenitor cell differentiation into skeletal myotubes and cardiac myocytes. The formation of skeletal myotubes was promoted through the use of basal lamina-mimetic peptide nanofibers inspired by the chemical structures of laminin and fibronectin, two proteins strongly represented in the skeletal muscle extracellular matrix. We demonstrated that our basal lamina mimetic peptide nanofiber system actively interacts with the cells it contains and enhances their differentiation within 3 days. Morphological analysis and immunocytochemical stainings indicated the formation of differentiated myotubes.

We also designed glycosaminoglycan-mimetic peptide amphiphiles to mimic the glycosaminoglycans found in the myocardium. Glycosaminoglycans have been reported to play substantial roles in growth factor binding and the induction of angiogenesis, and their mimicry through peptide amphiphile nanofibers is promising as a combined approach for generating multifunctional cardiovascular tissue engineering scaffolds. We demonstrated that peptide nanofibers enhance the adhesion of cells to the surface and induce cardiac myoblast cells to differentiate into cardiomyocytes through both gene expression analysis and immunostainings.

In summary, myogenic platforms were developed by programming signal rich environment from self-assembled peptide nanofibers inspired from the components of the ECM to induce the differentiation of cells. These bioactive nanofiber systems serve as promising platforms for muscle tissue engineering applications.

Keywords: Peptide nanofibers, extracellular matrix, biomimetic, basal lamina, skeletal muscle tissue, laminin, fibronectin, glycosaminoglycan, myocardial regeneration.

ÖZET

BİYOAKTİF PEPTİT AMFİFİLLER İLE ÇİZGİLİ KAS VE KALP KASI OLUŞUMU İÇİN MİKROÇEVRESEL SİNYALLERİ PROGRAMLAMA

İmmihan Ceren Garip
Malzeme Bilimi ve Nanoteknoloji Programı, Yüksek Lisans
Tez Yöneticisi: Yrd. Doç. Dr. Ayşe Begüm Tekinay
Ağustos, 2014

Hücrelerarası ekstrasellüler matris, hücre yapışması, hareketi, farklılaşması ve ölümü gibi hücresel olaylarda önemli düzenleyici ve yönlendirici roller oynamaktadır. Dokunun görevini yerine getirebilmesi ve yenilenebilmesi için, matris elemanları, hücrelere yapısal olarak destek olmakla birlikte, hücrelerin hareket edip farklılaşmalarını sağlayacak yüzey görevi de görmektedirler. Ayrıca, hücrelerde tepki oluşturacak sinyallerin düzgün bir şekilde hücrelere sunulmasını sağlayarak, reseptörlerin aktive edilip sinyal iletiminin sağlanmasında rol alırlar. Bu nedenle hücre-matris etkileşimi ve matrise bağlı sinyaller hücrelerin normal fonksiyonlarını yerine getirmelerinin yanı sıra dokunun yenilenmesinde de önemlidir. Bu tezde, kas dokusunun doğal çevresini taklit eden biyoaktif peptit nanofiberler tasarlanarak, öncül hücrelerin çizgili kas ve kalp kası hücrelerine dönüşmelerindeki etkileri araştırılmıştır. İlk olarak, çizgili kas oluşumunu indüklemek için, çizgili kas hücrelerarası matrisinde bulunan laminin ve fibronectin proteinlerinin kimyasal yapılarından esinlenerek, bazal laminayı taklit eden peptit nanofiberler tasarlanmıştır. Bu peptit nanofiber sisteminin hücrelerle etkileştiği ve üç gün içerisinde farklılaşmayı arttırdığı gösterilmiştir. Morfolojik ve immunojenik boyamalar farklılaşmış myotüplerin oluştuğunu göstermiştir.

Ayrıca, kalp dokusunun hücrelerarası iskele yapısında bulunan glikozaminoglikanların kimyasal yapıları kullanılarak glikozaminoglikanları taklit edebilen peptit nanofiberler tasarlanmıştır. Büyüme faktörlerine bağlandığı ve damarlanmayı indüklediği bilinen glikozaminoglikan taklidi peptit nanofiberler tümleşik kardiyovasküler doku mühendisliği iskeleleri için umut verici yapılardır. Bu

çalışmada, peptit nanofiberlerin hücre yapışmasını arttırdığı ve kardiyak miyoblast hücrelerinin kalp kası hücrelerine farklılaştığı gösterilmiştir. Bu farklılaşma gen ekspresyonu analizi ve immunoboyamalarla kanıtlanmıştır.

Özet olarak, kas oluşumunu indükleyen, hücrelerarası iskelenin yapısal elemanlarından esinlenilerek tasarlanan, kendiliğinden toplanan peptit nanofiber platformlar hücrelerin farklılaşmasını desteklemişlerdir. Bu biyoaktif nanofiber sistemlerin kas doku mühendisliği uygulamalarında kullanılması umut vaadetmektedir.

Anahtar Kelimeler: Peptit Nanofiberler, Hücrelerarası İskele, Biyomimetik, Basal Lamina, Çizgili Kas dokusu, Laminin, Fibronektin, Glikozaminoglikan, Kalp kası Rejenerasyonu.

ACKNOWLEDGEMENTS

First of all, I would like to thank and express my gratitude to my advisor Dr. Ayşe Begüm Tekinay for her support and guidance at all times. She not only supported my scientific career but also contributed to my personal development. I also would like to thank Dr. Mustafa Özgür Güler for his guidance and support. This work could not be accomplished without Dr.Güler.

I would like to thank Murat Kılınç, Nuray Gündüz and Gülcihan Gülseren for their collobration and friendship in different projects which could not be possible without their sincere efforts.

I was lucky to work with Hakan Ceylan from whom I learned many techniques. I am greatfull for his kindness and contributions to my technical skills and view of science. Also, all NBT and BML lab members were there when I needed them. It was great to know and work with them. I would like to thank Elif Arslan, Yasin Tümtaş, Didem Mumcuoğlu, Berna Şentürk, Melis Göktaş, Seher Yaylacı, Gülistan Tansık, Gözde Uzunallı, Melike Sever, Mevhibe Geçer, Büşra Mammadov and Seda Koyuncu for their support and friendship.

I would like to thank UNAM (National Nanotechnology Research Center) for providing facilities and equipments for my research and to thank TUBITAK (The Scientific and Technological Research Council of Turkey) for financial support, provided in the form of a BIDEB 2210-E MSc fellowship.

I have also special thanks to Öncay Yaşa, who was with me either in good and bad times with endless support.

Lastly, I always feel the love and support of my family with me. I owe the greatest thanks to them.

TABLE OF CONTENTS

LIST OF ABBREVIATIONS

BrdU	**:**	Bromodeoxyuridine
CD	**:**	Circular Dichroism
CS	**:**	Chondroitin Sulfate
cTnT	**:**	Cardiac Troponin T
C2C12	**:**	Mouse Myoblast Cells
DCM		Dichloromethane
DMEM	**:**	Dulbecco's Modified Eagle Medium
DMF		Dimethlyformamide
FGF	**:**	Fibroblast Growth Factor
GAG	**:**	Glycosaminoglycan
GAPDH		Glyceraldehyde 3-phosphate dehydrogenase
GF	**:**	Growth Factor
HM-PA	**:**	Heparin Mimetic Peptide Amphiphile
HS	**:**	Heparan Sulfate
HSPG	**:**	Heparan Sulfate Proteoglycan
H9C2	**:**	Ventricular Rat Myoblast Cells
Mlc-2v		Ventricular Myosin Light Chain
MHC	**:**	Myosin Heavy Chain
PA	**:**	Peptide Amphiphile
SEM	**:**	Scanning Electron Microscope
TCP	**:**	Tissue Culture Plate
TEM	**:**	Transmission Electron Microscope
VEGF	**:**	Vascular Endothelial Growth Factor

LIST OF FIGURES AND TABLES

CHAPTER 1.

INTRODUCTION

1.1 Overview of Skeletal Muscle Tissue

Skeletal muscle is a highly complex, hierarchically organized and heterogeneous tissue that is attached to, and allows the movement of, the various bones of the skeleton. It serves a multitude of functions, the most important of which is to generate longitudinal forces. This is established by the contraction of multiple myofibrils inside uniaxially directed bundles of myofibers [1], which are bundled together and attached to the skeleton by tendons.

Skeletal muscle is composed of thousands of muscle fibers (myofibers) that are formed during development by the fusion of mononucleated myoblasts of mesodermal origin. Myofibers are multinucleated cellular syncytia and, since the generation of force requires substantial energy, must be supported constantly through an extensive network of blood vessels. As their constituent cells are terminally differentiated, mature muscle fibers are not capable of self-renewal. However, skeletal muscle is a dynamic tissue and can either increase or decrease its mass in response to a variety of environmental signals, such as starvation, exercise and nutrients [2]. This self-renewal capacity is derived from a subpopulation of cells called satellite cells or myoblasts, which reside beneath the basal lamina. They constitute up to 1-5% of total skeletal muscle nuclei, depending on age and muscle fiber composition [3]. These cells, first described in 1961, are found in healthy muscle fibers, remain in the mitotic quiescent state G0 and express CD 34, M-cadherin, PAX 7, syndecan 3 and c-met [4]. Satellite cells are unipotent adult stem cells and possess an exceptional self-renewal capacity. This ensures their persistence within the muscle while preserving the muscle's ability to regenerate and repair after injury. These cells are activated in response to severe muscle damage, which triggers their asymetrical division and proliferation. Through asymmetrical division, some of these myocytes repopulate the stem cell niche, while others differentiate into myoblasts and rebuild the muscle by fusing with one another or with residual myofibers [5]. As such, large numbers of new myotubes are formed only a few days after acute muscle damage, [6] which serves as a testament to the remarkable regenerative capacity of skeletal muscle. This regeneration is regulated by locally produced growth factors that control cellular proliferation and differentiation [7].

Characteristics of the skeletal muscle fibers

Skeletal muscle cells are postmitotic, multinucleated myotubes formed during the embryonic development by the fusion of myoblasts. The myotube matures into the long muscle cell, which possess diameter of 10 to 100 μm and lengths of up to several centimeters. Their total lengths can vary from several millimeters to more than 30 cm [8].

Skeletal muscle fibers are characterized by their striated myofibrils, which are precisely organized contractile and regulatory proteins composed of repeating units arranged in series known as sarcomeres [9]. Myofibrils are the smallest functional unit of a myofiber and a muscle fiber is composed of hundreds of myofibrils, which occupy about 80% of the sarcoplasm and are surrounded by mitochondria (also called sarcosomes). Myofibrils are principally composed of two major filaments formed by contractile proteins: thin filaments contain actin, while thick filaments incorporate myosin as well as many other cytoskeletal proteins [10]. The capacity of the myofiber to produce force is directly related to the number of parallelly arranged sarcomeres within a muscle fibe

1.2 Skeletal Muscle Extracellular Matrix and Regeneration

The extracellular matrix (ECM) is the non-cellular component present within all tissues and organs, and plays an important role not only in providing a structural framework for the cellular constituents but also by regulating cell behavior by initiating crucial biochemical and biomechanical cues that are required for tissue morphogenesis, differentiation and homeostasis [11]. The ECM serves as a substrate for cell migration, modulates growth factor activity and transmits instructive and permissive signals from the microenvironment to cells to support their functional integrity [12]. In muscle development, the primary role of the ECM is to function as a structural support for cell attachment, resulting in cell-to-extracellular matrix interactions that are required for cell migration. Depending on the tissue and development stage of the organism, ECM has a diverse nature and composition, containing several distinct families of molecules with disparate evolutionary origins. Although all ECMs are principally composed of water, proteins and polysaccharides, each tissue has an ECM with a unique composition and topology. ECM

glycoproteins include both collagens and a diverse array of non-collagenous proteins such as laminins, tenascins and fibronectin [13].

Skeletal muscle is a hierarchically organized tissue and its ECM is ordered in several layers around whole muscle, mucle fascicles and muscle fibers. A layer of connective tissue, called the epimysium, surrounds each muscle, and bundles or fascicles of muscle cells are grouped together by perimysia, which are derived from the epimysial layer and contain the nerves and blood vessels that run through the muscle. Lastly, each muscle fiber is surrounded by a basal lamina and a mesh-like sheath of connective tissue called the endomysium. The basal lamina serves as a scaffold for muscle fiber formation and recovery from injury [14]. Figure 1.1 demonstrates the structure of skeletal muscle tissue and connective layers.

1.2.1 Function and composition of the basal lamina

The basement membrane that surrounds muscle fibers is closely associated with the sarcolemma, and provides a protective niche in which muscle regenerative cells (satellite cells) reside [14]. It is a specialized ECM sheath composed of both an internal basal lamina and an external reticular lamina. The basement membrane is now known to be critical in muscle fiber structure and function. The actin cytoskeletons of muscle fibers are linked to their basal laminae, which support muscle function and protect against contraction-induced damage. Genetic studies of muscular dystrophy patients and animal models of muscular dystrophy have demonstrated the importance of the basement membrane in the maintenance of muscle integrity. In addition to the maintenance of muscle integrity, it is also essential in the promotion of myogenesis and muscle development. [15].

The muscle ECM is formed by numerous components, including collagen, perlecan, laminin, entactin, fibronectin and several glycoproteins and proteoglycans. These proteins function as a scaffold that provides mechanical support for the cells and facilitates the formation of parallel myofibers by coordinating their attachment and alignment.

Collagens are the most abundant proteins in the animal kingdom and, as a general feature, function to limit the distensibility of tissues, which are effectively 'kept in place' by the enormous tensile strengths of collagen fibrils [16]. The muscle basement

membrane consists primarily of a type IV collagen network; however, types VI, XV, and XVIII are also present within the matrix [17]. Fibronectin in particular is important for the maintenance of skeletal muscle, because it can bind to both the integrin receptors on cells and other molecules in the ECM.

At the sarcolemma, laminins are bound by integrins and α-dystroglycan [18]. Laminins are among the best studied of basement membrane components and can bind directly to type IV collagen, and may also be indirectly linked by fibronectin [19]. Laminins are composed of three chains (α, β and γ) that exist in different combinations and form at least 16 different types of laminins. Laminins 211 and laminin 221 in the mature muscle bind to each other and to matrix proteins and serve to connect the muscle networks. Laminin-211 in the basement membrane is extremely important for the maintenance and stabilization of differentiated muscle [20]. Interactions between matrix glycoproteins provide potential mechanisms for lateral force transmission from the myofiber [21]. Together with the branched network structure of type IV collagen, these glycoproteins form the basis for basement membrane architecture.

1.2.2 Course of Differentiation

During embryonic development, skeletal muscle arises from mesodermal precursor cells [22]. Adult skeletal muscles have a robust system of repair. It has been found that a large number of new myotubes arise within a couple days of acute muscle damage. Normally, satellite cells are quiescent and remain in the G0 phase of the cell cycle until they receive certain stimuli [6]. Satellite cells express various proteins, including Pax7, CD34, c-met, Mcadherin, syndecan-3 and syndecan-4 [23-24], that are important for their activation and proliferation in response to muscle damage. Several common stimuli that trigger the activation of satellite cells include exercise, injury from myotoxins, disease, denervation or other muscle damage. Following damage to the skeletal muscle, growth factors (GFs) and cytokines, such as hepatocyte growth factor, epidermal growth factor; platelet-derived growth factor BB; and members of the insulin-like growth factor (IGF) and fibroblast growth factor family [25] are released from the ECM [26], myofibers, endothelial cells, interstitial cells [27] and leukocytes [28]. Interactions among these GFs and receptors on

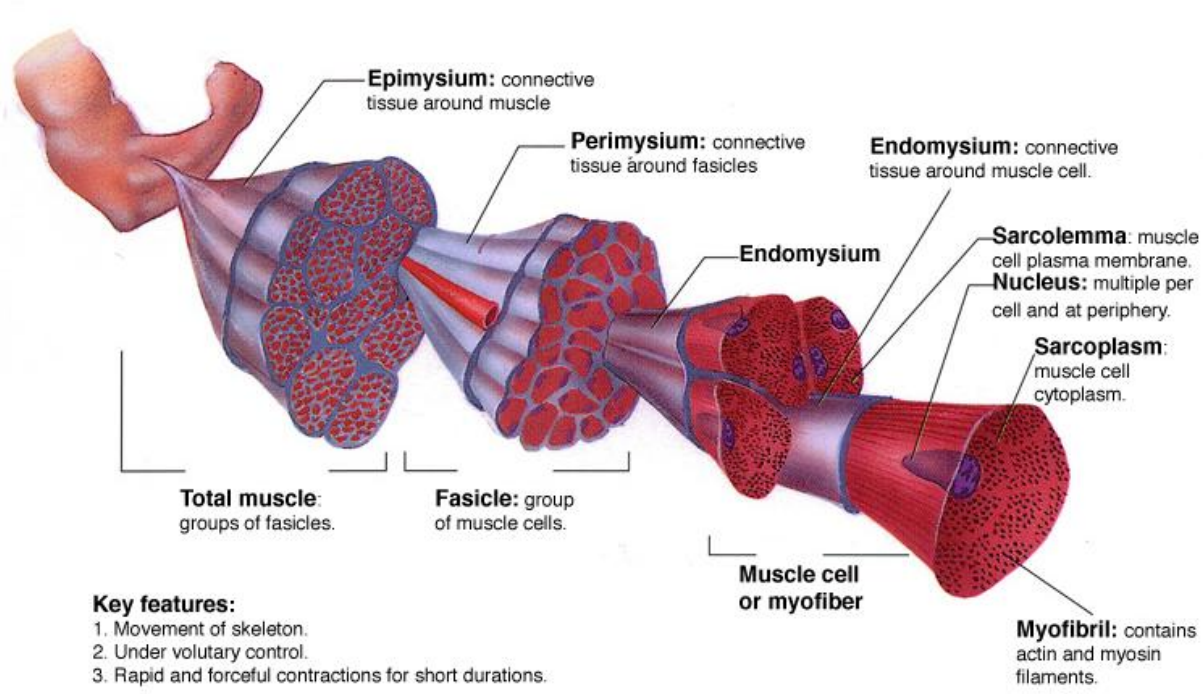

Figure 1.1 Hierarchical organization of skeletal muscle tissue. Epimysium is the outermost layer that surrounds whole muscle tissue, perimysium is the connective tissue around fascicles and endomysium surrounds muscle fiber. Image acquired from wadeyoder.com.

quiescent satellite cells trigger satellite cell activation and result in their asymmetric proliferation. Activated satellite cells downregulate Pax7 expression and upregulate MyoD and Myf5 transcriptional activators, which direct these precursor cells to the myogenic linage [29-30]. MyoD/Myf5 positive cells first become myoblasts and then stop proliferating and terminally differentiate into cells that begin expressing myogenin, myosin heavy chain (MHC), and muscle creatine kinase (MCK), which are muscle-specific genes. These myoblasts continue proliferating until they reach a sufficient number to begin fusing with existing fibers or with other myoblasts to form new multinucleated myotubes, which later on mature into muscle fibers [31]. These sequential events are regulated through ECM components, growth factors and cytokines and occur within a dynamic microenvironment. Therefore, programming the environmental signals to induce the differentiation of progenitor cells for regenerative purposes is a challenging yet promising approach for functional restoration of damaged tissue. As the focus of the present work is differentiation of skeletal muscle cells with bioactive scaffolds using advanced nanoscale systems, the next section will be devoted to an in-depth discussion of muscle injuries and tissue engineering strategies for the regeneration of muscle tissue.

1.2 Muscle Injuries and Tissue Engineering Strategies for Repair

Damage to skeletal muscle may occur throughout life due to exercise and contraction, abnormalities in the immune system, acute physical and chemical injury, or muscle degenerative diseases. Skeletal muscle injuries are a common cause of severe long-term pain and physical disability. Acute damage to skeletal muscle can occur by physical or chemical trauma. For example, excessively hot or cold temperatures and sharp or blunt traumas induce rapid myofiber necrosis. Likewise, ischemia/reperfusion also causes acute muscle damage. Also, during organ transplantation surgery, stroke and hypovolemic shock, or prolonged periods of zero blood flow induce muscle dysfunction through the loss of cellular energy supplies and results in the accumulation of potentially toxic tissue metabolites. Restoration of blood flow is essential for the rescue of ischemic muscle. Therefore, there is a strong need to improve the short- and long-term management of skeletal muscle injuries. According to the principle of conservative management, muscle injuries heal conservatively. It follows the RICE protocol (rest, ice, compression, and elevation). Other therapies also exist, including the local application of heat and passive motion

exercises or drug therapy, which typically consists of nonsteroidal anti-inflammatory drugs (NSAIDs) and intramuscular corticosteroids [32]. However, current treatment methods do not seem to obtain complete restoration of normal functionality, and new biological therapies could represent new and more effective strategies for the restoration of muscle tissue. Current biological strategies for the management of muscle injuries are growth factor therapy [33-36], cell therapy [37], platelet-rich plasma (PRP) therapy [38-39] and tissue engineering scaffolds.

In skeletal muscle injuries, tissue engineering represents a biological alternative for the replacement of large tissue loss after severe damage. Tissue engineering could allow skeletal muscle fibers to be grown in culture and then transplanted into a patient to improve their physical and psychological symptoms. A comprehensive understanding of tissue structure and the ability to imitate its molecular composition are important to effectively grow tissues for therapeutic use. Biomaterials that emulate the natural tissue structure can be designed and used as controlled microenvironments for regeneration and tissue development.

Efficient skeletal muscle regeneration is strongly correlated with the properties of the biomaterials used for scaffold generation and with the regenerative potential of the cells used for scaffold seeding. Biomaterials with different physiochemical features and compositions, as well as different biological characteristics, have been used to fabricate efficient tissue engineering scaffolds. Both natural and synthetic materials are used to mimic the structural and biomechanical properties of the native tissue. Materials commonly used as scaffolds are hydrogels, polymer scaffolds (PLA, PLLA, PDMS) [40-42] and natural products such as collagen [43], fibrin [44-45] hyaluronan [41], chitosan [46] and matrigel. Kroehne *et al*. have used collagen scaffolds with parallel oriented pores to reproduce the three-dimensional organization of skeletal muscle and showed that this scaffold has the ability to induce skeletal muscle-like tissue regeneration [43]. In addition, Ma *et al.* reported the ability of 3-D collagen scaffolds seeded with myoblasts to improve muscle healing with an increased quantity of innervated and vascularized regenerated muscle fibers [47]. Fibrin is another natural material used as a scaffold and Page *et al*. demonstrated that fibrin microthread scaffolds provide an efficient delivery system for cell-based therapies and improve the regeneration of a large defect in the tibialis anterior of the mouse [48].

Another approach is the use of decellularized tissues as scaffolds, which readily provide the native extracellular microenvironment experienced by cells. Borschel *et al.* used acellular muscles with injected myoblasts and showed the production of longitudinal contractile force upon electrical stimulation after differentiation [49]. In another study, Sicari *et al*. implanted porcine urinary bladder ECM scaffold to mice and demonstrated new skeletal muscle formation. Moreover, in a parallel human clinical study, scaffold-treated patients with volumetric muscle loss showed similar outcomes with mice and improved limb strength during physical therapy [50].

In addition to its composition, the structural features of biomaterial are important for the alignment of cells, since skeletal muscle tissue is ordered into aligned bundles and tissue constructs should be aligned to function after engraftment. Therefore, biodegradable materials with parallel oriented pores and aligned or grooved morphologies have been used to reproduce the three-dimensional organization of skeletal muscle. Ricotti *et al*. fabricated electrospun nanofibrous PHB scaffolds and demonstrated that the aligned nanofibrous mesh decreases the proliferation activity and provides a higher differentiative stimulus [51]. In another study, grooved polystyrene substrates were conjugated with RGD and were shown to enhance adhesion, growth and differentiation of C2C12 cells [52].

1.4 Heart And Cardiac Muscle Tissue

Heart is an organ that operates as an engine for the circulatory system. It accomplishes this task with a tissue structure that is specially adapted to meet the demands of constant activity during times of rest and exercise. It has three layers; epicardium, myocardium and endocardium, where myocardium is the muscular middle layer of the heart wall. Myocardium is composed of cardiac muscle fibers, which occupy most of the tissue volume but constitute only 30% of the total number of cells in a normal adult heart. Remaining cell populations are non-cardiomyocyte cell types, among which cardiac fibroblasts represent the vast majority [53].

Heart contraction is an autonomic function of the peripheral nervous system, and the myocardium stimulates contractions and relaxations to pump blood from the ventricles and to allow the atria to receive blood, respectively.

Cardiac muscle is involuntary, so functionally, it is smilar to smooth muscle. However, anatomically cardiac muscle more closely resembles skeletal muscle due to being striated as a result of the parallel arrangement of actin and myosin filaments. Cardiac muscle fibres are long, cylindrical cells with one or sometimes two nuclei which are centrally located within the cell. Also, the cardiac muscle has several unique features such as intercalated discs, which are connections between two adjacent cardiac cells and help muscle cells to contract rapidly as a single unit. Intercalated discs are irregular transverse thickenings of the sarcolemma that contain desmosomes and gap junctions and ensure proper functioning of the cardiac muscle as an effective pump [54-55].

1.4.1 Myocardial extracellular matrix

There is a connective tissue layer between the muscle fibers, analogous to the endomysium of skeletal muscle, and it supports capillary network necessary to meet the high metabolic demand of strong continuous activity. The ECM not only facilitates the exchange of mechanical, electrical and chemical signals during homeostasis, but also plays essential roles in development, remodeling and signaling in the cardiovascular system [56]. This three-dimensional structure acts as a framework for myocytes, fibroblasts and endothelial cells contained in the myocardium and the vasculature to align and build a network. ECM components are also important in determining the mechanics of myocardium, pericardium, blood vessels and valves [57].

The extracellular space can be divided into solid and fluid components, of which organization, composition and density are dynamic both in normal and pathological conditions. The fluid components of the matrix contribute to the distribution of soluble factors and other molecules related to different processes. Also, these components act as binding sites for soluble factors and effect their distribution and availability. Other components play roles in accumulating water due to their hydrophilic nature and therefore providing resistance to compression. The extracellular space and its components also serve to connect the cellular components of the myocardium, effectively linking each individual cell and coordinating the contraction of the whole tissue. In addition, cellular and acellular signals and ECM components involved in cell-ECM interactions during post-myocardial infarction (MI) or hypertensive remodeling may contribute to the progression toward recovery or heart failure by playing agonistic or antagonistic roles [56].

The ECM is a collection of macromolecular proteoglycans, glycoproteins, proteases, collagens, growth factors and cytokines. Fibroblasts and vascular smooth muscle cells (VSMC) primarily contribute to the secretion of fibronectin and collagens type I and III, while VSMCs, myocytes and endothelial cells produce type IV collagen and laminins [58].

Proteoglycans have recently begun to receive increased attention for their potential signalling roles. During the synthesis of proteoglycans; glycosaminoglycans, which are polysaccharide chains consisting of repeating amino sugar and uronic acid disaccharide units, are covalently linked to the core protein, sulphated and then secreted into the microenvironment. Glycosaminoglycans (GAGs), and especially sulphated GAGs, have a strongly negative charge, which attracts water and results in large hydrodynamic volumes. When the muscle is placed under pressure, the water is removed and GAGs return to their original volume, which allows proteoglycans to act as a lubricant and makes them essential in tissues undergoing continuous cycles of pressure-relief, such as cartilage or cardiac muscle [59]. Furthermore, glycosaminoglycans also play major roles in cell signalling, angiogenesis [60], axonal growth [61], tumor progression [62], and anti-coagulation [63].

Heparan sulphate is a common glycosaminoglycan and can bind to multiple growth factors and cytokines through polysaccharide chains. These factors include vascular endothelial growth factor (VEGF), BMPs, and fibroblast growth factors (FGFs), and TGF-βs, which have been demonstrated to be important for cardiac development [64].

Numerous studies have revealed that ECM composition differs during different physiological states and differences in the microenvironment are largely driven by cell-cell and cell-matrix interactions within the developing and adult heart. Alterations in the signaling pathways that regulate the production of ECM components, or perturbations in their expression patterns, can lead to congenital heart diseases and cardiac malfunctions [64].

1.5 Cardiovascular Diseases and Cardiac Regeneration

One of the leading causes of death worldwide, ischemic heart disease is characterized by reduced blood supply to the heart muscle, which leads to a deficit in the production of the energy required for cardiac contraction. It is a multi-factorial

condition, resulting from a combination of genetics, life style and environment factors. Risk factors for ischaemic heart disease include family history, LDL cholesterol, high blood pressure and obesity.

Acute myocardial infarction (AMI) is a subcategory of ischaemic heart disease and occurs when the blood supply is completely cut at the level of a coronary artery [65], leading to a permanent tissue ischemia. While death does not always occur, the disease nonetheless results in the large-scale loss of cardiac muscle, diminishes the contraction capability of the heart [66] and frequently causes heart failure.

Current therapies for AMI include medical treatment, heart transplantation and implantation of mechanical ventricular assist devices. With the exception of transplantation and mechanical assistance devices, current pharmacological, interventional or operative therapies for the disease suffer from an inability to compensate the decreased pumping capacity of heart following the irreversible loss of functional cardiomyocytes [67]. Thus, new solutions are required to regenerate the damaged myocardium, to overcome the bad prognosis of patients with heart failure, and to address the shortage of heart donors.

Cellular repair strategies for heart disease include direct transplantation of cells into the damaged tissue, tissue engineering techniques for the *ex vivo* development of replacement tissue and therapies that prompt the heart to regenerate damaged tissues.

Cell Therapy

The basis of cell therapy is the repopulation of injured myocardium by transplantation of healthy cells. Although heart was once thought to be a terminally differentiated organ and therefore incapable of replenishing lost myocytes, Beltrami *et al*. have demonstrated that mammalian cardiac myocytes retain some capacity for division [68] and identified endogenous cardiac progenitor cells, which retain some potential for differentiation into endothelial cells, smooth muscle cells and cardiac myocytes [69]. Following the discovery that native progenitor cells exist in the adult heart, the delivery of these progenitor cells have been studied as a method to facilitate the generation of a functional myocardium, and this has eventually been translated into the clinic as a cell-based therapy to treat heart disease [70]. However, a key concern for stem cell transplantation is the selection of cell source, which

determines the safety and efficacy after engraftment. In addition, clinical trials with bone marrow progenitors have shown modest improvements in ventricular function [70-72].

Various cell types have been considered as candidates for therapeutic delivery in humans, including BMCs, myocardium or adipose tissue derived cells (which were already used in clinical trials), endothelial progenitors, hematopoietic stem cells and pluripotent stem cells [65,67].

Currently, bone marrow is the most frequent source of cells used for cell therapy. Jackson *et al.* have reported that the transplantation of bone marrow with labelled haematopoietic stem cells followed by myocardial infarction results in a low rate of cardiomyocyte differentiation from the transplanted cells [73]. However, many other studies in animals could not demonstrate cardiomyocyte differentiation from haematopoietic progenitor cells, [74-75] nor did they find any improvement in cardiac function following haematopoietic stem cell transplantation [76]. On the other hand, bone marrow-derived cells have been used in small clinical trials with apparent success, [77-79] yet most studies demonstrated modest cell therapy-mediated improvements in ventricular function [80].

Another source for cell therapy is endogenous cardiac progenitor cells, since the initial discovery had demonstrated that there existed an endogenous population of progenitor cells resident in the mammalian heart. The advantage of this approach is the feasibility of autologous transfer, although the *ex vivo* expansion of these cells is necessary. However, a principal problem with cardiac progenitors is the lack of definitive markers [65]. Small populations of stem cells in the mammalian myocardium express the cell-surface markers Kit12 or Sca1 [81]. Animal studies reported that these cells differentiated into cardiomyocytes, smooth muscle cells and vascular endothelium, replacing the majority of the infarcted tissue and improving ventricular function significantly when engrafted to heart [82-83].

1.6 Cardiovascular Tissue Engineering Strategies

As an extension of cell transplantation, tissue engineering with biocompatible scaffolds can provide an appropriate structural and three-dimensional

microenvironment to integrate myocytes with the host tissue and develop the vasculature necessary to support blood flow.

Design of the biomaterial scaffold is important to mimic the native cardiac tissue in terms of mechanical properties, structure of the underlying matrix, and presence of vasculature. As such, tissue engineering constructs should be mechanically robust yet flexible, electrophysiologically stable, vascularized or capable of vascularization after implantation, non-immunogenic and contractile [84].

Recent studies have explored the possibility of using decellularized hearts as scaffolds; however, although decellularized scaffolds are suitable for replacing native tissue with a new tissue layer of the same thickness, injectible hydrogels are less invasive in acute MI [85].

A common approach is to seed cardiomyocytes onto porous scaffolds, typically from a biodegradable polymer such as poly(lactic-coglycolicacid) or natural polymers such as collagen and fibrin [86]. Zimmermann *et al*. developed collagen gels into which cardiomyocytes are embedded and mechanically conditioned in a cyclic stretching device, and studies with this gel suggest that some of the cardiomyocytes survive after transplantation into uninjured hearts and undergo further proliferation [87].

Similarly, Zhang *et al.* used fibrin gels and compared the maturation of human embryonic stem cell-derived cardiomyocytes in 2D monolayers and 3D patch cultures. As a result, they observed that cells in 3D fibrin-based patches exhibited longer sarcomeres and increased expression of genes associated with contractile function [86].

Another study has shown that porous alginate scaffolds with seeded cardiomyocytes yield 3D high-density cardiac constructs and optimized the cell seeding requirements for a uniform distribution in a 3-dimensional structure [88].

The ability to support vascularization is one of the most important requirements for biomaterial or tissue engineering constructs to correctly facilitate the regeneration of damaged myocardial tissue [89]. 3D cell constructs generally lack the vascular network that exists in normal tissues. However, a bioengineered myocardial tissue graft requires persistent neovascularization, or angiogenesis, for its growth and survival after implantation. This factor is essential because cardiomyocytes are very sensitive

to prolonged ischemia and may die by necrosis and apoptosis if deprived of oxygen, and the engineered heart muscle should survive the ischemic period to maintain viability and function [84]. Strategies to promote vessel formation include cell tri-culture, use of growth factors and peptides and the engineering of novel proangiogenic scaffolds [90].

Xiang *et al.* reported succesful neovascularization in the infarct area following implantation of collagen-GAG scaffolds in combination with bone marrow-derived mesenchymal stem cells [91].

Leor *et al.* also used porous sodium alginate scaffolds to grow fetal rat cardiac cells within a 3D biograft, and transplanted this scaffold into cardiac tissue. Intensive neovascularization from the neighbouring coronary network was observed through histological analysis [92]. In another study, Chiu *et al.* developed angiogenic and cardioprotective peptide-encapsulated collagen–chitosan hydrogels and observed increased formation of mature blood vessels after the injection of the hydrogel into rat myocardium. The increase in mature blood vessel numbers in turn enhanced the presence of cardiomyocytes while reducing tissue loss 3 weeks post-MI [93].

Another approach for cardiac tissue regeneration is the site-specific delivery of angiogenic growth factors from tissue-engineered devices to stimulate localized vessel recruitment to the cell transplant and wound area. For example, Perets *et al*. constructed a porous alginate scaffold that incorporates tiny poly (lactic-co-glycolic acid) microspheres capable of controlling the release of angiogenic factors such as bFGF, which was released from the scaffolds in a controlled manner *in vitro* and accelerated the vascularization of the mesenteric membrane in the rat peritoneum [94]. Figure 1.2 demonstrates the current myocardial tissue engineering strategies.

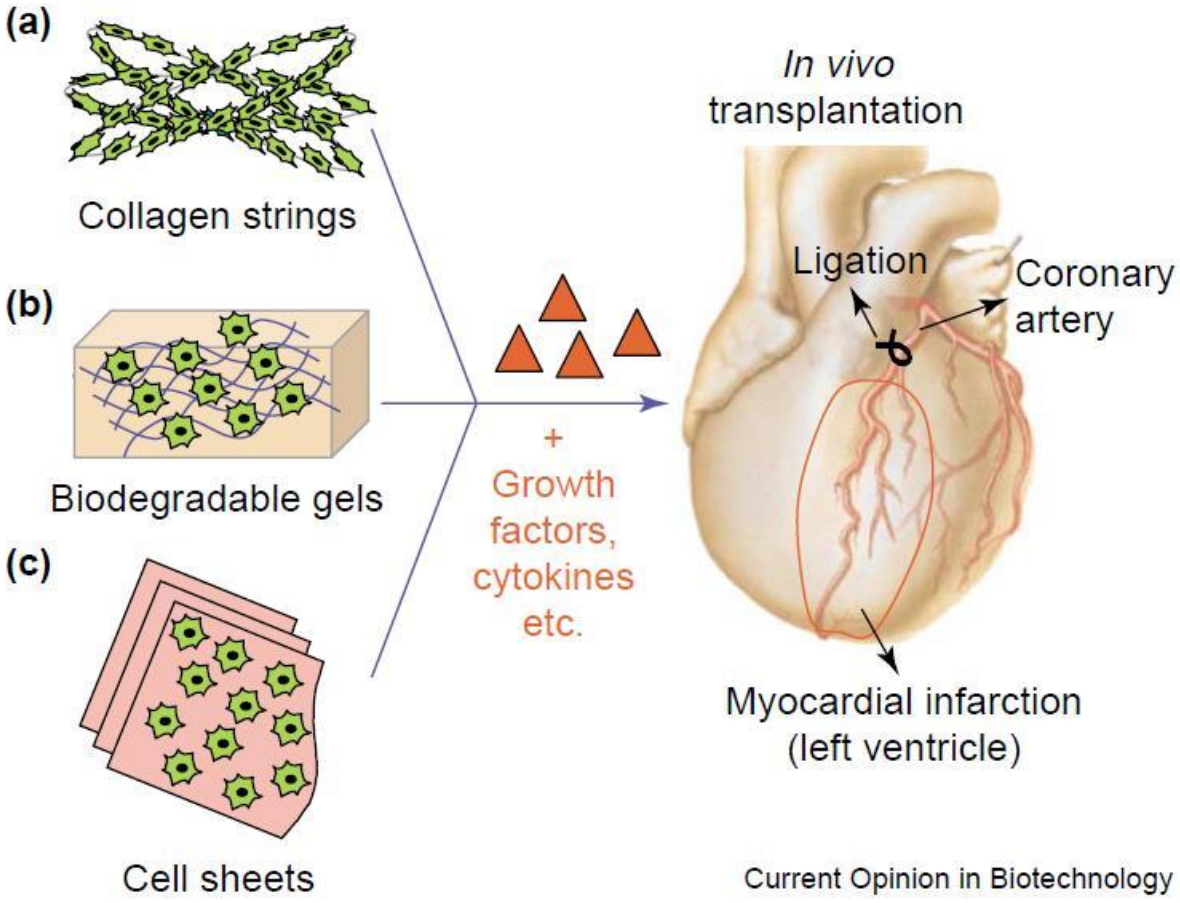

Figure 1.2 Scheme of the present major strategies for cardiac tissue engineering using (a) collagen strings, (b) biodegradable gels or (c) cardiac cell sheets (Adapted with permission from Zammaretti et al. Current Opinion in Biotechnology 2004, 15:430–434.)

Angiogenesis can also be promoted under certain structure geometries. Madden *et al.* created methacrylate-based hydrogel scaffolds consisting of interconnected pores, which were 30–40 mm in diameter, by microtemplating and showed that this system

supports the growth of hESC-derived cardiomyocytes *in vitro* and is proangiogenic, promotive of vessel infiltration and able to reduce scarring *in vivo* [95].

Another approach to increase vacularization is biomimetics, which encompasses the design of scaffolds that physically and chemically resemble growth factors or the ECM of heart tissue. Narmoneva *et al*. cocultured endothelial cells (EC) and neonatal cardiac myocytes (CM) in 3-D RADA-peptide hydrogels and demonstrated that, when these cells are cultured together, interactions between the cells promote myocyte reorganization and the endothelial cells form capillary-like networks, which in turn promote spontaneous contractions [96].

Webber *et al.* designed peptide amphiphile-based supramolecular nanostructures which mimic the activity of VEGF and facilitate increased tissue perfusion and functional recovery in ischemic tissue [97]. Mammadov *et al.* also used peptide amphiphiles to mimic heparan sulphate and showed that glycosaminoglycan mimetic nanofibers bind to the growth factors secreted by cells and enhance angiogenesis without the addition of exogenous growth factors [98].

In this thesis, we synthesized heparin sulphate-mimetic peptide nanofibers, which were previously shown to induce angiogenesis [98], and examined their effect on the induction of cardiomyocyte differentiation *in vitro*. This study is combined with an *in vivo* myocardial infarction model and an analysis of peptide-mediated revascularization in the infracted area. We therefore assessed the regenerative potential of an ECM-mimetic peptide amphiphile scaffold to heal the myocardium after infarction.

1.7 Motivation and Goals

Peptide amphiphiles allow incorporation of various functional biological signals into their primary sequence and form higher order nanostructures that display complex architectures and biochemical characteristics similar to those of native tissue microenvironments under physiological conditions. These properties make them ideal candidates as bioactive scaffolds for regenerative medicine and tissue engineering applications. Peptide sequences derived from the active sites of the ECM components, which have important roles in muscle regeneration and development, were incorporated into peptide amphiphile nanofibers to create a

microenvironment that can both physically support cellular growth and supply the bioactive signals required for the induction of differentiation. In the first chapter, I discussed the effect of biomimetic peptide amphiphiles designed to mimic the basal lamina of skeletal muscle on the differentiation of myoblast cells. In the second chapter, I focused on angiogenic peptide amphiphiles and their effect on cardiomyocyte differentiation.

CHAPTER 2.

BASAL LAMINA MIMETIC PEPTIDE NANOFIBERS FOR SKELETAL MUSCLE DIFFERENTIATION

Part of this study was submitted to be published as “Basal Lamina Mimetic Nanofibrous Peptide Networks for Skeletal Myogenesis”, Immihan Ceren Garip, Nuray Gunduz, Murat Kilinc, Mustafa O. Guler and Ayse B. Tekinay.

2.1 INTRODUCTION

Skeletal muscle tissue constitutes 40% of the total body weight and is crucial for physical locomotion. Traumatic injury, tumor excision, congenital defects or myopathies compromise muscle function and mobility and necessitate muscle tissue reconstruction [99]. Muscle stem cell transplantation is a promising treatment against skeletal muscle trauma; however, isolated stem cells drastically lose their ability to form myotubes and function adequately after in vitro expansion. Therefore, antagonism between differentiation and proliferation hampers the therapy [100]. On the other hand, transplantation of non-cultured muscle stem cells to damaged muscle tissue immediately after isolation is quite effective in new myotube formation; however, it is required to harvest approximately 3-4 kg of muscle tissue to regenerate 1 x 10^5 mm^3 of muscle [101-102]. As such, due to lack of donor tissue availability, autologous graft surgery is limited. Another one of the most important issues in muscle disorders is the infiltration of connective tissue to the site of injury. Presence of connective tissue inside the muscle which does not possess any contractile capability leaves non functional scar even after healing. Such scars lead to severe weakness in muscles and increase the possibility of fat accumulation within muscle throughout aging. Proper treatment to muscle injuries such as tears or traumas requires use of sophisticated materials to prevent infiltration of connective tissue. To this end, regenerative medicine is a promising alternative solution for the treatment of myopathies as well as regeneration of age-related muscle wasting in elderly people. It is still challenging to engineer skeletal muscle, yet numerous techniques are being developed [51,103-105]. One of the strategies is fabrication of aligned scaffolds for engineering muscle tissue. Aviss *et al*. fabricated align polymer fibers with PLGA and demonstrated differentiated long myotubes by immunostainings [104]. Similarly, myotube assembly was shown on nanofibrous and micropatterned polymers by Huang *et al*. They concluded that microgrooves cause the alignment of myoblasts and cytoskeletal proteins and promote myotube assembly along the nanofibers [106].

Biomimicry to generate favorable microenvironment for induction of differentiation is another promising strategy. ECM mimetic scaffolds for differentiation and tissue regeneration are under investigation for many tissues including bone, cartilage,

myocardium and nerve. For skeletal muscle, basal lamina could be target of biomimetic strategies. Basal lamina is a type of ECM that surrounds muscle fibers and takes role in fiber force transmission, repair and maintenance. Fibrous architecture and biochemical components of basal lamina support development and function of skeletal muscle. Thus, scaffolds mimicking basal lamina are promising candidates for efficient muscle tissue regeneration [107]. Since nano- to micrometric topography is known to greatly influence cellular behavior including differentiation [108], micro and nanofabrication techniques are currently used to develop skeletal muscle constructs, with specific focus on topographical features to induce alignment of myotubes [42,109-110]. Similarly, ECM proteins such as collagen, fibronectin and laminin or their cell adhesion domains are used to coat the engineered surfaces for triggering cell growth and differentiation [111-112]. Previously, it has been shown that laminin has an important role in myogenic differentiation by stimulating proliferation and motility of cells and leading them to bipolar shape of fused cells [113]. The YIGSR and IKVAV peptide sequences derived from β1 and α1 cell binding domains of laminin, respectively, have been utilized to imitate the natural microenvironment in tissue engineering strategies. The RGD peptide is another important cell adhesion epitope found in many proteins including fibronectin[114] and was also shown to promote migration and fusion of cells in an in vitro myogenesis model system.

Peptide amphiphiles enable incorporation of various functional biological signals into their primary sequence and give rise to formation of higher order nanostructures that display complex architecture and biochemical characteristics of native tissue microenvironment under physiological conditions. Owing to their inherent biocompatibility and tailorable properties, variety of studies demonstrated peptide amphiphiles as versatile tools for the design of artificial ECM-like scaffolds [115]. Various shapes including high-aspect ratio nanofibers and nano-networks can be generated through programmed self-assembly driven by multiple types of non-covalent interactions. These properties make them ideal candidates as bioactive scaffolds for regenerative medicine and tissue engineering applications.

This chapter presents utilization of laminin-mimetic and fibronectin-mimetic self-assembled peptide nanofibers for myogenic induction of progenitor cells. These peptide amphiphiles resemble the structure of basement membrane skeletal muscle cells. I describe below the design and characterization of peptide nanofibers and the

affect of these nanofibers on myogenic cell behaviors such as viability, proliferation and differentiation.

2.2 EXPERIMENTAL

2.2.1 Chemicals and Solutions

9-Fluorenylmethoxycarbonyl (Fmoc) and tert-butoxycarbonyl (Boc) protected amino acids, [4-[α-(2',4'-dimethoxyphenyl)Fmoc-aminomethyl]phenoxy] acetamidonorleucyl-MBHA resin (Rink amide MBHA resin), 2-(1H-Benzotriazol-1-yl)-1,1,3,3 tetramethyluronium hexafluorophosphate (HBTU) and Lauric acid were purchased from NovaBiochem, ABCR and Merck. Piperidine, Acetic anhydride, Dichloromethane (DCM) and Dimethylformamide (DMF), N, N-diisopropylethylamine (DIEA), trifluoroacetic acid (TFA) : triisoproplysilane (TIS) were purchased form Sigma.

Cell Culture Reagents:

Dulbecco's Modified Eagle Medium (DMEM), Penicillin/streptomycin (PS) antibiotic combination and fetal bovine serum (FBS) were purchased from Invitrogen Gibco.

2.2.2 Synthesis of Peptide Amphiphiles

Peptide amphiphile molecules were synthesized using solid phase peptide synthesis method with Rink amide MBHA resin and aspartic acid loaded and glutamic acid loaded Wang resin. FN-PA (Lauryl-VVAGERGD-OH) and E-PA (Lauryl-VVAGE-OH) were synthesized on Fmoc-Asp-Wang and Fmoc-Glu-Wang resins, respectively. LM-PA (Lauryl-VVAGKKIKVAV-Am) and K-PA (Lauryl-VVAGK-Am) were synthesized on Rink amide resins. For coupling of amino acids, 1.95 molar equivalents of HBTU and 3 equivalents of DIEA for 1 equivalent of starting resin were used with 2 equivalents of amino acid in 10 mL of dimethylformamide (DMF). Each amino acid coupling took 2 h and removal of Fmoc protecting group was performed with 20% piperidine/dimethylformamide (DMF) solution for 20 min. Lauric acid addition was performed similarly to amino acid coupling except that coupling time was 4 h. In order to acetylate the unreacted amine groups after each coupling step, 10% acetic anhydride–DMF

solution was used after each coupling. Dichloromethane (DCM) and DMF were used for washing steps. Peptide cleavage from the resin and deprotection were carried out with 95% cleavage cocktail (95:2.5:2.5 trifluoroacetic acid (TFA): triisopropylsilane (TIS): water) for 2 h at room temperature. Excess TFA was removed by rotary evaporation. Ice-cold diethyl ether was used to precipitate the remaining PA solution overnight at -20 °C. Centrifugation was used to collect the precipitate and ultrapure water was used to dissolve the PA precipitate. Solution was frozen at −80 °C and then lyophilized for 3 days.

To characterize synthesized peptide amphiphiles, a quadruple time of flight (Q-TOF) mass spectrometer with electrospray ionization (ESI) source equipped with a reverse-phase analytical high performance liquid chromatography (HPLC) was used. Agilent Zorbax Extend-C18 2.1 x 50 mm column was used for negatively charged peptide molecules and Zorbax SB-C8 4.6 x 100 mm column was used for positively charged peptide molecules respectively. A gradient of water (0.1% formic acid and 0.1% NH_4OH) and acetonitrile (0.1% formic acid and 0.1% NH_4OH) were used for liquid chromatography. In order to purify synthesized peptide amphiphiles, reverse-phase preparative HPLC equipped with Zorbax Extend-C18 21.2 x 150 mm column for negatively charged peptide molecules and Zorbax SB-C8 21.2 x 150 mm column for positively charged peptide molecules was used. A gradient of water (0.1% Acetonitrile and 0.1% NH_4OH) and acetonitrile (0.1% formic acid and 0.1% NH_4OH) were used. Furthermore, positively-charged peptide amphiphiles were treated with 0.1 M HCl solution in order to remove residual TFA at the end.

Table 2.1 Mass and molecular weights of synthesized peptide amphiphiles

Name	Sequence	Exact Mass	Molecular Weight
LM-PA	Lauryl-VVAGKKIKVAV-NH_2	1291.93	1292.74
FN-PA	Lauryl-VVAGERGD	983.57	984.15
E-PA	Lauryl-VVAGE	655.42	655.82
K-PA	Lauryl-VVAGK- NH_2	653.48	653.90

2.2.3 Preparation of Peptide Nanofiber Gels

Solutions were prepared by dissolving PAs in sterile double distilled water and their pH values were adjusted to 7.4. Each PA molecule was separately heated at

70 °C for 5 min and then mixed at a different volume ratio to have final neutral charge. Following 30 s sonication, mixture of PA combinations were reheated at 70 °C for another 5 min. Plates and coverslips were then coated with PA mixtures. With the annealing procedure, homogenous coating over the surface was achieved. After 30 min of incubation at 37 °C, coatings were left to dry overnight under sterile conditions.

2.2.4 Characterizations of Self-Assembled Peptide Nanostructures

Chemical and mechanical characterizations of peptide amphiphiles were performed using CD, SEM, TEM, and rheology.

2.2.4.1 Secondary Structure Analaysis by Circular Dichroism:

LM-PA, FN-PA and E-PA were mixed at 2 x 10^{-4} M concentration. Peptides were heated for 5 min, mixed, sonicated and heated again for 5 min before measurement. Following cooling of mixtures at room temperature, scanning was done between 190 nm to 300 nm using a digital integration time of 1 s, a band width of 1 nm and with standard sensitivity. Secondary structures of individual PA molecules were also analyzed by using 2 x 10^{-4} M concentration. Molar elipticity was calculated with the data obtained from measurements

2.2.4.1 Scanning Electron Microscopy:

SEM samples were prepared by mixing 1% (wt/V) LM-PA and FN-PA at 2:3 ratio and LM-PA and E-PA at 2:3 ratios to have neutral charge. All the samples were prepared with same annealing procedure. Before serial ethanol dehydration step, gels were put onto silicon wafers and incubated for 20 min cooling and stabilization. Then serial ethanol dehydration step was performed. After gradual ethanol dehydration, gels were dried in a critical point dryer (Tousimis, Autosamdri-815B, Series C critical point dryer) and coated with 5 nm Au/Pd before imaging. PA gels were then observed with scanning electron microscopy (SEM, FEI Quanta 200 FEG) at 10 kV.

2.2.4.3 Transmission Electron Microscopy:

For analysis samples were prepared with same annealing procedure, 1 mM E-PA and 1 mM FN-PA were mixed with 1 mM LM-PA in 3:2 volumes and after heating and cooling, mixtures were put on a 200-mesh carbon TEM grid for 5 min

followed by 2 wt% uranyl acetate staining for 40 s. Further, sample was left at flow hood to dry until a dried film was obtained. For E/K-PA 0.5 mM E-PA was mixed with 1 mM K-PA. TEM and STEM images were acquired at 300 kV.

2.2.4.4 Mechanical Characterization by Rheology:

Total volume of 300 µL of 1% (wt/V) PAs was used to analyze mechanical properties of gels. After heating, individual PAs were mixed on the center of the plate, whose temperature was set to 70 °C, and incubated for 5 min. Oscillatory Rheology (Anton Paar Physica RM301 rheometer) operating with a 25 mm parallel plate configuration was used for measurement, after 15 min of cooling, with 0.5 mm gap distance, 100 - 0.1 rad/s angular frequency and 0.5% shear strain.

2.2.5 Cell Culture

2.2.5.1 Cell Adhesion and Viability

Viability of Cells

Cytotoxicity of samples was evaluated using Live-Dead Assay (Invitrogen). C2C12 cells were seeded in DMEM supplemented with 10% FBS and %1 Penn/Strep under conditions of 5% CO2 at 37 ^{0}C.

Well plates were coated with LM/E-PA, LM/FN-PA and E/K-PA. Coating was done as mentioned in the nanofiber formation section. Before coating process, solutions were sterilized under UV for at least 1 h. Gel formation was achieved at 37 °C for 30 min and drying was performed under laminar flow hood overnight. Before experiments, dried plates were further sterilized under UV light for 1 h and washed with medium to remove unbound nanofibers. C2C12 cells were cultured in 96-well plate in 200 µL medium per well with seeding density of 5 x 10^3 cells/well for 24 h. After 24 h of standard incubation, plate was centrifuged for 5 min at 2500 rpm to keep dead cells on the surface. Then wells were washed with 1x PBS and 2 min centrifugation was done in each step. Calcein AM and Ethidium Homodimer reagents were diluted in PBS so that they had 2 µM and 4 µM concentration, respectively. After subsequent 40 min incubation at dark, cells were observed under fluorescent microscope. Experiment was carried out with n=4 and, images were taken from 5 different locations per

well. Live and dead cells were counted with ImageJ (NIH) software. Viability was assessed by calculating ratio of live cells over total cell number.

Cell Adhesion:

C2C12 cells were incubated for 1 h in serum free DMEM medium supplemented with 4 mg/mL Bovine Serum Albumin (BSA) and 50 mg/mL cyclohexamide at standard culture conditions in 75-cm tissue culture flask before seeding. After 1 h, cells were removed from tissue culture plate by trypsinization and seeded onto the coated 96-well plates at a density of 3 x 10^3 cells/well. After 2 h incubation in serum-free medium at standard culture conditions, Calcein AM (Invitrogen) staining (2 μM) for 40 min was performed. Cell adhesion was quantified directly by counting the number of cells using Image J program from the images taken with fluorescent microscope. Images were taken from 5 different random locations per well, and experiment was carried out with n=4. Results were then normalized to tissue culture plate counts.

2.2.5.2 Cell Proliferation

Proliferation of cells on LM/E-PA and LM/FN-PA coatings was assessed using BrdU assay (Roche). Cells were seeded onto PA coated 96-well plate and uncoated tissue culture plates (TCP) at a density of 3 x 10^3 cells/well. Cells were incubated in standard cell culture medium supplemented with 100 μM BrdU labeling solution for 48 h. At the end of the incubation, BrdU incorporation assay was performed. Cells were fixed with FixDenat solution for 30 min and anti BrdU-POD solution was added into wells. Following 90 min incubation and tapping, substrate solution was added into wells and proliferation rates of the cells were quantified by measuring the absorbance (370 nm, with 492 nm reference wavelength) with microplate reader.

2.2.6 Cell Differentiation

Cells were seeded at a density of 5000 and 15000 onto 96-well plate and 24 well plates respectively. Before differentiation induction, they were cultured in 10% FBS and %1 Penn/Strep under conditions of 5% CO2 at 37 ^{0}C for 2 days to let them reach confluence. Afterwards, their culture medium was replaced with DMEM: Ham's F10 Nutrient mix supplemented with 2% FBS, 1% penicillin/streptomycin and 10 μg/mL

insulin. In all experiments, media were changed every day. Cells were used at passage numbers between 8-10.

2.2.6.1 Morphology

During differentiation period, cells on 96-well plate were controlled every day under inverted microscope. Images were taken from 4 different random locations per well, and experiment was carried out with n=3. Number, length and diameter of differentiated myotubes were count by using Image J, and its cell counter plugin. Scale bar in the figures were used to set the measurement length from μm to pixel and length measurement tool of the program was used to analyze the myotube lengths and diameters.

2.2.6.2 Myogenin and Myosin Heavy Chain Gene Expression

Quantitative RT-PCR was used for gene expression analyses. Total RNA was isolated from C2C12 samples using TRIzol (Invitrogen) reagent. Nanodrop 2000 (Thermoscientific) was used to assess yield and purity of extracted RNA. Primer sequences were designed using Primer 3 software (Table 2.1). The reaction efficiencies for each primer set were evaluated with standard curve using 2-fold serial dilutions of total RNA. cDNA synthesis from RNA and qRT-PCR were performed using SuperScript III Platinum SYBR Green One-Step qRT-PCR Kit (Invitrogen). Myosin Heavy Chain and Myogenin gene expression profiles were analyzed at day 0, 3 and 4. Reaction conditions were briefly as follows: 55 °C for 5 min, 95 °C for 5 min, 40 cycles of 95 °C for 15 s, 60 °C for 30 s, and 40 °C for 1 min, followed by a melting curve to confirm product specificity. For analysis of the expression data, primary gene expression data was normalized to the expression level of GAPDH. A comparative Ct method was used to analyze the results. Gene expression was normalized to GAPDH and TCP.

Table 2.2 Primer sequences of myogenin and myosin heavy chain for C2C12 cells.

Gene	Primer Sequence: Forward/Reverse	Annealing Temp.
Myogenin	5’-ACCTTCCTGTCCACCTTCAG-3’ 5’-CACCGACACAGACTTCCTCT-3’	58.5 ºC

Myosin Heavy Chain	5’-GGAGTACAAGAACGAGGGCA -3’ 5’-TTGAAGGAGGTGTCTGTCGC-3’	59.9 ºC

2.2.6.3 Myosin Heavy Chain Immunocytochemical Staining

Antibodies against Myosin heavy chain were used for immunocytochemistry as a late marker of myotube differentiation. C2C12 cells were seeded onto PA coated surfaces and glass surface (15 mm) at a density of 8 x 10^3 cells/cm^2. After reaching confluency, differentiation was induced with low serum medium. Medium was changed every day. Cells were fixed in 4% paraformaldehyde/PBS for 10 min and permeabilized in 0.1% Triton X-100 for 15 min. To reduce nonspecific binding, samples were incubated with 3% (w/v) bovine serum albumin/PBS for 2 h and treated with 10 µg/mL Myosin heavy chain primary antibody (R&D MAB4470) overnight at 4 °C. After overnight incubation with primary antibody, samples were incubated with Alexa Fluor 488 goat anti-mouse secondary antibody at 1:300 dilutions for 1 h at room temperature. Extensive washing with PBS was performed between each steps. All samples were counterstained with 1 µM To-PRO-3 (Invitrogen) and 1:500 diluted phalloidine in PBS for 20 min at room temperature and mounted with Prolong Gold Antifade Reagent (Invitrogen). Negative controls were obtained by omitting primary antibody and incubating with 1% normal goat serum/PBS. Samples were imaged using confocal microscope (Zeiss LSM510).

2.3 RESULTS AND DISCUSSION

2.3.1 Sythesis and Characterization of Peptide Amphiphiles

Four different peptide amphiphile molecules were designed and synthesized by solid phase peptide synthesis to form nanofibers which presents chemical groups in Laminin and Fibronectin structure. Peptide amphiphiles were designed as a composition of hydrophobic alkyl group, β-sheet driving group and charged group. Lauric acid added at the end of peptide gives a hydrophobic character to peptide amphiphile which triggers hydrophobic collapse during self-assembly. For β-sheet forming part, four non-polar aminoacids were used; Val-Val-Ala-Gly (VVAG). Laminin-derived sequence "IKVAV" (Lauryl-VVAGKKIKVAV-Am) and fibronectin-derived sequence "RGD" (Lauryl-VVAGERGD) were incorporated into peptide amphiphiles (LM-PA and FN-PA, respectively) to generate a 2D myogenic environment. As a counter negatively charged peptide amphiphile, E-PA (Lauryl-VVAGE-OH) with only one glutamic acid after VVAG sequence was designed. LM-PA is positively charged at pH 7.4 whereas FN-PA and E-PA are negatively charged. To form gel, positivley charged LM-PA was mixed with either FN-PA or E-PA so that two network was generated. One of them includes only "IKVAV" signal while other one presents both "IKVAV" and "RGD" signals. Also, to form non-bioactive control group, positively charged K-PA (Lauryl-VVAGK-Am) was synthesized adding lysine aminoacid to N-terminus of peptide amphiphile and mixed with negatively charged E-PA (Figure 2.1).

2.3.1.1 Mass Spectrometry and HPLC Purification

QTOF-LCMS was used to verify synthesized peptide amphiphiles accordingly. Expected masses for all PA molecules are 1291.93 for LM-PA, 983.57 for FN-PA, 655.42 for E-PA and 653.48 for K-PA as shown in Table 2.2. We obtained 1292.97 for LM-PA, 982.54 for FN-PA, 654.41 for E-PA and 654.50 for K-PA (Figure 2.2, and Figure 2.3).

2.3.1.2 Circular Dichroism

Circular Dichroism (CD) analysis was performed to understand the secondary structure of peptide amphiphiles. CD measures the differential absorbance of left-

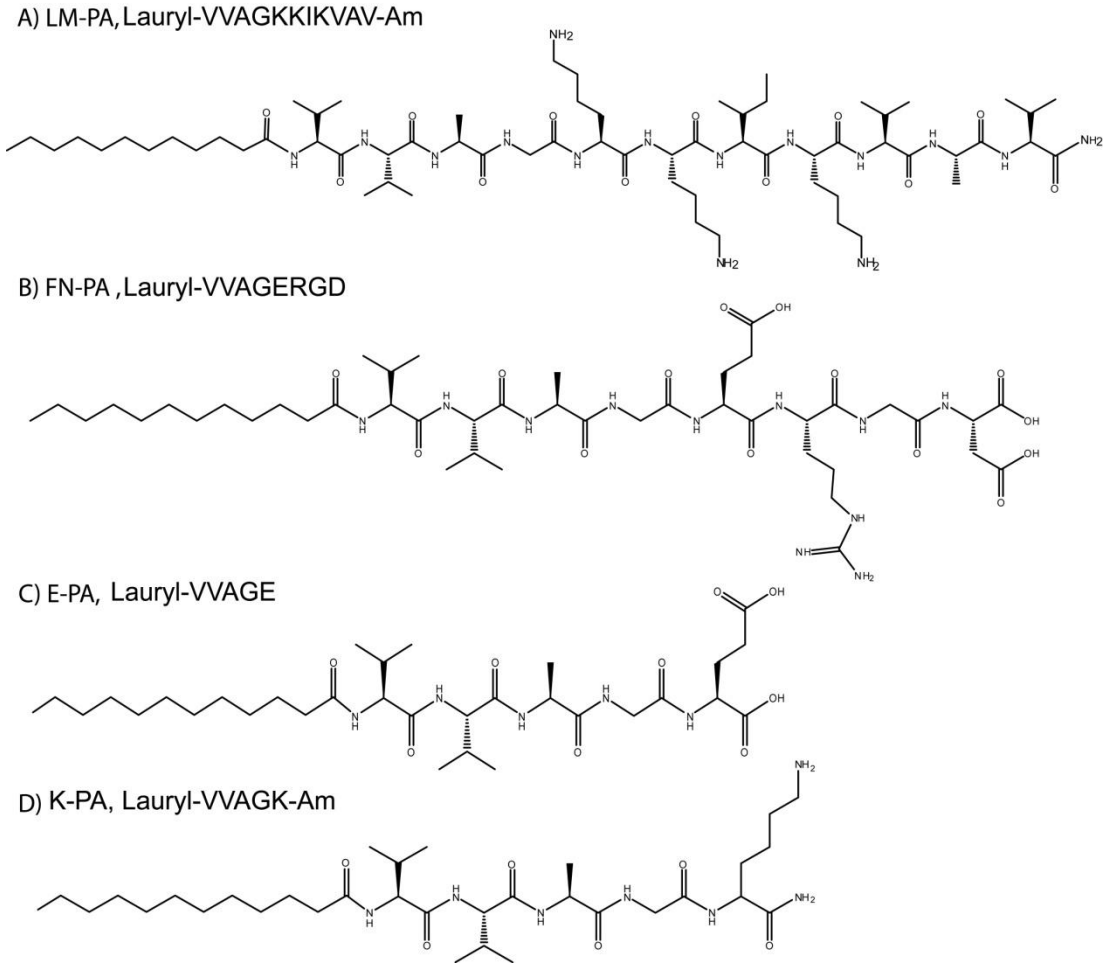

Figure 2.1 Chemical structures of peptide amphiphile molecules, A) LM-PA, B) FN-PA, C) E-PA and D) K-PA

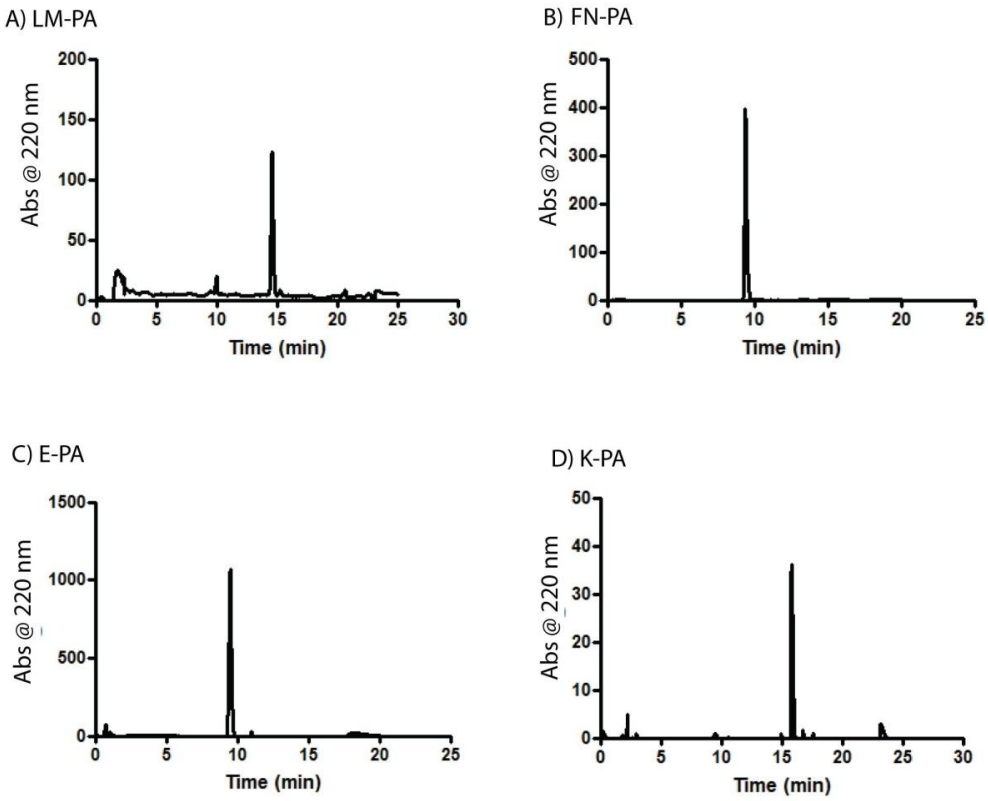

Figure 2.2 Liquid Chromatography of A) LM-PA, B) FN-PA, C) E-PA and D) K-PA

LM-PA

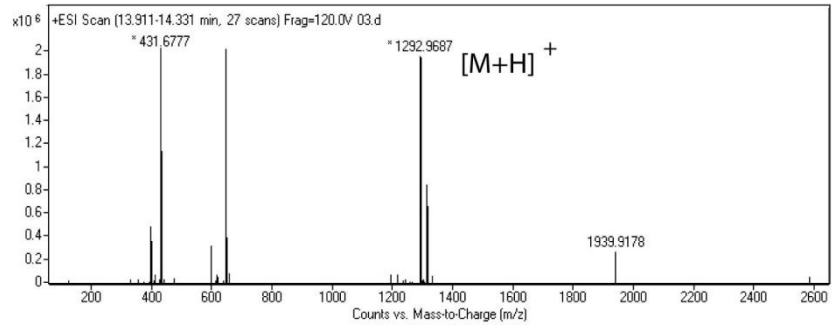

FN-PA

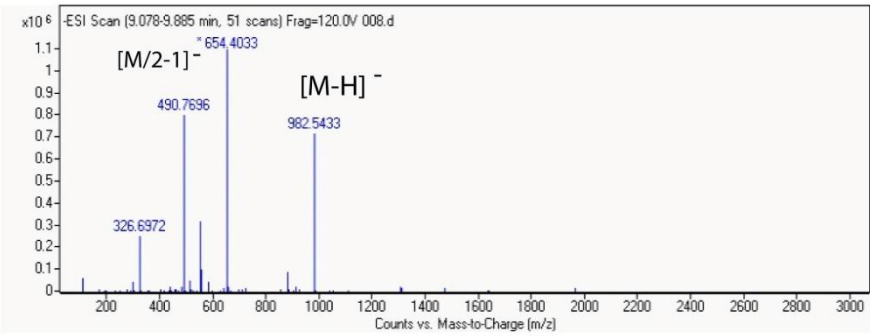

E-PA

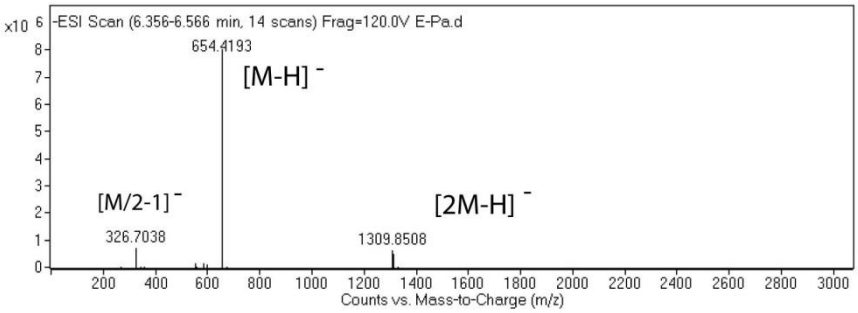

K-PA

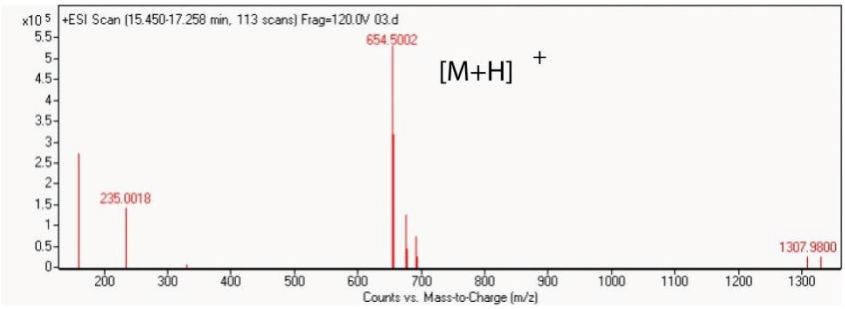

Figure 2.3. Electrospray ionization mass spectra of A) LM-PA, B) FN-PA, C) E-PA and D) K-P

handed and right-handed circularly polarized light which exhibited on optically active chiral molecules. The absorbance is provided by the amide group forming the peptide backbone by acting as a chromophore in the far UV region. While none of the PAs were found to display an ordered structure by itself, CD spectra of the PA mixtures revealed a minimum at 220 nm and a maximum at 200 nm, which indicate β-sheet secondary structure in both annealed and normal LM/FN-PA, LM/E-PA and E/K-PA combinations (Figure 2.4).

2.3.1.3 Scanning Electron Microscopy

To characterize self-assembly of peptide amphiphiles, nanofiber formation and morphology of the peptide network, SEM imaging was performed. SEM imaging reveals that nanofibers formed upon mixing oppositely charged peptide amphiphiles LM/FN-PA, LM/E-PA and E/K-PA. (Figure 2.5). These peptide networks with its porous and nanofibrous morphology, mimicks the physical architecture of native ECM of cell.

2.3.1.4 Transmission Electron Microscopy

TEM imaging was also performed to further analyze nanofiber formation and individual nanofibers. TEM images revealed that nanofibers formed upon charge neutrilization of oppositely charged peptide amphiphiles. Nanofibers were observed with 6 – 10 nm diameters and lengths up to a few microns (Figure 2.5). Moreover, bundling of nanofibers for E/K-PA was observed.

2.3.1.5 Oscillatory Rheology

Rheology experiment was applied to peptide nanofibers in order to analze gel formation upon mixing oppositely charged peptide amphiphiles. Gel formation is defined when storage modulus (G′) is higher than the loss modules (G″) where a shift from viscous liquid to gel form is taken place. LM/FN-PA and LM/E-PA mixtures showed higher storage moduli (G′) than loss (G″) moduli, which was consistent with the formation of a gel. The 1% (wt/v) gels exhibited storage moduli of between 1-3 kPa with loss moduli of 100-500 Pa. At the 0.1% strain, both LM/E-PA and LM/FN-PA combinations were similar in terms of mechanical properties.

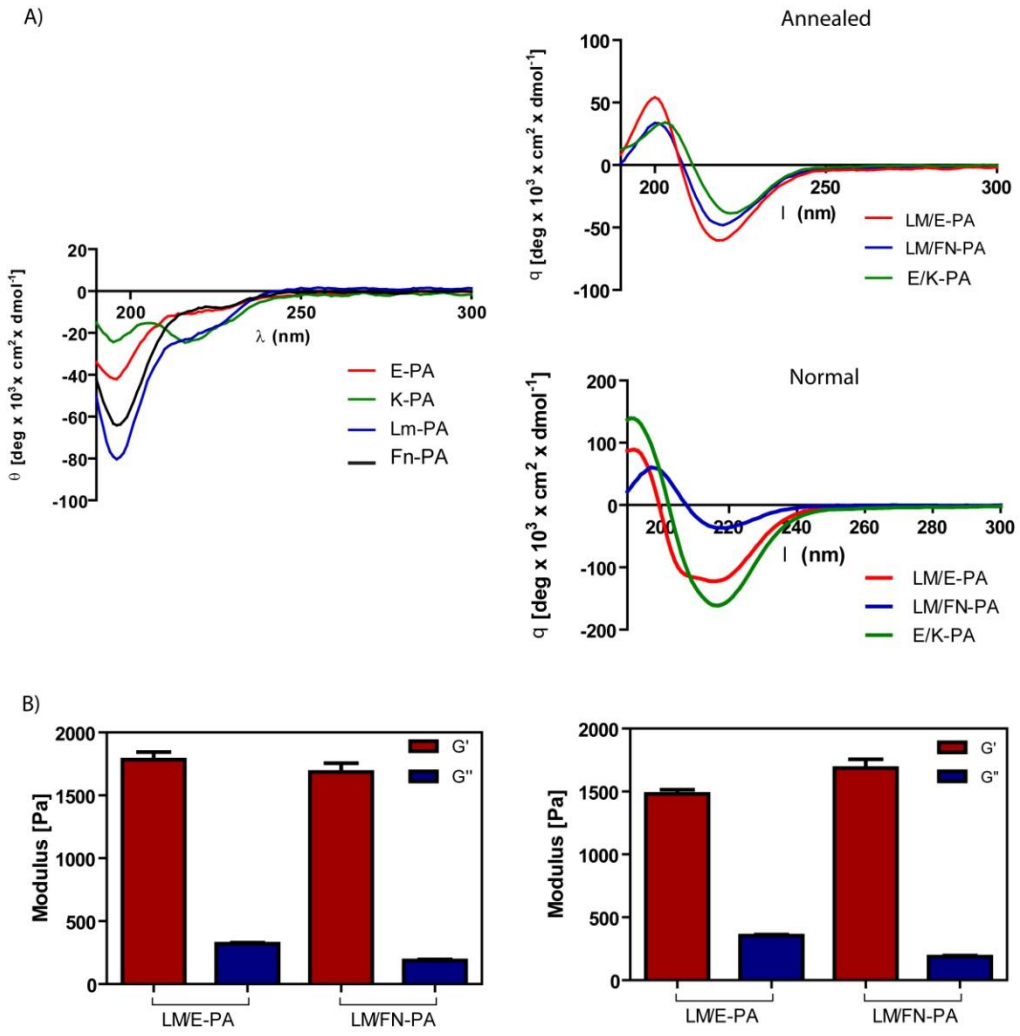

Figure 2.4 Characterization of peptide amphiphile molecules by using circular dichoism and oscillatory rheology. A) Secondary structure characterization of annealed and normal PA molecules with circular dichoism, and B) storage and loss moduli of PA mixtures prepared through annealing and without annealing procedure, to compare mechanical differences between standard and annealing protocol.

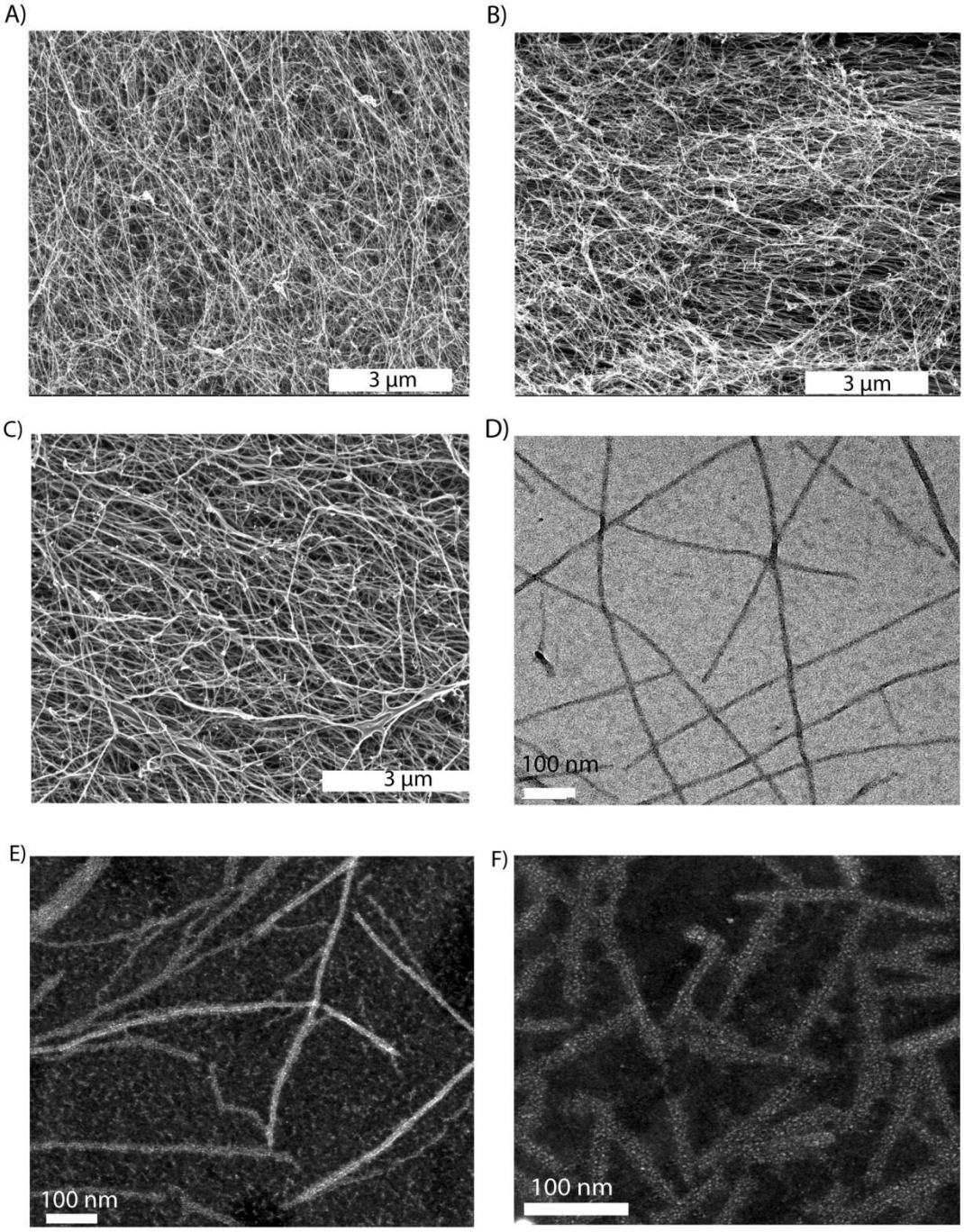

Figure 2.5 Characterization of peptide amphiphile molecules by using scanning electron microscopy and transmission electron microscopy. A) SEM images of LM/FN-PA and B) LM/E-PA and C) E/K-PA gels that reveal the ECM mimicking morphology (Scale bars = 3 µm). Representative TEM images of individual nanofibers of (D) LM/E-PA and E) STEM image of LM/FN-PA, and F) E/K-PA (Scale bars = 100 nm).

Annealed PA gels showed higher storage moduli than unheated PA gels, such that the mechanical strength of the bulk annealed gels were higher than their unheated counterparts (Figure 2.4).

2.3.2 Cell Culture on Peptide Nanofibers

2.3.2.1 Design of 2D Cell Culture Experiments

Laminin and fibronectin mimetic PAs were coated onto tissue culture plates and coverslips to determine the effect of chemical groups on PAs to the cellular behaviors such as viability, spreading, proliferation and differentiation in two-dimensional cell culture. LM/E and LM/FN nanofibers were used to mimic basal lamina and E-PA/K-PA nanofibers were used as nan-bioactive control groups along with uncoated tissue culture plates which lack peptide nanofibers. C2C12 cells are used in all *in vitro* experiments due to their myoblast phenotypes and differentiation capacities.

2.3.2.2 Biocompatibility of Peptide Nanonetworks

Viability of myoblast cells was assessed with Calcein-AM staining. Calcein-AM is a cell-permeable and nonfluorescent dye which is converted into fluorescent calcein upon acetoxymethyl ester hydrolysis by intracellular esterases and gives green color. After 24 h of incubation in growth medium, cells on peptide nanofibers and tissue culture plates were stained with Calcein to utilize their viabilities. Calcein AM staining showed that LM/E-PA and LM/FN-PA nanofibers did not alter viability of C2C12 cells compared to uncoated tissue culture plate surface (Figure 2.6). Quantitative results of this viability assay was done by counting live and dead cells through Image J program and calculated by taking ratios of live cells to total number of cells. On LM/E-PA nanofiber networks, cells showed 97.31 % viability, whereon LM/FN-PA and TCP, 96.74% and 95.45% viability were calculated, respectively. This result demonstrated the biocompatibility of the PA system (Figure 2.6 D), which was further confirmed with microscopic observations of the morphologies of C2C12 cells. The spindle-like morphology of C2C12 cells was preserved during their culturing on LM/E-PA and LM/FN-PA nanofibers. Figures and quantitative results indicates that basal lamina mimetic peptide nanofibers do not have any toxic affect on cells and they provide biocompatible and biofriendly environments where cells

can live. However, cells cultured on a non-bioactive control peptide amphiphiles (E/K-PA) displayed decreased viability and clustering (Figure 2.7). Consequently, this combination was not used for further experiments. Overall, cellular viability was supported on bioactive peptide nanofibers and it was comparable with TCP, which indicates the biocompatibility of LM/E-PA and LM/FN-PA peptide nanofibers.

2.3.2.3 Adhesion and Proliferation of cells

Cell adhesion is mediated through interaction of cell surface proteins with ligands present in the proteins of the ECM. IKVAV and RGD are ligands found in ECM and binds to cells through cell surface receptors. We investigated the initial adhesion behavior of cells to the nanofibrous networks in the absence of any adhesion proteins, and by preventing cells from synthesizing new

adhesion proteins via cyclohexamide. After 2 h of adhesion, cells were stained with Calcein-AM and observed under fluorescent microscope and number of adhered cells was count on Image J. Results showed that cells on LM/FN-PA surfaces adhere slightly better than other groups, though this difference was not statistically significant. Quantified data showed that adhesion of cells to peptide amphiphile nanofibers were comparable with tissue culture plate results (Figure 2.8 D).

Proliferation profiles of cells on peptide nanofibers were assessed with BrdU incorporation assay. 5-bromo-2-deoxyuridine (BrdU) is a uridine derivative and a structural analog of thymidine and it can be incorporated into DNA during the synthesis-phase of the cell cycle as a substitute for thymidine, thereby serving as a marker for proliferation. After 48 h of incubation in growth medium, cells on LM/FN-PA coated surfaces proliferated significantly more than cells on LM/E-PA coated surfaces (Figure 2.8 E). This increase in proliferation is likely due to the additional effect of RGD. No significant difference in proliferative capacity was found between the LM/E-PA system and TCP. These results show that this fibrous, ECM-mimetic peptide amphiphile system provides a biocompatible and favorable environment for the growth and proliferation of C2C12 cells.

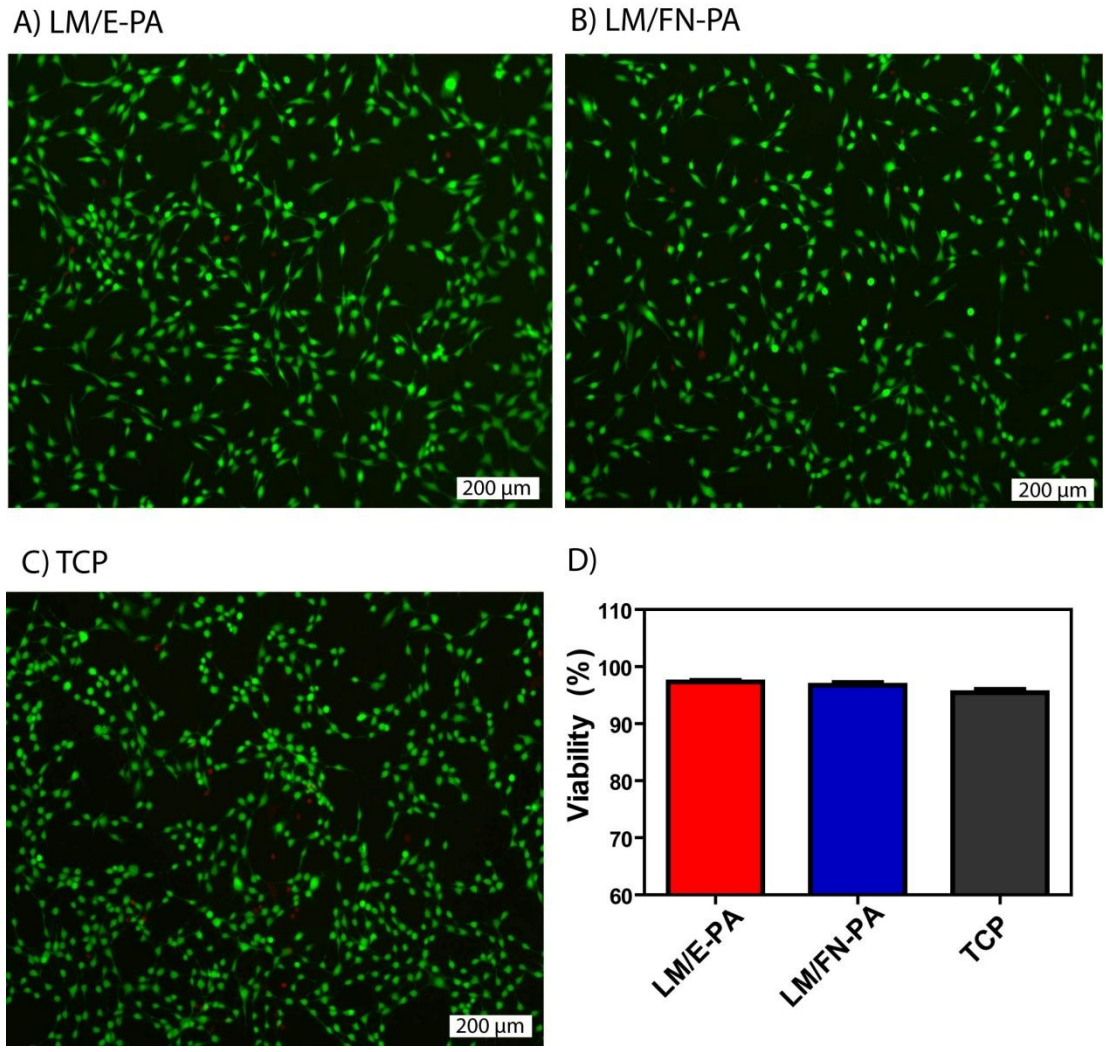

Figure 2.6 Viability of C2C12 cells on peptide nanofiber networks. Live-dead assay of C2C12 cells at 24 h. Dead cells were stained red and live cells were stained green. The scale bar is 200 µm in all images. (A) LM/E-PA, (B) LM/FN-PA and (C) TCP. (D) Relative viability of C2C12 cells on LM/FN-PA and LM/E-PA coated surfaces compared to tissue culture plate surface at 24 h

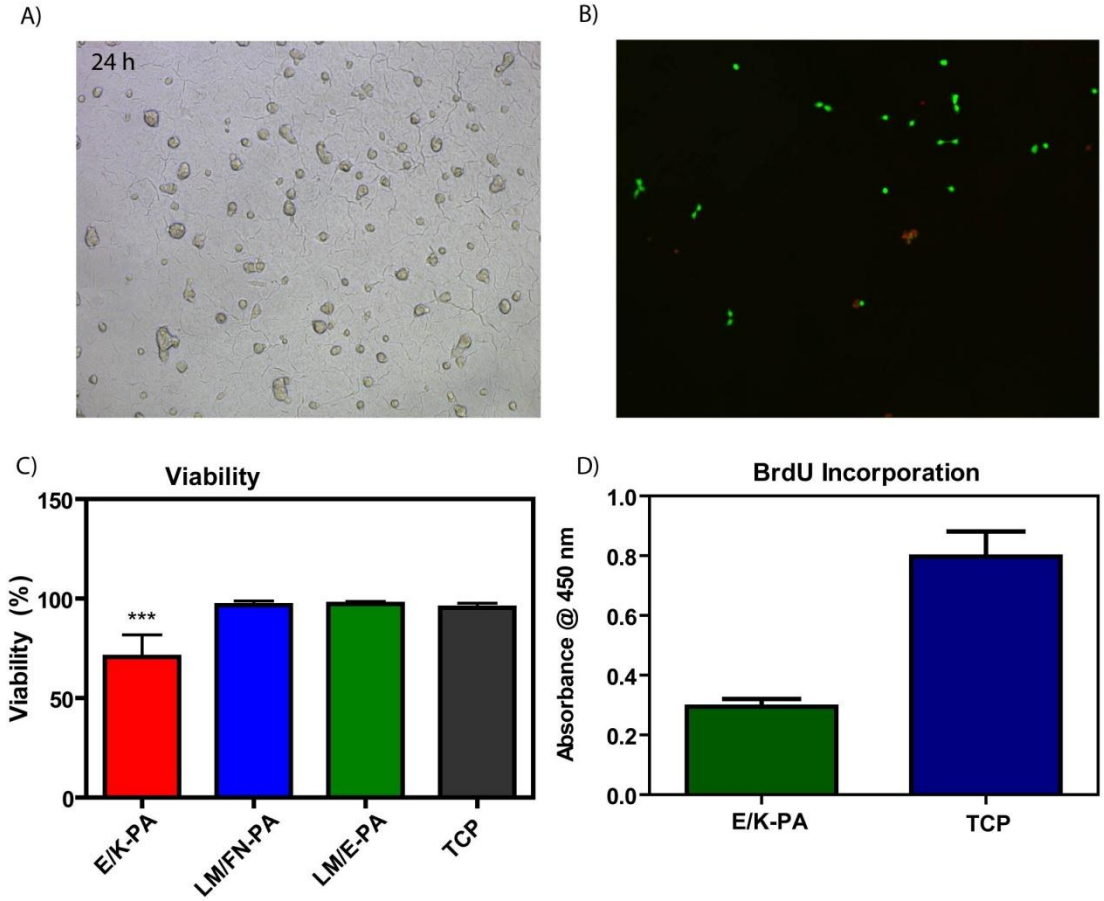

Figure 2.7 Cellular viability and proliferation of C2C12 cells on control peptide group. A) Optical microscope image of C2C12 cells on E/K-PA coating, 10x objective, B) live (green) and dead (red) cells stained with live/dead assay, C) quantitative analysis of viability assay and D) proliferation of cells cultured in E/K-PA.

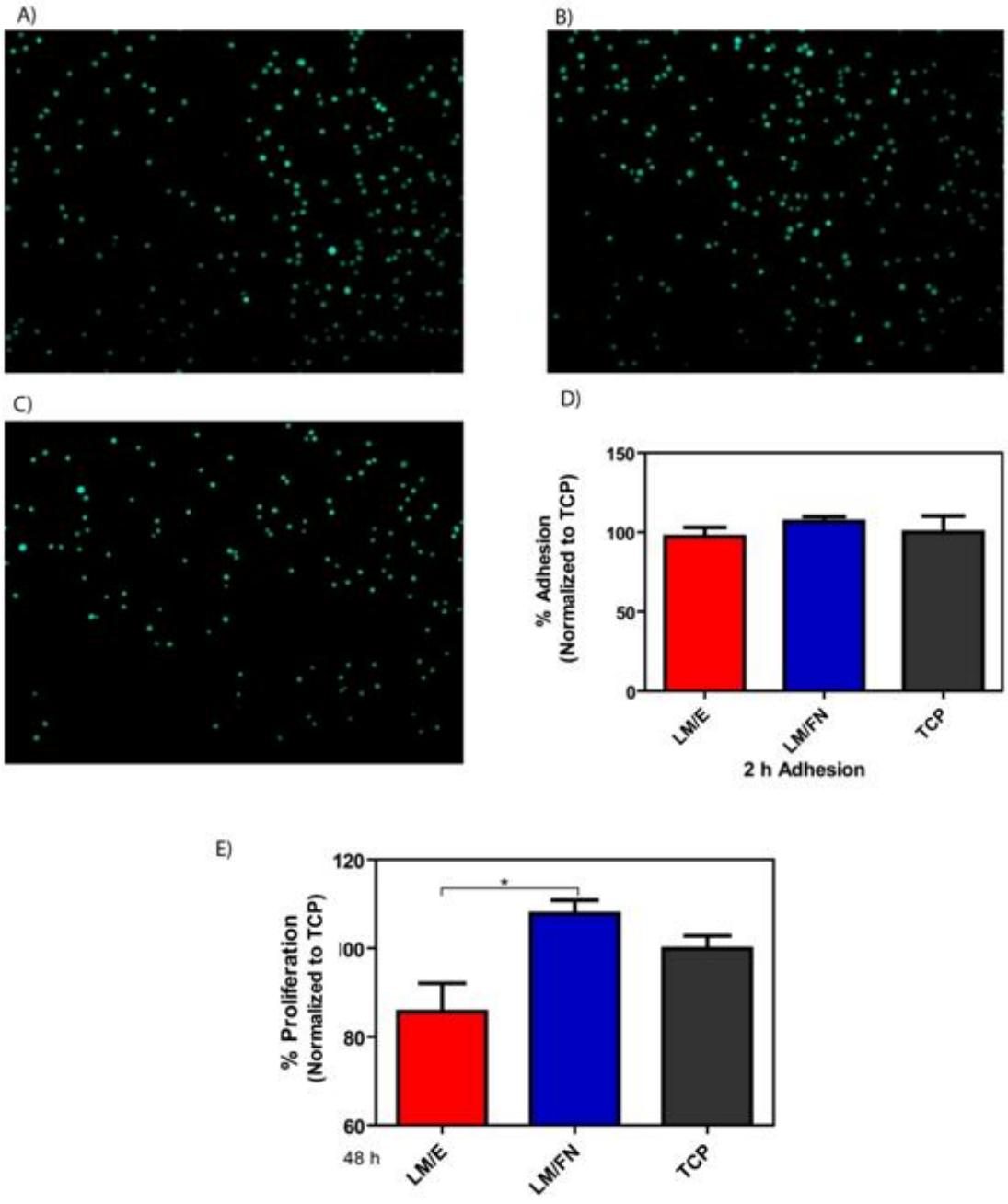

Figure 2.8 Adhesion and proliferation of C2C12 cells on peptide nanofiber networks. Fluorescence images of 2 h adhesion assay, A) C2C12 cells on LM/E-PA, B) LM/FN-PA and C) TCP and D) Relative adhesion of C2C12 cells normalized to TCP. E) Relative proliferation of cells normalized to TCP at 48 h. Error bars represent mean ± SEM (*$p<0.05$).

2.3.2.4 Morphology of Differentiated Cells

After induction of differentiation, morphology of the cells were checked every day under optical microscope. Significant changes in cell morphology were observed during the differentiation process since individual myoblast cells contact with each other and fuse to form multinucleated, long myotubes. Fusion of the cells was evident within 2 days, and the formation of elongated myotubes was observed after 3 days of incubation with reduced serum medium. Since myotubes have a tendency to delaminate from the surface after long-term incubation, quantitative analyses were done at day 3 and 4 to minimize the detachment of cells from the surface. Optical microscopy images clearly showed the formation of myotubes (Figure 2.9) after 3 days of incubation. Myotube lengths, diameters and numbers were also evaluated with light microscopy to quantitatively describe myotube morphology and development. Average myotube lengths were around 250 μm, albeit with a wide distribution range between 150-600 μm. While the cells cultured on LM/E-PA produced a greater number of myotubes compared to cells on TCP, differences regarding myotube numbers, lengths and diameters were not statistically significant between the groups. As such, all groups showed similar profiles in terms of quantitative myotube properties (Figure 2.10).

2.3.2.5 Gene Expression analysis

The expression of skeletal muscle differentiation markers was investigated by qRT-PCR to further analyze skeletal myogenesis, as well as to understand the effect of peptide amphiphile nanofibers on the expression of vital muscle differentiation genes. Myogenin is one of the myogenic transcription factors, and plays a key role in later stages of myogenesis. qRT-PCR analysis showed that myogenin expression increased significantly on LM/E-PA coated surfaces compared to TCP at day 3, although there was no significant difference between the expression levels of LM/E-PA and LM/FN-PA groups. However, at day 4, LM/E-PA group had a significantly higher expression of myogenin (2.46 fold relative to TCP) than both TCP and LM/FN-PA (Figure 2.11 A, B). This could be due to the presence of the proliferative RGD sequence on LM/FN-PA. Myosin heavy chain (MHC) is another late myogenic differentiation marker, of which expression was analyzed with qRT-PCR. MHC is an important protein for sarcomeric organization of differentiated myotubes. In parallel

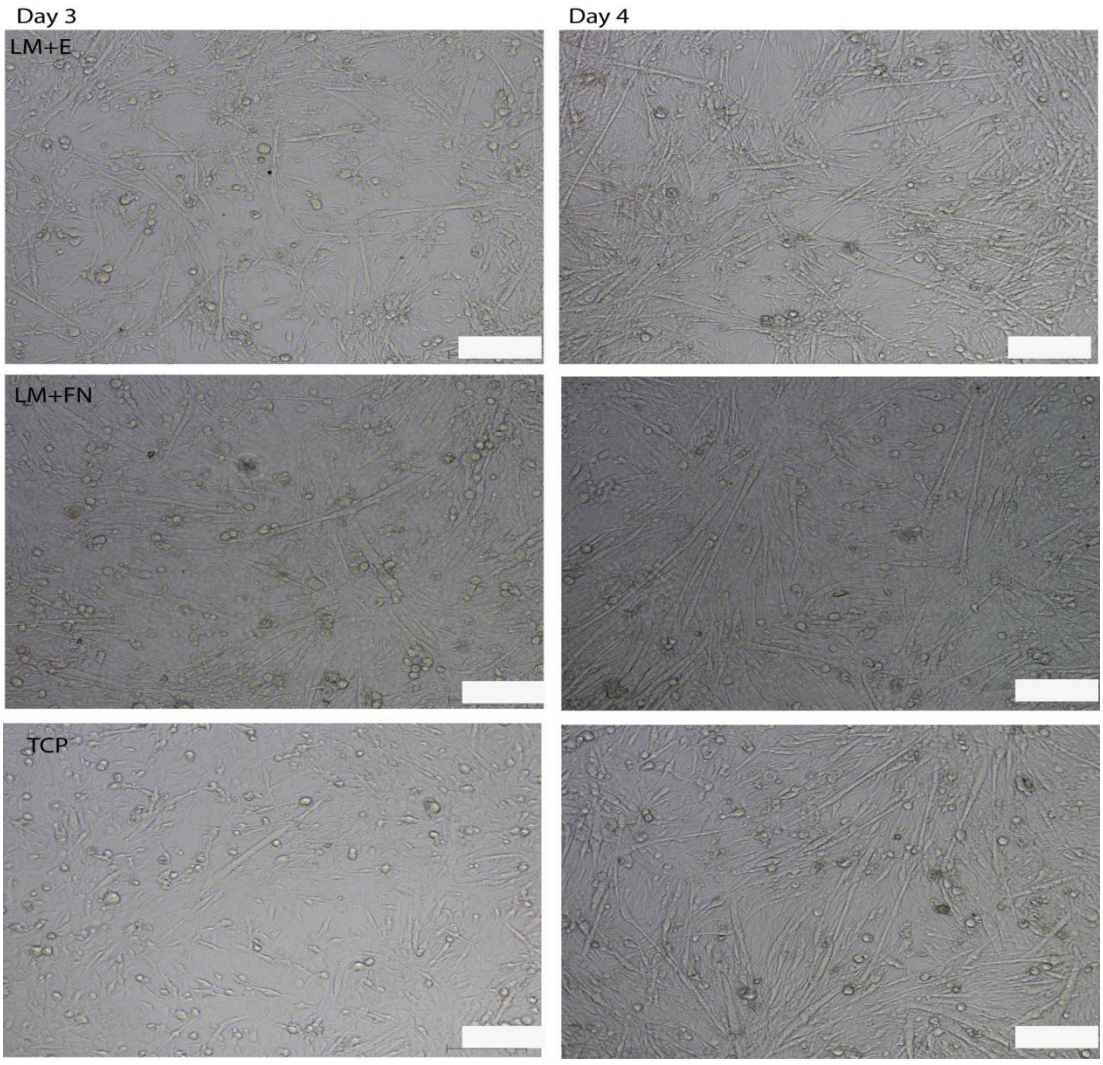

Figure 2.9 Bright-field images of C2C12 cells cultured on peptide nanofiber networks after 3 days and 4 days of myogenic induction. (Scale bars = 200 μm)

to myogenin expression, upregulation in MHC was also observed in LM/E-PA group compared to other groups, though it is not significant at both days 3 and 4 (Figure 2.11 C, D).

2.3.2.6 Immunocytochemical Staining

Myotubes were stained for sarcomeric myosin heavy chain expression to characterize and further confirm myogenic differentiation following culturing on bioactive peptide nanofibers at day 4. The differentiation of C2C12 cells toward mature skeletal muscle cells was evaluated by the analysis of stained cells. Confocal microscopy images showing MHC-positive differentiated cells (green) and nuclei (red) are shown in Figure 2.12. These results are in good agreement with the previous results, where MHC positive myotubes can be observed in all three groups. Myogenic fusion index, a metric reflecting the number of fused cells per total cell number, was calculated for all groups and found to be ca. 15% at day 4, with only slight differences between the groups (Figure 2.13). Maturation index, which denotes the prevalence of myotubes with 5 or more nuclei compared to total myotube numbers, was also measured. Roughly 30% of all myotubes were found to be mature in each group.

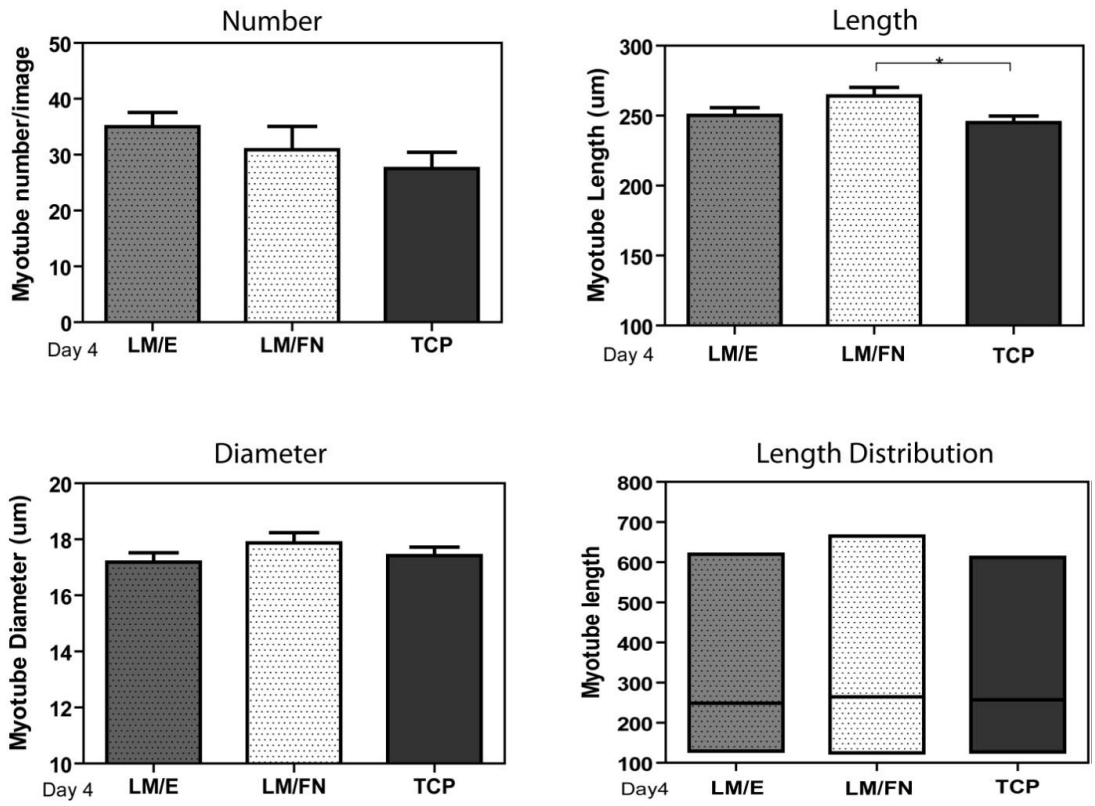

Figure 2.10 The relative myotube number, average length and diameter quantified with Image J. Error bars represent mean ± SEM.

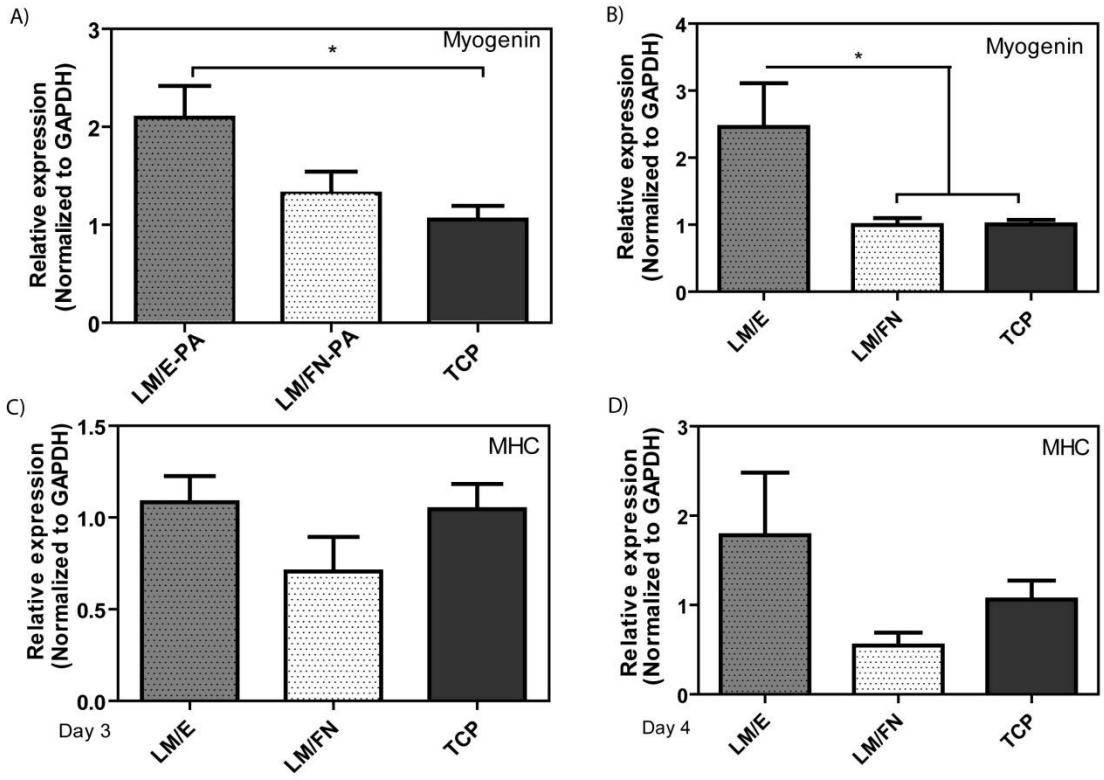

Figure 2.11 Gene expression analyses of C2C12 cells cultured on nanofiber networks after myogenic induction. A) Myogenin expression at day 3, B) Myogenin expression at day 4, C) Myosin Heavy Chain (MHC) expression at day 3, D) Myogenin expression at day 4. The expression level of each gene was normalized against TCP and GAPDH was used as the internal control. Error bars represent mean ± SEM, (*$p<0.05$).

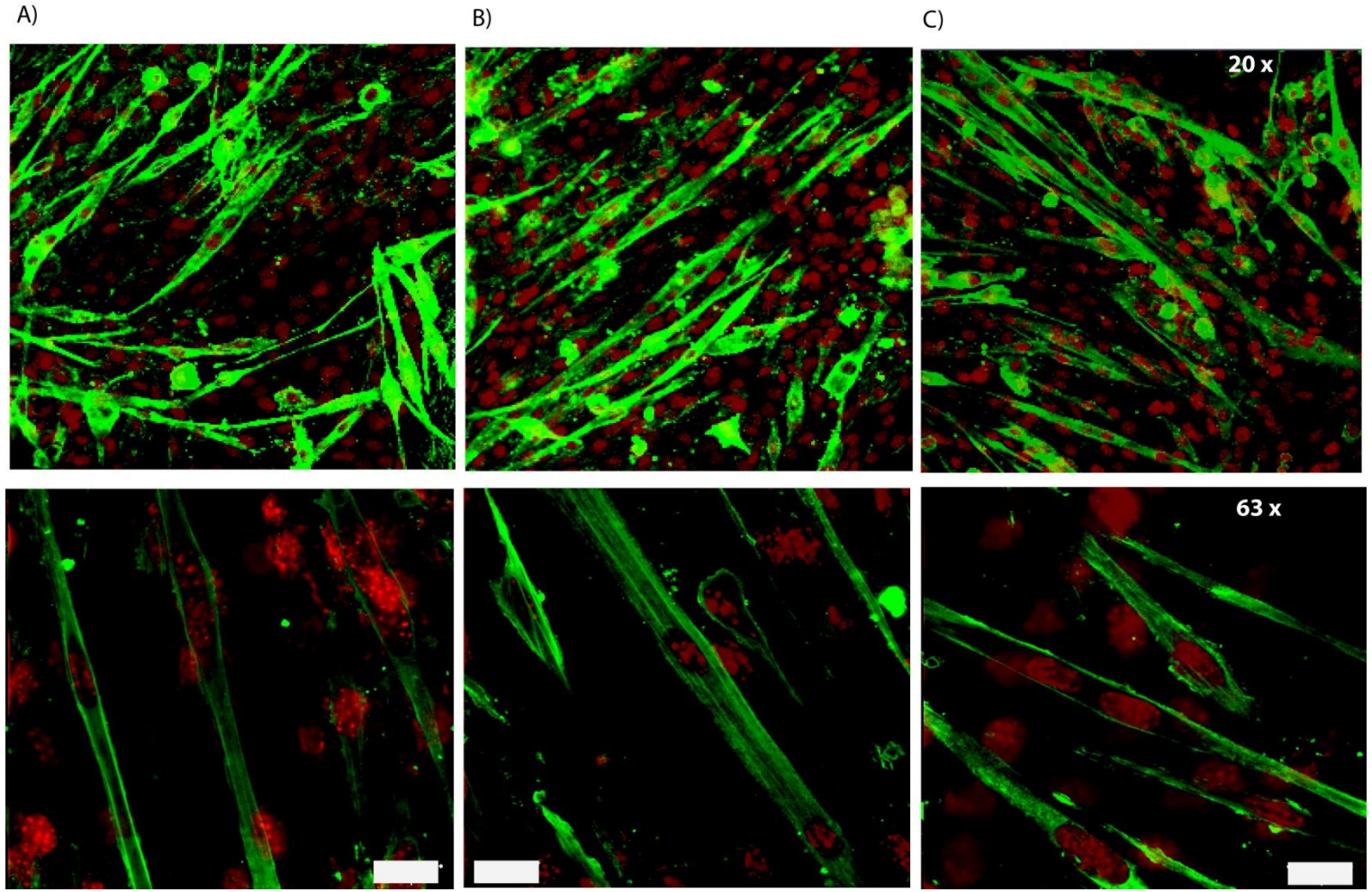

Figure 2.12 Representative immunofluorescent staining of Myosin Heavy Chain (MHC) and nuclei of myotubes 4 days after myogenic induction on the peptide nanofibers A) LM/E-PA, B) LM/FN-PA, and C) TCP. Green: MHC, Red: Nucleus. (Scale bar = 20 μm)

2.4 Conclusion

Bioactive peptide nanofiber based systems are effective materials for providing myogenic signals to augment muscle regeneration while simultaneously preventing the infiltration of connective tissue. The flexible nature of these systems allows the utilization of multiple strategies under both mechanical and biochemical channels. In this study, a peptide-based bioactive nanofiber system was used to create a favorable microenvironment with its fibrous architecture and biochemical signals for myogenic induction of skeletal myoblast cells. This system was developed to be bioactive and biocompatible, and was composed of self-assembled nanofibers functionalized with a myogenic inductive sequence and an adhesion sequence inspired from native basal lamina of skeletal muscle tissue. The presence of laminin-derived signals, in conjunction with the fibrous morphology of the nanofiber network, provides the chemical and structural support necessary for the differentiation of C2C12 cells, while the nanofibrous morphology by itself was not sufficient for neither cell adhesion nor cell viability. Our results showed that C2C12 cells remained viable and proliferative on both of the bioactive peptide nanofiber scaffolds, LM/FN-PA and LM/E-PA, following induction by decreasing serum concentrations supplemented with insulin, cells differentiated into elongated, multi-nucleated myotubes with myogenin and myosin heavy chain expression. Such properties indicate the myogenic potential of these platforms and reveal their potency for muscle regenerative medicine. Due to its biocompability, biodegradability and the ease of delivery by injection, our laminin derived signal-incorporating peptide amphiphile system offers a promising platform for future clinical applications.

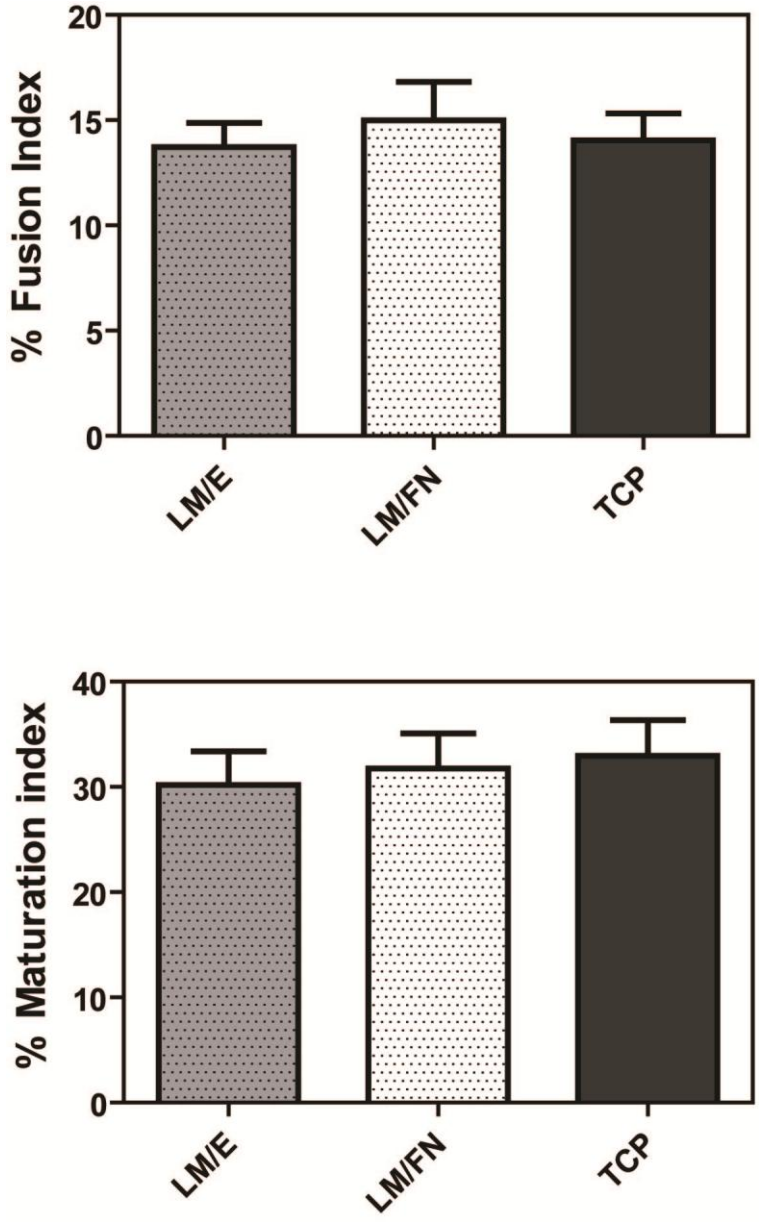

Figure 2.12 The relative fusion index and maturation index were calculated from images as reported in materials and methods. Error bars represent mean ± SEM.

CHAPTER 3. ANGIOGENIC PEPTIDE NANOFIBERS FOR CARDIOMYOCYTE DIFFERENTIATION

Part of this study will be submitted to be published as "Angiogenic Peptide Nanofibers Repair Cardiac Tissue Defect After Myocardial Infarction" Rufaihah Abdul Jalil, İmmihan Ceren Garip, Srirangam Ramanujam Vaibavi, Suganya Cheyyatraivendran Arularasu, Theo Kofidis, Mustafa O. Guler, Ayse B. Tekinay.

3.1 INTRODUCTION

Heart failure is one of the most common causes of death worldwide, and current therapies only delay the progression of the disease. Coronary heart disease is characterized by reduced blood supply to the heart and leads to myocardial infarction (MI), which causes apoptosis or necrosis in cardiomyocytes. Arrested blood and oxygen flow to the myocardium irreversibly damages the heart and causes pathological remodeling, myocardial loss, cardiac dysfunction and heart failure [116]. Current therapies include pharmacological therapy and percutaneous coronary intervention or coronary artery bypass surgery. However, the limited efficiency of current medical treatments generally results in final stage heart failure in several cases and these heart failure patients require heart transplantation (with limited availability) or the support of ventricular assisted devices, which have limited efficacy [117]. Therefore, the development of novel therapeutic strategies to regenerate lost myocardium could help millions of patients every year. Tissue engineering and regenerative medicine approaches are currently under investigation by many research groups for the potential repair of damaged myocardial tissues.

Cell therapy offers the promise of rebuilding the injured heart through a process similar to the one that is effective during natural tissue regeneration, and rapid translation of cell-based approaches to the clinic suggests that cell-based therapies can genuinely improve cardiac function. The mobilization of cells with factors such as cytokines is another related strategy for cardiac repair. However, many challenges still remain in stem cell-oriented therapeutic approaches and the optimal type of cell for many treatments have yet to be determined [65]. The optimal route of delivery and the long term survival and stability of the cells in the infarct area are other concerns related to cell-based therapies. Some of the current research focuses on improving our ability to guide the differentiation of stem cells, control their environment and deliver them in a suitable scaffold to increase the efficiency of the therapy. Another challange is the requirement for vascularization, as persistent ischaemia limits cell survival. Consequently, revascularization and enhanced angiogenesis are essential components of stem cell-based therapies. It was shown that induction of angiogenesis is a vital mechanism that may alleviate cardiac function after MI [118-119]. Cells located at a distance of 200 μm from the capillaries were shown to benefit from

the oxygen and nutrient transport, while cells that are located further away, are under oxygen and nutrient stress.

Heparan sulphate (HS) chains interact with a variety of proteins, including growth factors/morphogens and their receptors, chemokines, and ECM proteins. Interactions of HS with proteins vary with regard to their specificity, which often depends heavily on charge density rather than the carbohydrate sequence [120]. These interactions influence important processes in development, homeostasis and disease. In addition, HS is known to modulate the interaction of proangiogenic heparin-binding vascular endothelial growth factors and affect their bioavailability and interaction with VEGF receptor-2 (VEGFR2) and neuropilin co-receptor in endothelial cells [121-122]. As such, it is well established that HS plays a key role in vascularization and may serve as a potential target for biomimetic strategies.

Peptide-based scaffolds are suitable candidates for designing biomaterials to be used in tissue engineering applications, as they are biocompatible and display the ability to incorporate various bioactive chemical groups in their sequence. Peptide amphiphile molecules, with their adaptive nature and ability to self-assemble into nanostructures with highly variable properties, are high-fidelity models for studying the effects of bioactive and fibrous scaffolds on cellular differentiation. These nanofibers self-assemble into nanofibrous gels at physiological pH. Peptide nanofibers have the advantages of being biodegradable, hypo-immunogenic and suitable for sustained release of a growth factor through covalent bonding. Previously, we have developed a heparan sulphate-mimetic peptide amphiphile nanofiber scaffold which interacts with growth factors secreted by cells and induces angiogenesis without the addition of exogenous growth factors [98]. Through an innovative design, these heparin-mimetic peptide amphiphiles were decorated with sulphonate, hydroxyl and carboxylic acid groups in order to mimic heparan sulphate glycosaminoglycans, which are fundamental constituents of the extracellular matrices of many tissues.

This chapter discusses the *in vitro* effect of heparan sulphate-mimetic peptide nanofibers on the differentiation of cardiomyocytes for the purpose of generating a bioactive material which can repair damaged myocardium and induce angiogenesis. Peptide nanofibers used in this study provide a biochemically and morphologically suitable surface for H9C2 myoblast to adhere, thereby enhancing their survival and

differentiation. Below, we described the design and characterization of peptide nanofibers and their effects on myogenic behaviours.

3.2 EXPERIMENTAL

3.2.1 Chemicals and Solutions

9-Fluorenylmethoxycarbonyl (Fmoc) and tert-butoxycarbonyl (Boc) protected amino acids, [4-[α-(2',4'-dimethoxyphenyl)Fmoc-aminomethyl] phenoxy] acetamidonorleucyl-MBHA resin (Rink amide MBHA resin), 2-(1H-Benzotriazol-1-yl)-1,1,3,3 tetramethyluronium hexafluorophosphate (HBTU) and lauric acid were purchased from NovaBiochem, ABCR and Merck. Piperidine, acetic anhydride, dichloromethane (DCM) and dimethylformamide (DMF), N, N-diisopropylethylamine (DIEA), trifluoroacetic acid (TFA): triisoproplysilane (TIS) were purchased form Sigma.

Cell Culture Reagents:
Dulbecco's Modified Eagle Medium (DMEM), penicillin/streptomycin (PS) antibiotic combination and fetal bovine serum (FBS) were purchased from Invitrogen Gibco.

3.2.2 Synthesis of Glycosaminoglycan-mimetic Peptide Amphiphiles

To synthesize glycosaminoglycan-mimetic peptide amphiphiles, solid phase peptide synthesis was performed with standard Fmoc chemistry. Rink Amide MBHA resin or Fmoc-Glu (OtBu)-Wang resin was used as template where amino acids were added on. Amino acid couplings were performed as 2 equivalents of amino acids activated with 1.95 equivalents of HBTU and 3 equivalents of DIEA for 2 h. To remove Fmoc protection groups, 20% piperidine–DMF solution was used for 20 min. To permanently acetylate the unreacted amine groups after each coupling step 10% acetic anhydride–DMF solution was used. DMF and DCM were used as washing solvents after each step. To synthesize sulfonated PAs, p-sulfobenzoic acid was added to the side chain of lysine which has 4-methytrityl (Mtt) side chain protection as used for selective deprotection of amine groups. Mtt removal was performed by shaking resin for 5 min with TFA:TIS:H_2O:DCM in the ratio of 5:2.5:2.5:90. Cleavage of the PAs and protection groups from the resin was performed by using a

mixture of TFA: TIS: H_2O in the ratio of 95:2.5:2.5 for 3 h. Rotary evaporation was used to remove excess TFA from the peptide solution. PAs in the remaining solution were precipitated in ice-cold diethyl ether overnight. Next day, the precipitate was collected by centrifugation and dissolved in ultrapure water. This solution was frozen at -80 °C for 4 h and then lyophilized for 4-5 days.

3.2.3 Purification of Peptide Amphiphiles

To characterize synthesized peptide amphiphiles, a quadruple time of flight (Q-TOF) mass spectrometer with electrospray ionization (ESI) source equipped with a reverse-phase analytical high performance liquid chromatography (HPLC) was used. Agilent Zorbax Extend-C18 2.1 x 50 mm column was used for negatively charged peptide molecules and Zorbax SB-C8 4.6 x 100 mm column was used for positively charged peptide molecules, respectively. A gradient of water (0.1% formic acid and 0.1% NH_4OH) and acetonitrile (0.1% formic acid and 0.1% NH_4OH) were used for liquid chromatography. In order to purify synthesized peptide amphiphiles, reverse-phase preparative HPLC equipped with Zorbax Extend-C18 21.2 x 150 mm column for negatively charged peptide molecules and Zorbax SB-C8 21.2 x 150 mm column for positively charged peptide molecules was used. A gradient of water (0.1% acetonitrile and 0.1% NH4OH) and acetonitrile (0.1% formic acid and 0.1% NH4OH) were used. Furthermore, positively-charged peptide amphiphiles were treated with 0.1 M HCl solution in order to remove residual TFA at the end.

3.2.4 Characterizations of Self-Assembled Peptide Nanostructures

Chemical and mechanical characterizations of peptide amphiphiles were performed using SEM, TEM, CD, and rheology.

3.2.4.1 Circular Dichroism

To analyze secondary structures of PA molecules CD (JASCO J815 CD spectrapolarimeter) was used. 2 x 10^{-4} M concentration was used to mix GAG-PA and K-PA. Secondary structures of individual PA molecules were also analyzed at 2 x 10^{-4} M concentration. All measurements were performed with three accumulations from 300 nm to 190 nm wavelengths using a digital integration time of 1 s, a band width of 1 nm and with standard sensitivity. Quartz cuvettes with 1 mm path length

were used for measurements. Molar elipticity was calculated with the data obtained from measurements.

3.2.4.2 Scanning Electron Microscopy

To visualize nanofiber formation upon self assembly of peptide amphiphiles, SEM and TEM imaging were performed. For SEM imaging 30-40 μL of 10 mM PA mixtures (GAG-PA/K-PA and E-PA/K-PA) were placed onto silicon wafers and critical point dried after dehydrating sequentially in 20%, 40%, 60%, 80% and 100% ethanol. After gradual ethanol dehydration, gels were dried by using critical point dryer (Tousimis, Autosamdri-815B, Series C critical point dryer) and coated with 5 nm Au/Pd before imaging. Then, morphological properties of the PA gels were observed with SEM, FEI Quanta 200 FEG with ETD detector at high vacuum mode at 10 keV beam energy.

3.2.4.3 Transmission Electron Microscopy

For TEM analysis, 1 mM GAG-PA was mixed with 2 mM K-PA in equal volumes. After 5 min self-assembly, it was diluted 5 times and put on a 200-mesh carbon TEM grid for 1 min followed by 2 wt% uranyl acetate staining for 40 s and drying under flow hood. Imaging was performed using FEI Tecnai G2 F30 transmission electron microscope with TEM and STEM mode.

3.2.4.4 Oscillatory Rheology

Oscillatory Rheology (Anton Paar Physica RM301 rheometer) operating with a 25 mm parallel plate configuration at 25 ºC was used to investigate the mechanical properties of GAG-PA/K-PA gel. 10 mM GAG-PA and K-PA with a total volume of 250 μL were loaded on the center of the plate and measurement was done with 0.5 mm gap distance, 100 - 0.1 rad/s angular frequency and 0.1% shear strain.

3.2.5 Cell Culture

H9c2 cells derived from embryonic rat ventricle were a kind gift from Gazi University, Ankara, Turkey. Cells were cultured in a humidified, 37 °C, 5% CO2 incubator using 75 cm^2 polystyrene cell culture tissue flasks containing High Glucose DMEM supplemented with 15% fetal bovine serum (FBS), 1% penicillin/streptomycin (P/S) and 4 mM L-glutamine. Passaging of cells was carried out at cell confluence between 50 to 60% to save myoblastic population, using trypsin/EDTA. Cells were diluted 1:4 for subculturing. Differentiation induction was

carried out after cells became 80% confluent by adding high glucose DMEM supplemented with 1% FBS, 1% penicillin/streptomycin and 10 nM retinoic acid (RA, Sigma–Aldrich). In all experiments, media were changed every 2 days.

In vitro tests in this study were carried out on GAG-PA/K-PA coated well plates and cover slips unless otherwise mentioned. Coating was done by mixing PA molecules in equal volume with 1 mM and 2 mM concentration after pH adjustment and sonication. Before coating process, solutions were sterilized under UV for at least 1 h. Gel formation was achieved at 37 °C for 30 min and drying was performed under laminar flow hood overnight. Before experiments, dried plates were further sterilized under UV light for 1 h and washed with PBS to remove unbound nanofibers.

3.2.5.1 Cell Viability and Adhesion

Cell viability on the surface of nanofibers was tested with Alamar Blue viability assay. In this experiment, 3 different charges were tested and negatively, neutral and positively charged combinations were formed by mixing GAG-PA (1 mM) and K-PA with varying molar ratios (1:2, 1:3 and 1:4). Coated 96 well-plates were used for analysis and H9C2 cells were seeded at a density of 5×10^3 cells/well. After 24 h of standard incubation, Alamar Blue reagent was diluted 1:10 with serum-free medium and replaced with standard medium. After subsequent 4 h of incubation, absorbance was measured using microplate reader at 570 nm and 600 nm background. We continued with -1 charge combination (1:2 ratios) for further experiments.

Cell adhesion was performed under serum-free conditions. Cells were incubated for 1 h in serum free DMEM medium supplemented with 4 mg/mL Bovine Serum Albumin (BSA) and 50 mg/mL cyclohexamide at standard culture conditions before seeding. After 1 h, cells were removed from tissue culture plate by trypsinization and seeded onto the coated 96 well plates at a density of 5×10^3 cells/well. After 2 h of incubation in serum-free medium at standard culture conditions, Calcein AM (Invitrogen) staining (2 μM) was performed for 40 min according to the manufacturer's instructions. Cell adhesion was quantified directly by counting the number of cells using Image J (NIH) program from the images taken with fluorescent microscope. Images were taken from 4-5 different locations per well, and experiment was carried out with n=4. Results were then normalized to uncoated tissue culture plate.

3.2.5.2 Cell Proliferation

Proliferation of cells on GAG-PA/K-PA coating was assessed using BrdU assay after 72 h. Cells were seeded onto PA coated wells (1:2 molar ratio) and tissue culture plates (TCP) at a density of 3 x 10^3 cells/well. Cells were incubated in standard cell culture conditions for 72 h. 2 h prior to the experiment, cell medium was replaced with 10 μM BrdU labeling solution-containing standard maintenance medium. At the end of the time, BrdU incorporation assay was performed according to manufacturer's instructions. Briefly, cells were fixed with FixDenat for 30 min and after that anti BrdU-POD solution was added into wells. Following 90 min of incubation and tapping, substrate solution was added into wells and proliferation rates of the cells were quantified by measuring absorbance (370 nm, with 492 nm reference wavelength) with a microplate reader.

3.2.6 Gene Expression Analysis

Quantitative RT-PCR (qRT-PCR) analysis was used for gene expression analysis. Total RNA was isolated from C2C12 samples using TRIzol (Invitrogen) reagent. Nanodrop 2000 (Thermo scientific) was used to assess yield and purity of extracted RNA. Primer sequences were designed using Primer 3 software. The reaction efficiencies for each primer set were evaluated with standard curve using 2-fold serial dilutions of total RNA.

cDNA synthesis from RNA and qRT-PCR were performed using SuperScript III Platinum SYBR Green One-Step qRT-PCR Kit (Invitrogen) according to manufacturer's instructions. Ventricular myosin light chain-2 (Mlc-2v) and Myogenin genes' expression patterns were analyzed at day 0, 3 and 4. Reaction conditions were briefly as follows: 55 °C for 5 min, 95 °C for 5 min, 40 cycles of 95 °C for 15 s, 60 °C for 30 s, and 40 °C for 1 min, followed by a melting curve to confirm product specificity. For analysis of the expression data, primary gene expression data were normalized by the expression level of GAPDH. A comparative Ct method was used to analyze the results. Gene expression was normalized to GAPDH and TCP.

Table 3.1 Primer sequences and annealing temperatures with efficiencies

Gene	Primer Sequence: Forward/Reverse	Annealing Temp.
Myogenin	5’ TGGTCCCAACCCAGGAGATC 3’ 5’ AGAAGTGGTGGCGTCTGA C 3’	60 °C
Mlc-2v	5’ CCTGACGTCACCGGCAACC 3’ 5’ TGGGTGATGATGTGAACCAAA 3’	54 °C

3.2.7 Immunocytochemical Staining

Cardiac Troponin T was stained as a marker of cardiomyocyte differentiation. H9C2 myoblast cells were seeded onto PA coated surfaces and glass surface (15 mm) at a density of 1.5 x 10^4 cells/well. Differentiation was induced after reaching confluency. Medium was exchanged every day. For immunocytochemistry, cells were fixed in 4% paraformaldehyde/PBS for 10 min and permeabilized in 0.1% Triton X-100 for 15 min. To reduce nonspecific binding, samples were incubated with 3% (w/v) bovine serum albumin/PBS blocking reagent for 2 h and treated with 1:200 diluted Cardiac Troponin T primary antibody (Ms Ab33589) overnight at 4 °C. After overnight incubation with primary antibody, samples were incubated with Alexa Fluor 488 goat anti-mouse secondary antibody at 1:300 dilution for 1 h at room temperature. Extensive washing with PBS was performed between each step. All samples were counterstained with 1 μM TO-PRO-3 (Invitrogen) and 1:500 diluted phalloidine in PBS for 20 min at room temperature and mounted with Prolong Gold Antifade Reagent (Invitrogen). Negative controls were obtained by omitting primary antibody and incubating with 1% normal goat serum/PBS. Samples were imaged by using confocal microscope (Zeiss LSM510).

3.3 RESULTS AND DISCUSSION

3.3.1 Self-assembly and Characterization of Peptide Amphiphiles

Peptide amphiphile molecules used in this study, lauryl-VVAGEGD-K (p-sulphobenzoyl)-S-Am (GAG-PA) and lauryl-VVAGK-Am (K-PA) (Fig.3.1A and 3.1 B), were synthesized by solid phase peptide synthesis method and at physiological pH. Heparin-mimetic PA (GAG-PA) has a net charge of -3, whereas lysine-PA (K-PA) has a net charge of +1 at physiological pH (Figure 3.1). QTOF-LC/MS was used to verify synthesized peptide amphiphiles accordingly and observed mass of PAs as shown in Figure 3.2.

3.3.1.1 Circular Dichroism

Circular Dichroism (CD) analysis was performed to understand the secondary structure of peptide amphiphiles. None of the PAs were found to display an ordered structure by itself, while CD spectra of the PA mixtures revealed a minimum at 220 nm and a maximum at 200 nm, which indicate β-sheet secondary structure in GAG-PA/K-PA combination (Figure 3.3).

3.3.1.2 Zeta Potential Measurement

To determine the charge of the PA solutions and the system, zeta potential measurements were performed. GAG-PA was found to display a negative potential, while K-PA had a positive zeta potential. Self-assembled nanostructures formed upon mixing oppositely charged GAG-PA and K-PA revealed overall negative potentials (Figure 3.3 B).

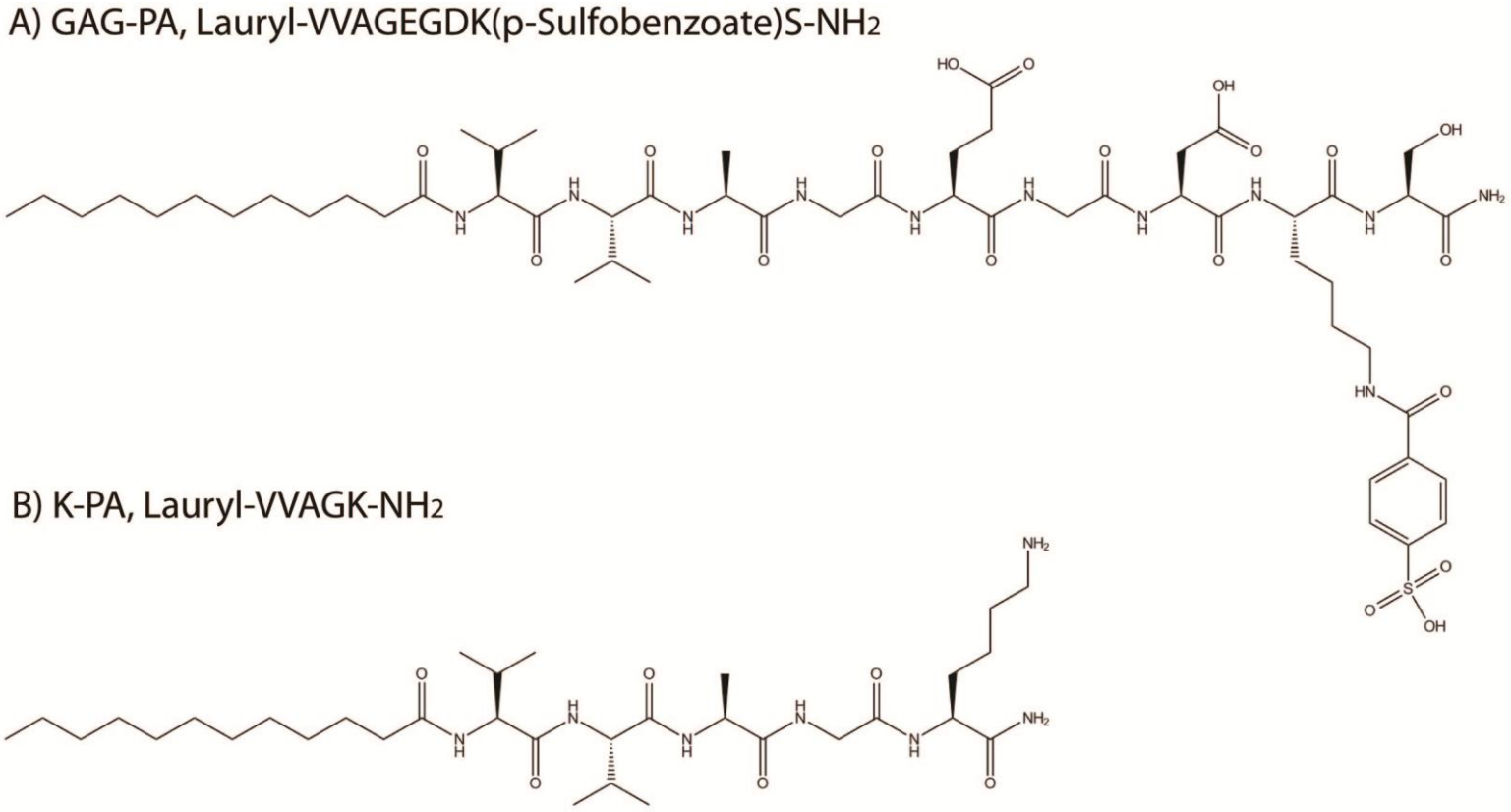

Figure 3.1 Chemical structures of peptide amphiphile nanofibers used in this study. Chemical structure of A) GAG-PA and B) K-PA

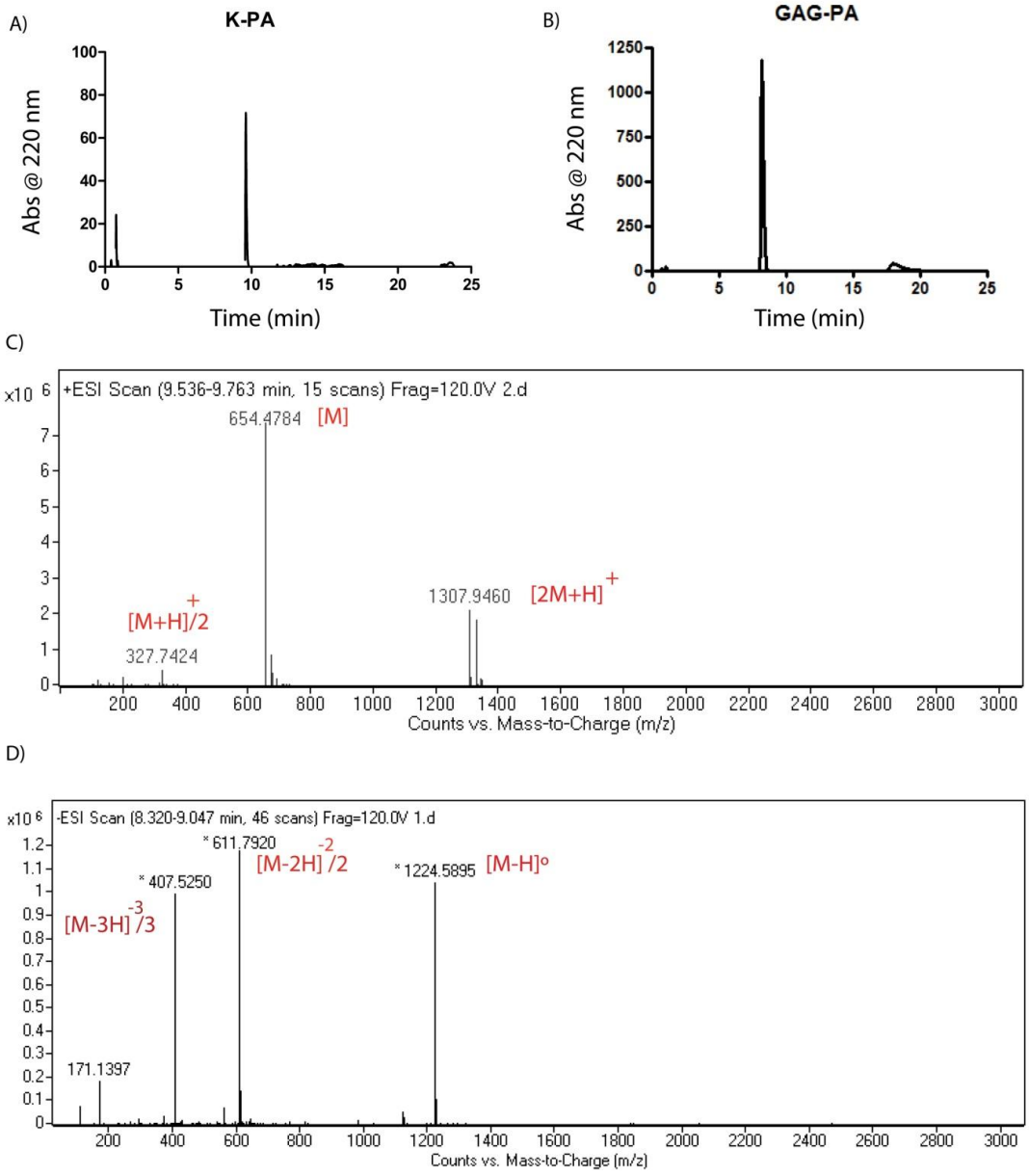

Figure 3.2 LC-MS chromatograms and electrospray ionization mass spectra of K-PA and GAG-PA. Liquid chromatography and Mass spectroscopy analysis of A, C) K-PA and B, D) GAG-PA.

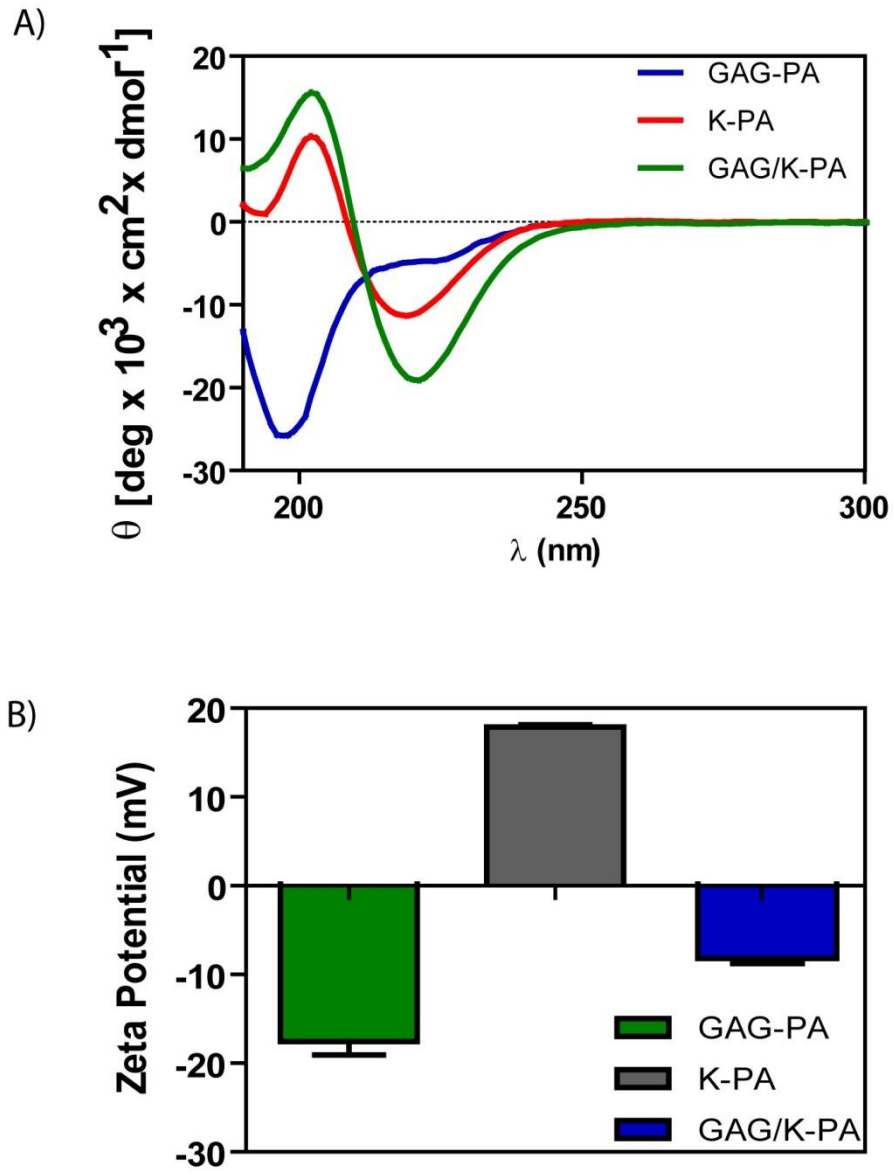

Figure 3.3 Characterization of PA molecules, A) circular dichroism spectra of PA molecules showing the β-sheet structure and B) zeta potentials of individual and mixed PA molecules.

3.3.1.3 SEM

To characterize self-assembly of peptide amphiphiles, nanofiber formation and morphology of the peptide network, SEM imaging was performed. SEM imaging revealed that nanofibers formed upon mixing oppositely charged peptide amphiphiles GAG-PA and K-PA (Figure 3.4). These peptide networks with its porous and nanofibrous morphology, mimic the physical architecture of native ECM of cells.

3.3.1.4 TEM

TEM imaging was also performed to further analyze nanofiber formation and individual nanofibers. TEM images revealed that nanofibers formed upon charge neutralization of oppositely charged peptide amphiphiles. Nanofibers were observed with 6 – 10 nm diameters and lengths up to a few microns (Figure 3.4).

3.3.1.5 Oscillatory Rheology

Rheology experiment was applied to peptide nanofibers in order to analyze gel formation upon mixing oppositely charged peptide amphiphiles. GAG-PA and K-PA mixture showed higher storage moduli (G′) than loss (G″) moduli, which was consistent with the formation of a gel. At 10 mM concentration, the gels exhibited storage moduli between 5-6 kPa and loss moduli between 300-400 Pa (Figure 3.5). Also, at coating concentration, the gel behavior was observed where storage moduli were higher than loss moduli.

3.3.2 Cell Culture on Peptide Nanofibers

To investigate the effect of Heparan sulphate mimicking peptide nanofiber system on cellular behavior, H9C2 myoblasts, derived from rat myocardia, were seeded on peptide coated surfaces or tissue culture plates. For viability analysis, GAG-PA and K-PA molecules were mixed in different molar ratios to display positive, neutral and negative final charges on different wells.

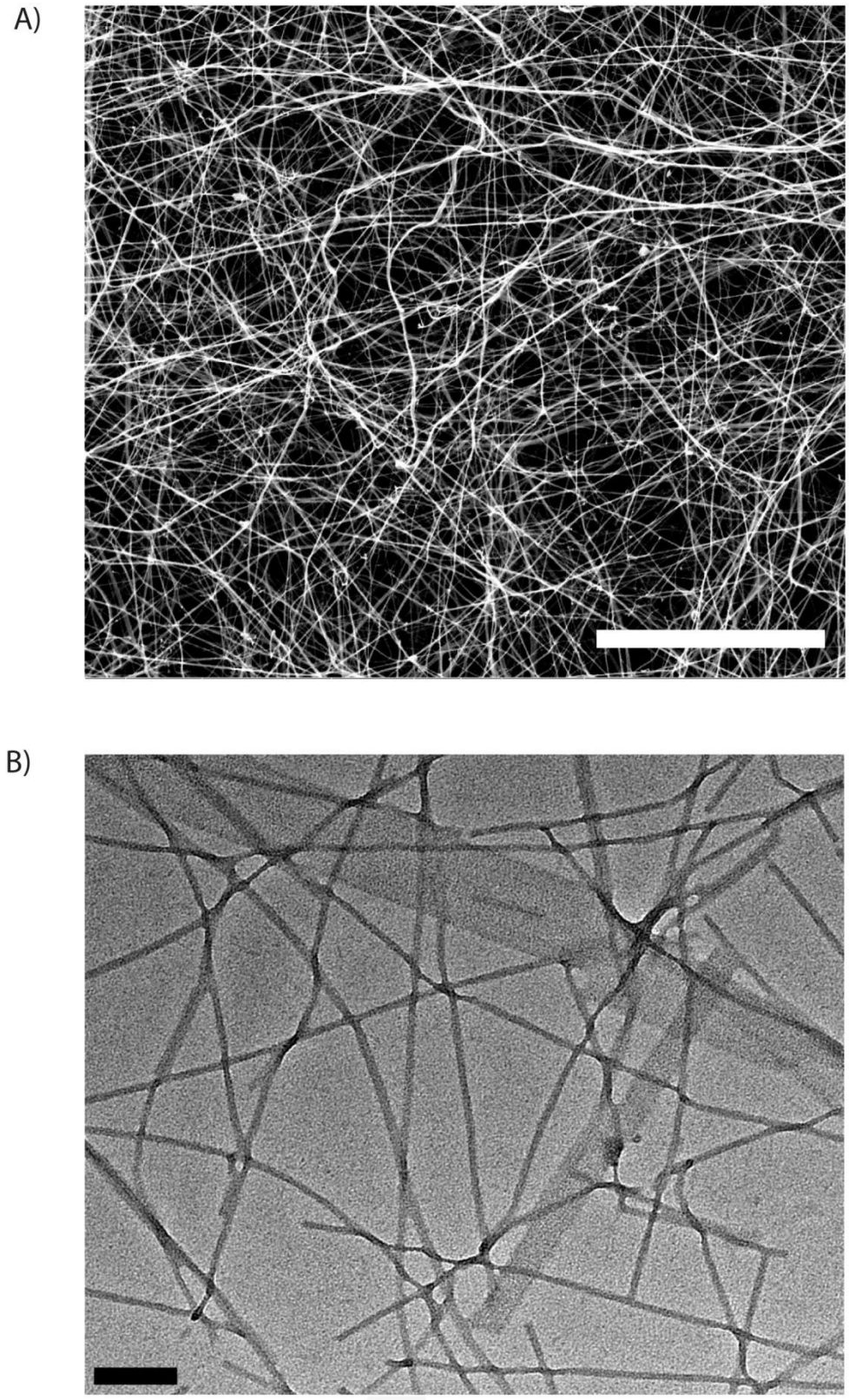

Figure 3.4 Morphological properties of PA molecules analyzed with electron microscopy. A) SEM and B) STEM images revealed the nanofibrous network that mimic the native matrix architecture.

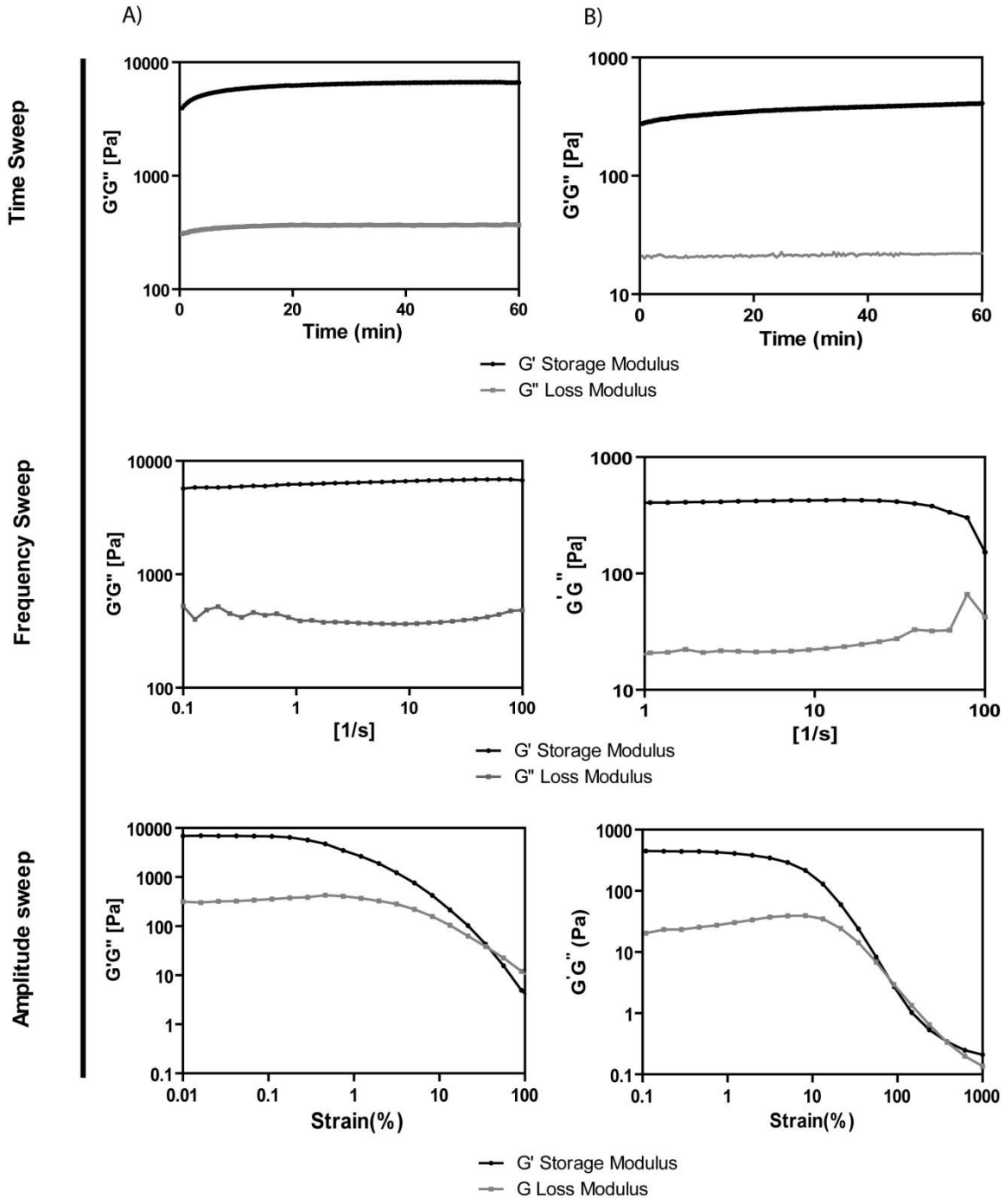

Figure 3.5 Mechanical characterization of peptide amphiphile network at 10 mM and 1 mM concentration by oscillatory rheology. A) Storage and loss moduli of PA system and frequency and strain sweep of 10 mM PA network showing the behavior of gels under varying strain/stress amplitudes and strain, respectively. B) Storage and loss moduli of 1 mM PA mixture showing the gel characteristic of the system and frequency and amplitude sweep tests results**.**

3.3.2.1 Biocompatibiblity of Peptide Nanonetworks

Viability of H9C2 after culturing for 24 h on bioactive peptide nanofibers was analyzed by Alamar Blue assay, and the results showed that peptide nanofiber network did not alter the viability of the cells compared to tissue culture plates and GAG/K-PA system is biocompatible with H9C2 cells at all three charge combinations (Figure 3.6). Cellular morphology was observed under optical microscope which further confirmed the viability results and showed that native cell morphology of H9C2 cells was preserved on PA-coated surfaces. In other experiments, molar ratios of mixtures were adjusted to yield a system with a net negative charge, matching the system utilized in our previous study on peptide-mediated angiogenesis. Proliferation capability of H9C2 cells on peptide nanofibers was analyzed by BrdU assay, and the results showed that the proliferation of cells on PA nanofibers was slightly less than these on tissue culture plates, but the difference between the groups was not statistically significant (Figure 3.6 B).

3.3.2.2 Adhesion of cells

We also investigated the initial adhesion behavior of H9C2 cells on heparan sulphate mimetic bioactive peptide nanofiber networks in the presence of BSA and the translation inhibitor cyclohexamide, which minimize the interference of endogenous proteins with the adhesion process. After 2 h of incubation, both the qualitative observation of Calcein AM staining (Figure 3.7) and quantitative data derived from the staining results demonstrated that cells adhered to the GAG/K-PA coated surface slightly more than TCP.

3.3.2.3 Gene Expression analysis

The H9C2 cells seeded on peptide nanofiber networks were induced to differentiate under reduced serum concentrations, accompanied by daily treatment with 10 nM all-trans-retinoic (RA) acid to stimulate cardiomyocyte differentiation, as RA has been known to affect the differentiation of cardiomyocytes, among other cell types.

A)

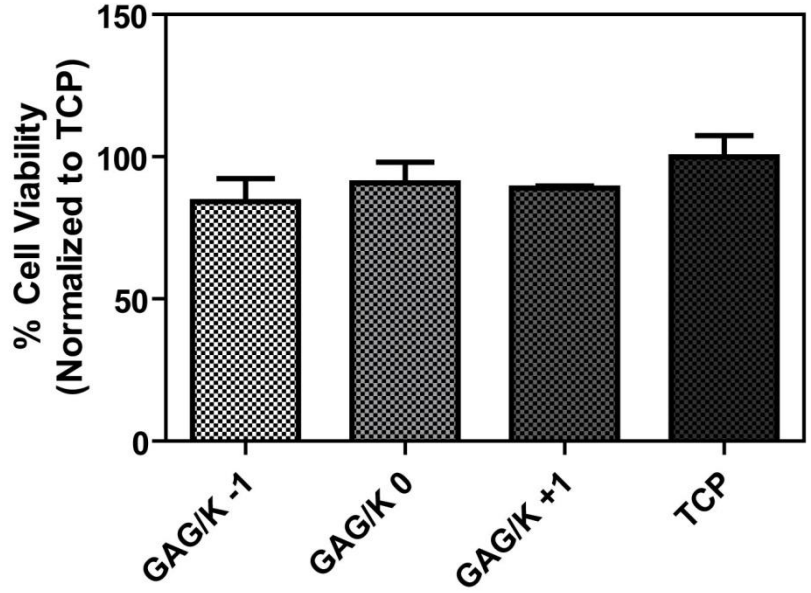

B)

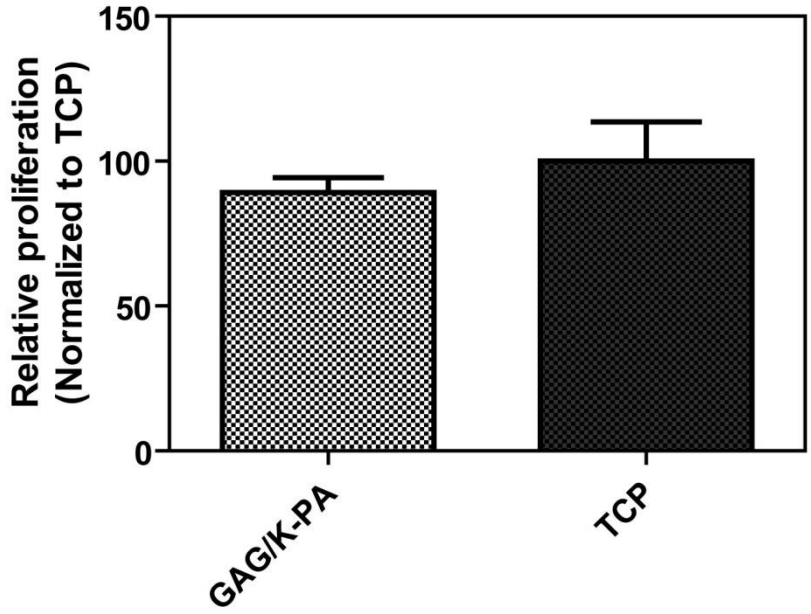

Figure 3.6 A) Viability of H9C2 cells cultured on GAG/K-PA coated surfaces and tissue culture plates at 24 h compared to TCP analyzed by Alamar Blue assay, B) relative proliferation of H9C2 cells normalized to TCP at 72 h, analyzed with BrdU incorporation.

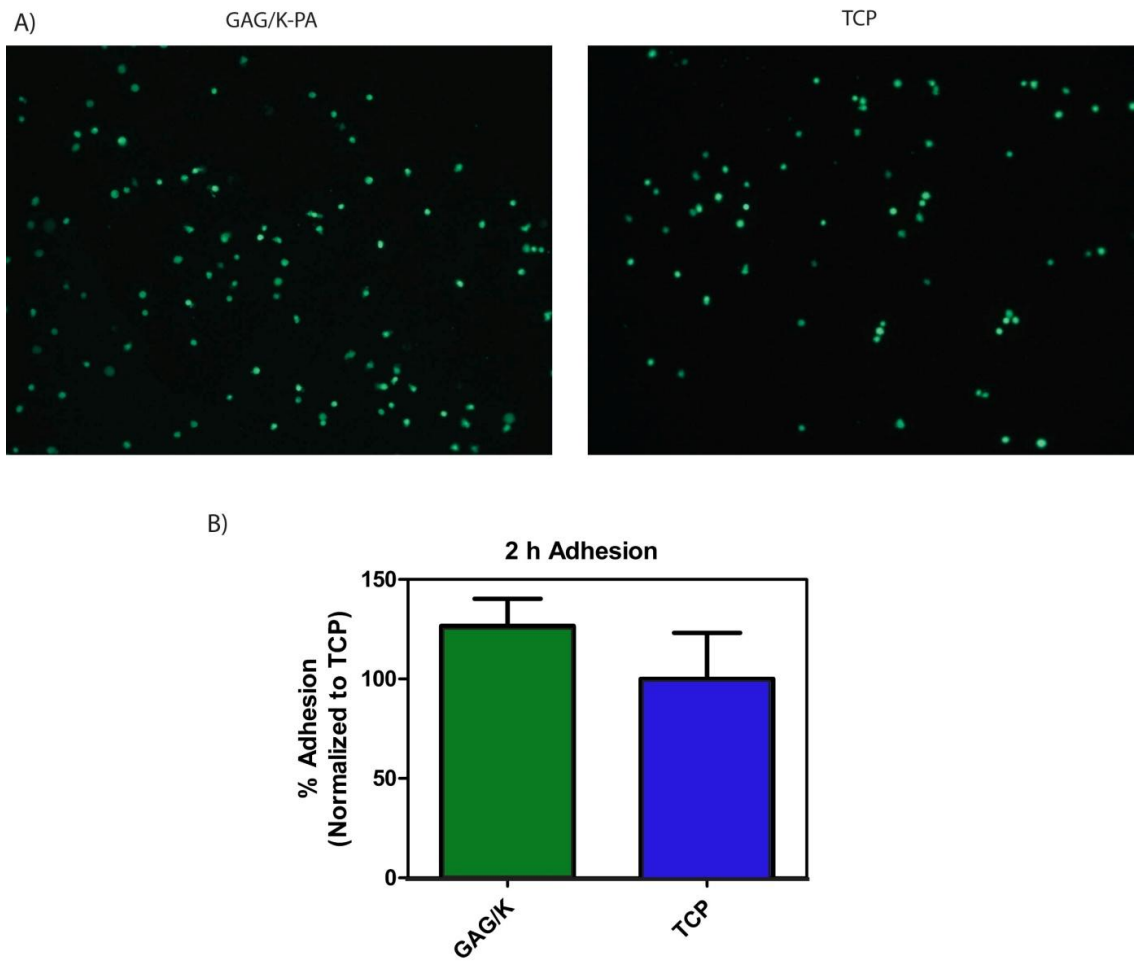

Figure 3.7 Adhesion of H9C2 cells cultured on GAG/K-PA coated surfaces and tissue culture plates. A) Representative Calcein-Am stained fluorescent images of adhered H9C2 cells on GAG/K-PA and TCP at 2 h, B) Relative adhesion of H9C2 cells to PA nanofibers at 2 h with respect to TCP.

The expression of cardiac specific marker ventricular myosin light chain 2 (Mlc-2v) and skeletal myogenic factor myogenin was analyzed by qRT-PCR to investigate the differentiation profiles of H9C2 cells towards the cardiomyocyte phenotype. Cells, which were seeded on bioactive peptide nanofibers and incubated in differentiation medium, showed higher Mlc-2v expression than the cells grown on TCP control at day 7. Culturing GAG/K-PA coated surfaces increased the expression of this cardiomyocyte differentiation marker earlier than the control system (Figure 3.8 A). In addition, there was no increase in the expression of the skeletal muscle marker myogenin when the experimental groups were compared (Figure 3.8 B). These results showed that the heparan sulphate mimetic PA nanofiber system induces cardiomyocyte differentiation of cardiac myoblast cells. When the cells were cultured on GAG/K-PA coating and induced with 2% FBS supplemented with 10 nM RA, their Mlc-2v expression increases *ca* 15 fold, compared to cells which were grown in growth medium. Therefore, from the expression profile we understood that, with additional effect of RA, cells on GAG/K-PA differentiate into cardiomyocyte while in growth medium they keep their myoblastic behavior (Figure 3.8 C).

We also analyzed the expression levels at day 10, but the expression of Mlc-2v was instead lower than that displayed by cells grown on TCP at day 10. This effect can be attributed to delayed differentiation of cells on TCP group compared to the PA nanofiber system.

3.3.2.4 Immunocytochemical Staining

Differentiation of H9C2 cells into cardiomyocytes was also investigated by analyzing the expression of cardiac troponin T (cTnT). The cTnT is an important cardiac-specific protein, and plays a role in cardiac muscle contraction and relaxation. Differentiated cardiomyocytes on heparin mimetic peptide nanofibers exhibited sarcomeric organization, observed through phalloidin staining after cells were cultivated in differentiation medium for 10 days. Also cTnT-positive (differentiated) cells were present on both GAG/K-PA coated surfaces and tissue culture plates (Figure 3.9) while cells incubated in growth medium did not reveal any staining for cTnT (Figure 3.10). SEM images also showed the normal morphology and size of cells incubated in growth medium.

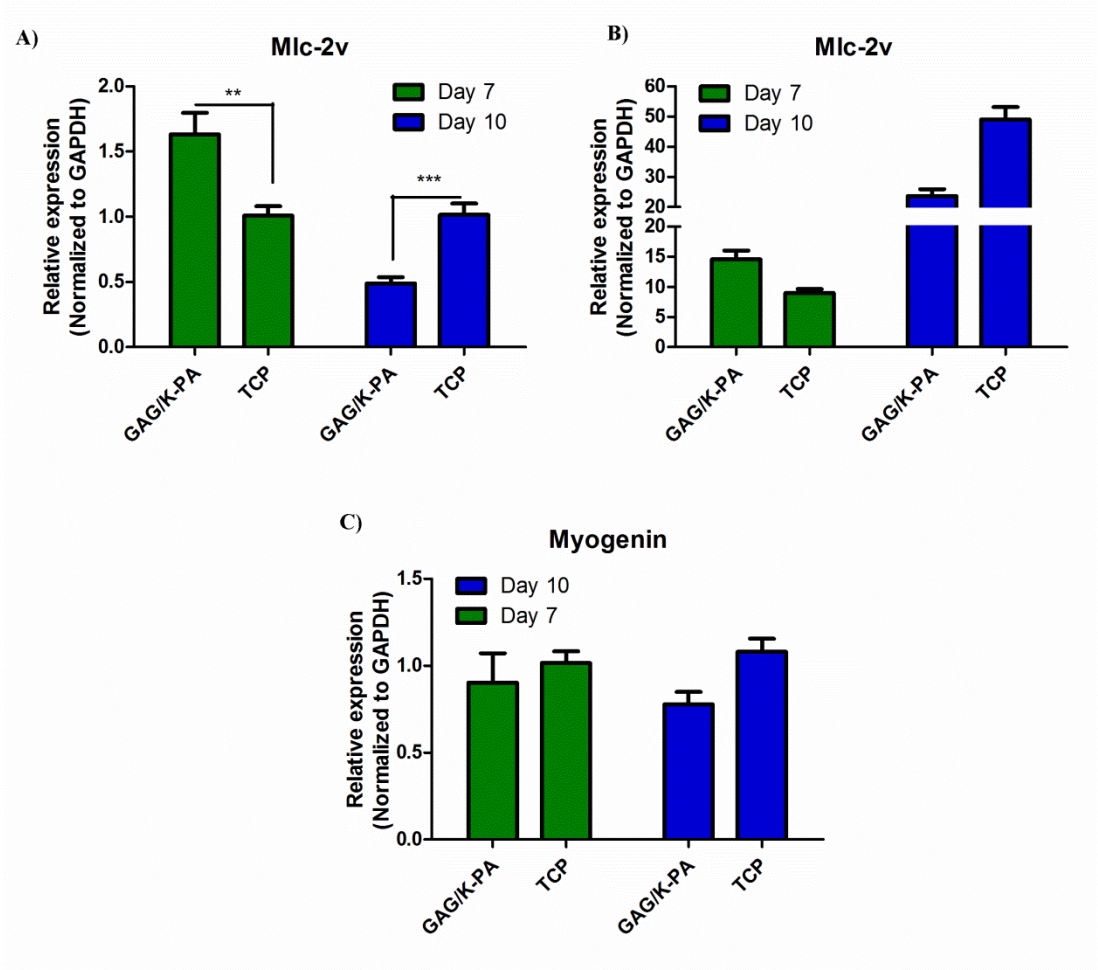

Figure 3.8 Gene expression analysis of Mlc-2v and myogenin. A) qRT-PCR analysis of cardiac differentiation marker, Mlc-2v in H9C2 cells incubated for 7 and 10 days in the presence of 10 nM RA, results were normalized to GAPDH and compared to TCP. B) Expression of Mlc-2v when the results were normalized to GAPDH and compared with Mlc-2v expression in growth medium. PA nanofiber system along with RA increases gene expression *ca.* 15 folds greater than uncoated TCP incubated with GM at day 7 and 20 fold higher at day 10. C) Expression analysis of skeletal muscle marker myogenin compared to TCP in the differentiation medium. $p<0.05$ indicates statistical significance.

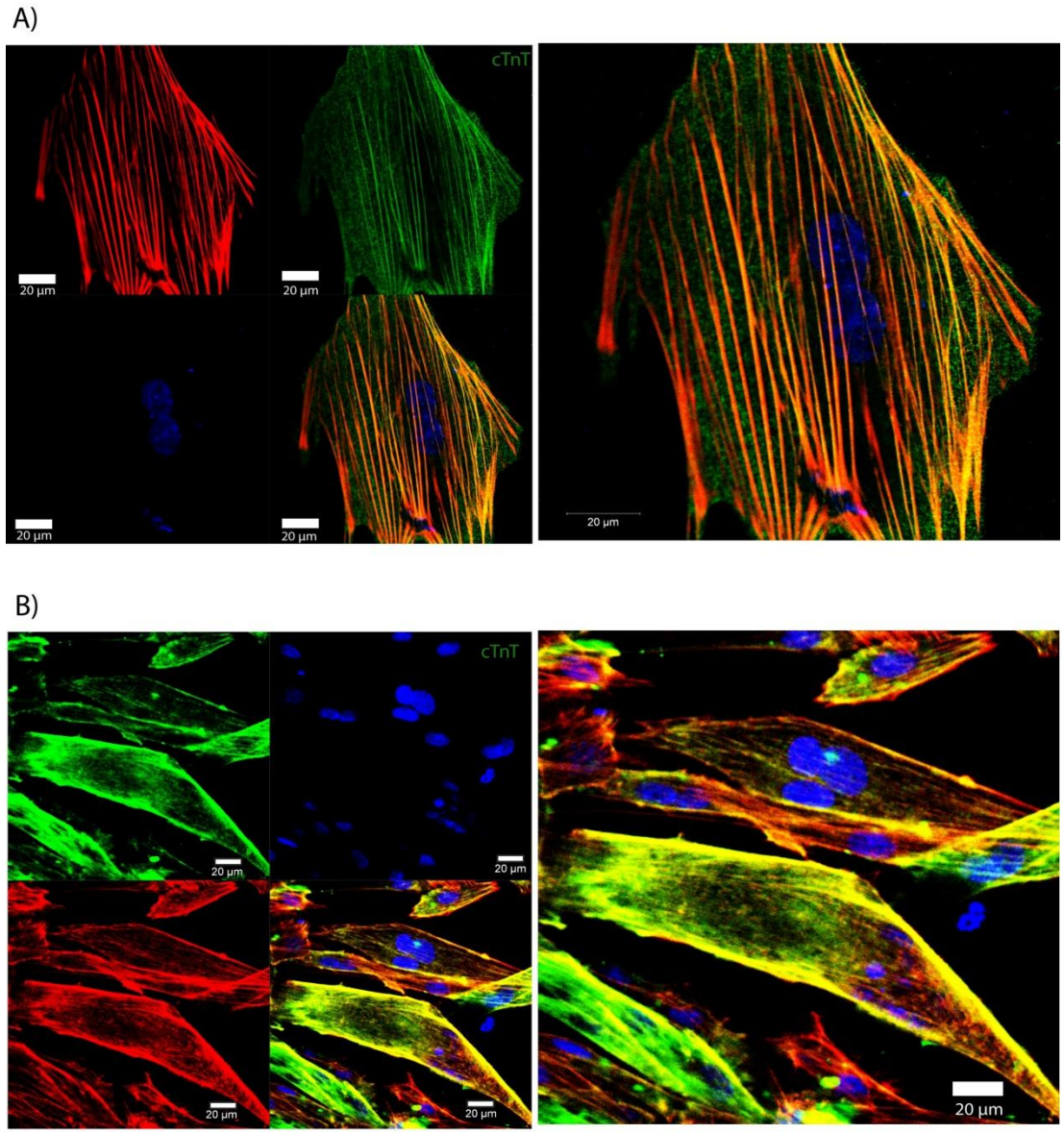

Figure 3.9 Immunocytochemistry staining of cardiac specific protein, cTnT, and cytoskeleton. Confocal images of cTnT staining in H9C2 cells cultured on GAG/K-PA for 10 days, D) Confocal images of cTnT staining in control TCP group. Green: cTnT, red: Actin, blue: nucleus. (Scale bar = 20 µm)

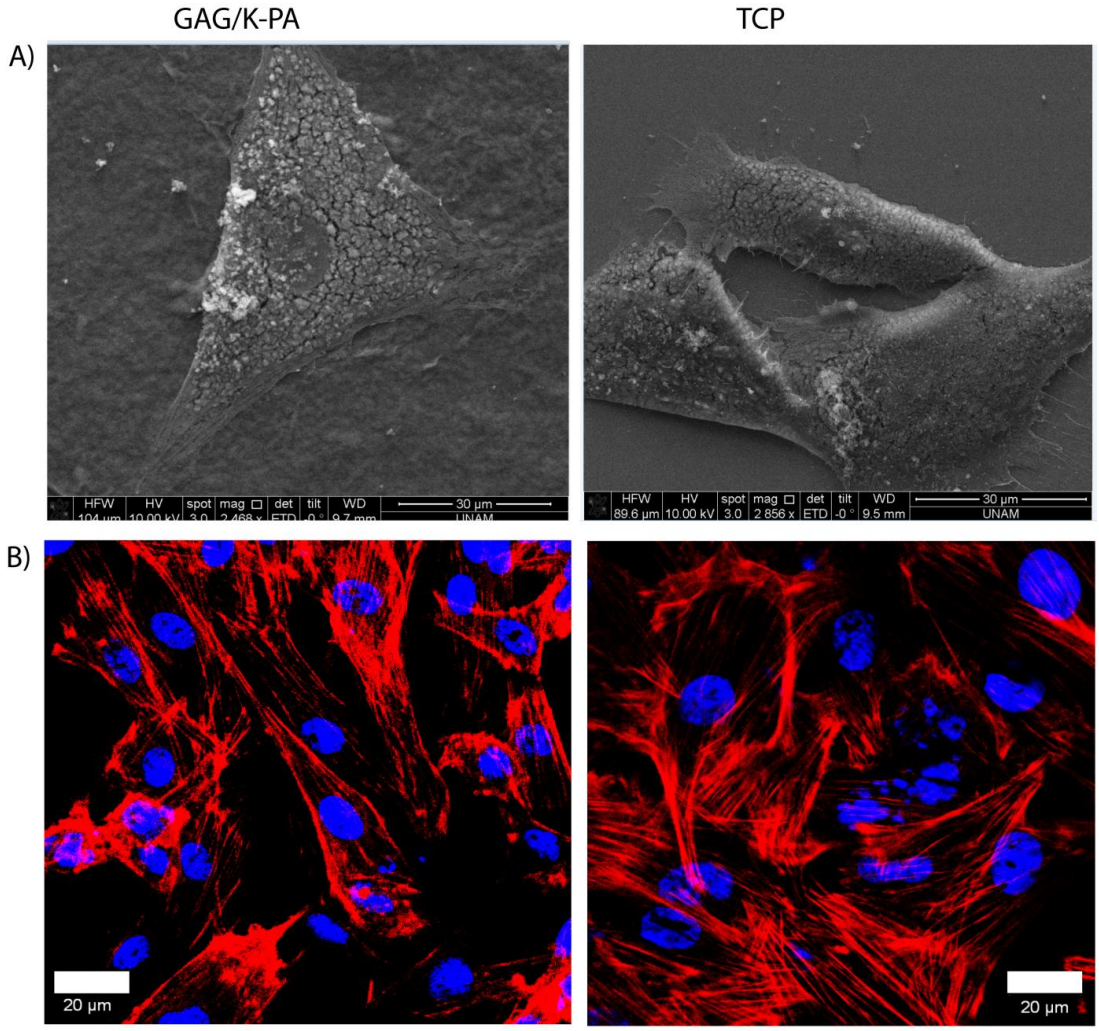

Figure 3.10 Characterization of cellular morphology with SEM imaging and confocal microscopy. A) SEM image of H9C2 cells incubated in 2% FBS supplemented with 10 nM RA for 10 days, B) H9C2 cells incubated in growth medium for 10 days kept their undifferentiated phenotype. Red=Phalloidin, Blue=ToPro staining. (Scale bar = 20 µm)

3.4 CONCLUSION

We aimed to generate a scaffold with both myogenic and angiogenic properties and accomplished this through the design of a peptide based bioactive nanofiber system that possesses carboxyl, hydroxyl and sulfonate groups to mimic the glycosaminoglycan residues found in the myocardium, which play an important role in growth factor binding and angiogenesis. In this way, we generated bioactive and biodegradable scaffolds to repair damaged myocardium and support vascularization after myocardial infarction. Glycosaminoglycan mimetic peptide nanofibers provided a biocompatible microenvironment for myoblast cell growth, spreading and proliferation. Furthermore, our results showed that H9C2 myoblast cells cultured on these nanofibers exhibited differentiation potential towards the cardiomyocyte phenotype and expressed the cardiomyocyte-specific marker ventricular myosine light chain significantly higher than the control group. Furthermore, the differentiation of H9C2 cells into cardiomyocytes was confirmed by the appearance of multinucleated cells that stained positive for cTnT, as well as the absence of the long myotubes, which are characteristic of skeletal muscle cells. The *in vitro* studies suggested that our heparan sulphate-mimetic bioactive and nanofibrous peptide system provides the necessary composition and architecture to support the adhesion, proliferation and cardiomyocyte-oriented differentiation of progenitor cells. In addition, the *in vivo* studies performed by our collaborators proved that our peptide hydrogels could effectively induce angiogenesis in infarct and periinfarct area after myocardial infarction in the rat model. Our results suggest that glycosaminoglycan-mimetic peptide nanofibers show great potential for cardiovascular tissue engineering strategies and offer a promising platform for future clinical applications.

CHAPTER 4.

CONCLUSION AND FUTURE PERSPECTIVES

An ideal myogenic construct should mimic the morphological, physiological and functional properties of the native muscle tissue. Therefore, the development of functional myogenic scaffold systems should take into account both the architecture and differentiation-enhancing capacities of native tissues, in addition to supporting cell adhesion and survival. Self-assembled peptide nanofibers are particularly advantageous in this capacity, as they can provide such an environment due to their versatile and functional structures. A great variety of peptide structures can be designed and synthesized to display desirable structural properties. To demonstrate the versatility of peptide-based nanofibers for regenerative medicine, we developed two different nanofibrous network systems by self-assembly. In the first study, laminin and fibronectin mimetic peptide nanofibers were designed to mimic the composition of the basal lamina of skeletal muscle fibers, which plays important roles in the migration, growth and differentiation of cells. Laminins in the basal lamina enhance the proliferation of myoblasts, stimulate their migration, and lead them to assume the bipolar shape characteristic of fusing cells, while fibronectin promotes the adhesion and migration of cells. To mimic these proteins, we decorated our peptide amphiphiles with IKVAV sequence, derived from the cell binding domain of laminin, and RGD cell adhesion sequence, derived from fibronectin. These functional groups supported the adhesion and viability of cells, as well as their differentiation. Adhesion and viability experiments revealed that laminin-mimetic and fibronectin-mimetic peptide nanofibers provide a biocompatible and adaptive microenvironment for skeletal myoblast cells' adhesion, growth and proliferation. Moreover, morphological observations revealed that cells cultured on these nanofibers fuse with each other and form multinucleated myotubes which were up to 600 μm length. In addition, laminin mimetic nanofibers exhibited enhanced myogenesis and greater expression of myogenic regulatory proteins compared to other groups. Immunological stainings of important skeletal muscle protein also confirmed the differentiation of cells and formation of long, multinucleated myotubes. As a result, this work indicates that our basal lamina mimetic peptide nanofiber system provides a favourable microenvironment for myoblast cells to grow, differentiate and form long myotubes. Due to the injectible characteristics of these nanofibers, they have potential applications in *in vivo* and clinical studies. To achieve this, *in vivo* muscle damage models could be used to inject peptide nanofibers and to evaluate their effect on regeneration of damaged muscle.

Furthermore, these systems could be design as a multifunctional for both regeneration of damaged tissue and delivery and slow release of drugs to the site of injury. If such system is combined with oligonucleotide therapy, it could be promising approach for people with muscle degenerative diseases such as muscular dystrophy.

In the second study, we developed glycosaminoglycan-mimetic peptide nanofibers to mimic the chemical groups on native glycosaminoglycans in the myocardial ECM, which are essential for the maintanence and vascularization of cardiac muscle. It is known that these glycosaminoglycans can interact with various growth factors and present them to the cell surface receptors to induce angiogenesis, which is important to secure the functioning of myocardium after infarction. Carboxyl, hydroxyl and sulfonate groups, which are abundant on the heparan sulphate glycosaminoglycans, were incorporated into the structure of our peptide amphiphiles to develop a peptide nanofiber scaffold that can induce cardiomyocyte differentiation and neovascularization for the regeneration of cardiovascular tissue after myocardial infarction. *In vitro* experiments revealed that the microenvironment provided by glycosaminoglycan-mimetic peptide nanofibers is biocompatible and conductive to the growth and proliferation of cardiac myoblast cells. Both gene expression analyses and immunocytochemical stainings supported our findings that myoblast cells were differentiated into the cardiomyocyte profile on our peptide amphiphile hydrogels. In the *in vivo* part of this study, glycosaminoglycan-mimetic peptide nanofibers were shown to promote neovascularisation by recruiting vascular cells and activating their proliferation and maturation. Enhanced neovascularization was found to eventually improve cardiac function after MI in rats. Consequently, both *in vitro* and *in vivo* studies indicate that glycosaminoglycan-mimetic peptide nanofibers offer great promise for clinical application and could be used directly or in combination with growth factors to rescue ischemic tissue after myocardial infarction.

Overall, these works offer a general strategy for the development of functional myogenic and angiogenic platforms by the bottom-up design and synthesis of molecules that self-assemble into well ordered nanostructures that can be functionalized depending on the needs at hand and the application of interest. To fully evaluate their efficiency and future succes of our strategy, *in vivo* studies may be performed and later translated into clinical studies.

REFERENCES

1 Stern-Straeter, J., Riedel, F., Bran, G., Hormann, K. & Goessler, U. R. Advances in skeletal muscle tissue engineering. *In Vivo* **21**, 435-444 (2007).

2 Matsakas, A. & Patel, K. Skeletal muscle fibre plasticity in response to selected environmental and physiological stimuli. *Histol Histopathol* **24**, 611-629 (2009).

3 Otto, A., Collins-Hooper, H. & Patel, K. The origin, molecular regulation and therapeutic potential of myogenic stem cell populations. *J Anat* **215**, 477-497, doi:DOI 10.1111/j.1469-7580.2009.01138.x (2009).

4 Dhawan, J. & Rando, T. A. Stem cells in postnatal myogenesis: molecular mechanisms of satellite cell quiescence, activation and replenishment. *Trends Cell Biol* **15**, 666-673, doi:DOI 10.1016/j.tcb.2005.10.007 (2005).

5 Tabebordbar, M., Wang, E. T. & Wagers, A. J. Skeletal Muscle Degenerative Diseases and Strategies for Therapeutic Muscle Repair. *Annual Review of Pathology: Mechanisms of Disease, Vol 8* **8**, 441-475, doi:DOI 10.1146/annurev-pathol-011811-132450 (2013).

6 Wagers, A. J. & Conboy, I. M. Cellular and molecular signatures of muscle regeneration: Current concepts and controversies in adult myogenesis. *Cell* **122**, 659-667, doi:DOI 10.1016/j.cell.2005.08.021 (2005).

7 Kurek, J. B., Bower, J. J., White, J. D., Muldoon, C. M. & Austin, L. Leukaemia inhibitory factor and other cytokines as factors influencing regeneration of skeletal muscle. *Basic Appl Myol* **8**, 347-360 (1998).

8 Miller, J. H., Lewontin, R. C., Gelbart, W. M. & Griffiths, A. J. F. *Molecular Cell Biology 4th Edition & Cd-rom*. (Macmillan Higher Education, 2002).

9 Choi, Y. M. & Kim, B. C. Muscle fiber characteristics, myofibrillar protein isoforms, and meat quality. *Livest Sci* **122**, 105-118, doi:DOI 10.1016/j.livsci.2008.08.015 (2009).

10 Craig, R. & Woodhead, J. L. Structure and function of myosin filaments. *Current Opinion in Structural Biology* **16**, 204-212, doi:http://dx.doi.org/10.1016/j.sbi.2006.03.006 (2006).

11 Frantz, C., Stewart, K. M. & Weaver, V. M. The extracellular matrix at a glance. *Journal of Cell Science* **123**, 4195-4200, doi:Doi 10.1242/Jcs.023820 (2010).

12 Velleman, S. G., Shin, J., Li, X. H. & Song, Y. Review: The skeletal muscle extracellular matrix: Possible roles in the regulation of muscle development and growth. *Canadian Journal of Animal Science* **92**, 1-10, doi:Doi 10.4141/Cjas2011-098 (2012).

13 Rozario, T. & DeSimone, D. W. The extracellular matrix in development and morphogenesis: A dynamic view. *Developmental Biology* **341**, 126-140, doi:DOI 10.1016/j.ydbio.2009.10.026 (2010).

14 Sanes, J. R. The basement membrane/basal lamina of skeletal muscle. *Journal of Biological Chemistry* **278**, 12601-12604, doi:DOI 10.1074/jbc.R200027200 (2003).

15 Campbell, K. P. & Stull, J. T. Skeletal muscle basement membrane-sarcolemma-cytoskeleton interaction minireview series. *Journal of Biological Chemistry* **278**, 12599-12600, doi:DOI 10.1074/jbc.R300005200 (2003).

16 Hay, E. D. *Cell Biology of Extracellular Matrix*. (Springer US, 1991).

17 Gillies, A. R. & Lieber, R. L. Structure and Function of the Skeletal Muscle Extracellular Matrix. *Muscle & Nerve* **44**, 318-331, doi:Doi 10.1002/Mus.22094 (2011).
18 Ervasti, J. M. & Campbell, K. P. A Role for the Dystrophin-Glycoprotein Complex as a Transmembrane Linker between Laminin and Actin. *J Cell Biol* **122**, 809-823, doi:DOI 10.1083/jcb.122.4.809 (1993).
19 Rao, C. N., Margulies, I. M. K. & Liotta, L. A. Binding Domain for Laminin on Type-Iv Collagen. *Biochem Bioph Res Co* **128**, 45-52, doi:Doi 10.1016/0006-291x(85)91642-0 (1985).
20 Vachon, P. H., Loechel, F., Xu, H., Wewer, U. M. & Engvall, E. Merosin and laminin in myogenesis; Specific requirement for merosin in myotube stability and survival. *J Cell Biol* **134**, 1483-1497, doi:DOI 10.1083/jcb.134.6.1483 (1996).
21 Grounds, M. D., Sorokin, L. & White, J. Strength at the extracellular matrix-muscle interface. *Scand J Med Sci Spor* **15**, 381-391, doi:DOI 10.1111/j.1600-0838.2005.00467.x (2005).
22 Messina, G. *et al.* Skeletal Muscle Differentiation of Embryonic Mesoangioblasts Requires Pax3 Activity. *Stem Cells* **27**, 157-164, doi:DOI 10.1634/stemcells.2008-0503 (2009).
23 Cossu, G., Tajbakhsh, S. & Buckingham, M. How is myogenesis initiated in the embryo? *Trends Genet* **12**, 218-223, doi:Doi 10.1016/0168-9525(96)10025-1 (1996).
24 Cornelison, D. D. W., Filla, M. S., Stanley, H. M., Rapraeger, A. C. & Olwin, B. B. Syndecan-3 and syndecan-4 specifically mark skeletal muscle satellite cells and are implicated in satellite cell maintenance and muscle regeneration. *Developmental Biology* **239**, 79-94, doi:DOI 10.1006/dbio.2001.0416 (2001).
25 Brzoska, E., Ciemerych, M. A., Przewozniak, M. & Zimowska, M. Regulation of Muscle Stem Cells Activation: The Role of Growth Factors and Extracellular Matrix. *Vitam Horm* **87**, 239-276, doi:Doi 10.1016/B978-0-12-386015-6.00031-7 (2011).
26 Taipale, J. & KeskiOja, J. Growth factors in the extracellular matrix. *Faseb J* **11**, 51-59 (1997).
27 Christov, C. *et al.* Muscle satellite cells and endothelial cells: Close neighbors and privileged partners. *Mol Biol Cell* **18**, 1397-1409, doi:DOI 10.1091/mbc.E06-08-0693 (2007).
28 Tidball, J. G. Inflammatory Cell Response to Acute Muscle Injury. *Med Sci Sport Exer* **27**, 1022-1032, doi:Doi 10.1249/00005768-199507000-00011 (1995).
29 Beauchamp, J. R. *et al.* Expression of CD34 and Myf5 defines the majority of quiescent adult skeletal muscle satellite cells. *J Cell Biol* **151**, 1221-1233, doi:DOI 10.1083/jcb.151.6.1221 (2000).
30 Zammit, P. S. *et al.* Muscle satellite cells adopt divergent fates: a mechanism for self-renewal? *J Cell Biol* **166**, 347-357, doi:DOI 10.1083/jcb.200312007 (2004).
31 Peault, B. *et al.* Stem and progenitor cells in skeletal muscle development, maintenance, and therapy. *Mol Ther* **15**, 867-877, doi:DOI 10.1038/mt.sj.6300145 (2007).
32 Longo, U. G. *et al.* Tissue Engineered Strategies for Skeletal Muscle Injury. *Stem Cells Int*, doi:Unsp 175038
Doi 10.1155/2012/175038 (2012).

33 Husmann, I., Soulet, L., Gautron, J., Martelly, I. & Barritault, D. Growth factors in skeletal muscle regeneration. *Cytokine & Growth Factor Reviews* **7**, 249-258, doi:http://dx.doi.org/10.1016/S1359-6101(96)00029-9 (1996).
34 Kasemkijwattana, C. *et al.* Use of growth factors to improve muscle healing after strain injury. *Clin Orthop Relat R*, 272-285 (2000).
35 Menetrey, J. *et al.* Growth factors improve muscle healing in vivo. *J Bone Joint Surg Br* **82B**, 131-137, doi:Doi 10.1302/0301-620x.82b1.8954 (2000).
36 Sato, M., Ito, A., Kawabe, Y., Nagamori, E. & Kamihira, M. Enhanced contractile force generation by artificial skeletal muscle tissues using IGF-I gene-engineered myoblast cells. *J Biosci Bioeng* **112**, 273-278, doi:DOI 10.1016/j.jbiosc.2011.05.007 (2011).
37 Quintero, A. J., Wright, V. J., Fu, F. H. & Huard, J. Stem Cells for the Treatment of Skeletal Muscle Injury. *Clin Sport Med* **28**, 1-+, doi:DOI 10.1016/j.csm.2008.08.009 (2009).
38 Anitua, E. *et al.* New insights into and novel applications for platelet-rich fibrin therapies. *Trends in Biotechnology* **24**, 227-234, doi:DOI 10.1016/j.tibtech.2006.02.010 (2006).
39 Wright-Carpenter, T. *et al.* Treatment of muscle injuries by local administration of autologous conditioned serum: A pilot study on sportsmen with muscle strains. *Int J Sports Med* **25**, 588-593, doi:DOI 10.1055/s-2004-821304 (2004).
40 Saxena, A. K., Marler, J., Benvenuto, M., Willital, G. H. & Vacanti, J. P. Skeletal muscle tissue engineering using isolated myoblasts on synthetic biodegradable polymers: Preliminary studies. *Tissue Eng* **5**, 525-531, doi:DOI 10.1089/ten.1999.5.525 (1999).
41 Drury, J. L. & Mooney, D. J. Hydrogels for tissue engineering: scaffold design variables and applications. *Biomaterials* **24**, 4337-4351, doi:Doi 10.1016/S0142-9612(03)00340-5 (2003).
42 Shimizu, K., Fujita, H. & Nagamori, E. Alignment of Skeletal Muscle Myoblasts and Myotubes Using Linear Micropatterned Surfaces Ground With Abrasives. *Biotechnology and Bioengineering* **103**, 631-638, doi:Doi 10.1002/Bit.22268 (2009).
43 Kroehne, V. *et al.* Use of a novel collagen matrix with oriented pore structure for muscle cell differentiation in cell culture and in grafts. *J Cell Mol Med* **12**, 1640-1648, doi:DOI 10.1111/j.1582-4934.2008.00238.x (2008).
44 Beier, J. P. *et al.* Tissue engineering of injectable muscle: Three-dimensional myoblast-fibrin injection in the syngeneic rat animal model. *Plast Reconstr Surg* **118**, 1113-1121, doi:DOI 10.1097/01.prs.0000221007.97115.1d (2006).
45 Matsumoto, T. *et al.* Three-Dimensional Cell and Tissue Patterning in a Strained Fibrin Gel System. *Plos One* **2**, doi:Artn E1211
Doi 10.1371/Journal.Pone.0001211 (2007).
46 Khademhosseini, A. *et al.* Co-culture of human embryonic stem cells with murine embryonic fibroblasts on microwell-patterned substrates. *Biomaterials* **27**, 5968-5977, doi:DOI 10.1016/j.biomaterials.2006.06.035 (2006).
47 Ma, J. Q., Holden, K., Zhu, J. H., Pan, H. Y. & Li, Y. The Application of Three-Dimensional Collagen-Scaffolds Seeded with Myoblasts to Repair Skeletal Muscle Defects. *J Biomed Biotechnol*, doi:Artn 812135
Doi 10.1155/2011/812135 (2011).

48 Page, R. L. *et al.* Restoration of Skeletal Muscle Defects with Adult Human Cells Delivered on Fibrin Microthreads. *Tissue Engineering Part A* **17**, 2629-2640, doi:DOI 10.1089/ten.tea.2011.0024 (2011).
49 Borschel, G. H., Dennis, R. G. & Kuzon, W. M. Contractile skeletal muscle tissue-engineered on an acellular scaffold. *Plast Reconstr Surg* **113**, 595-602, doi:Doi 10.1097/01.Prs.0000101064.62289.2f (2004).
50 Sicari, B. M. *et al.* An Acellular Biologic Scaffold Promotes Skeletal Muscle Formation in Mice and Humans with Volumetric Muscle Loss. *Sci Transl Med* **6**, doi:ARTN 234ra58
DOI 10.1126/scitranslmed.3008085 (2014).
51 Ricotti, L. *et al.* Proliferation and skeletal myotube formation capability of C2C12 and H9c2 cells on isotropic and anisotropic electrospun nanofibrous PHB scaffolds. *Biomedical Materials* **7**, doi:Artn 035010
Doi 10.1088/1748-6041/7/3/035010 (2012).
52 Wang, P. Y., Thissen, H. & Tsai, W. B. The roles of RGD and grooved topography in the adhesion, morphology, and differentiation of C2C12 skeletal myoblasts. *Biotechnology and Bioengineering* **109**, 2104-2115, doi:Doi 10.1002/Bit.24452 (2012).
53 Jugdutt, B. I. Remodeling of the myocardium and potential targets in the collagen degradation and synthesis pathways. *Curr Drug Targets Cardiovasc Haematol Disord* **3**, 1-30 (2003).
54 Bennett, P. M., Maggs, A. M., Baines, A. J. & Pinder, J. C. The transitional junction: A new functional subcellular domain at the intercalated disc. *Mol Biol Cell* **17**, 2091-2100, doi:DOI 10.1091/mbc.E05-12-1109 (2006).
55 Gutstein, D. E., Liu, F. Y., Meyers, M. B., Choo, A. & Fishman, G. I. The organization of adherens junctions and desmosomes at the cardiac intercalated disc is independent of gap junctions. *Journal of Cell Science* **116**, 875-885, doi:Doi 10.1242/Jcs.00258 (2003).
56 Bowers, S. L. K., Banerjee, I. & Baudino, T. A. The extracellular matrix: At the center of it all. *J Mol Cell Cardiol* **48**, 474-482, doi:DOI 10.1016/j.yjmcc.2009.08.024 (2010).
57 Fomovsky, G. M., Thomopoulos, S. & Holmes, J. W. Contribution of extracellular matrix to the mechanical properties of the heart. *J Mol Cell Cardiol* **48**, 490-496, doi:DOI 10.1016/j.yjmcc.2009.08.003 (2010).
58 Corda, S., Samuel, J. L. & Rappaport, L. Extracellular matrix and growth factors during heart growth. *Heart Fail Rev* **5**, 119-130, doi:10.1023/A:1009806403194 (2000).
59 Gandhi, N. S. & Mancera, R. L. The Structure of Glycosaminoglycans and their Interactions with Proteins. *Chem Biol Drug Des* **72**, 455-482, doi:DOI 10.1111/j.1747-0285.2008.00741.x (2008).
60 Iozzo, R. V. & San Antonio, J. D. Heparan sulfate proteoglycans: heavy hitters in the angiogenesis arena. *J Clin Invest* **108**, 349-355, doi:Doi 10.1172/Jci13738 (2001).
61 Holt, C. E. & Dickson, B. J. Sugar codes for axons? *Neuron* **46**, 169-172, doi:DOI 10.1016/j.neuron.2005.03.021 (2005).
62 Liu, D. F., Shriver, Z., Gi, Y. W., Venkataraman, G. & Sasisekharan, R. Dynamic regulation of tumor growth and metastasis by heparan sulfate glycosaminoglycans. *Semin Thromb Hemost* **28**, 67-78, doi:Doi 10.1055/S-2002-20565 (2002).

63 Casu, B., Guerrini, M. & Torri, G. Structural and conformational aspects of the anticoagulant and anti-thrombotic activity of heparin and dermatan sulfate. *Curr Pharm Des* **10**, 939-949 (2004).
64 Lockhart, M., Wirrig, E., Phelps, A. & Wessels, A. Extracellular matrix and heart development. *Birth Defects Res A Clin Mol Teratol* **91**, 535-550, doi:10.1002/bdra.20810 (2011).
65 Segers, V. F. M. & Lee, R. T. Stem-cell therapy for cardiac disease. *Nature* **451**, 937-942, doi:Doi 10.1038/Nature06800 (2008).
66 Laflamme, M. A. & Murry, C. E. Regenerating the heart. *Nature Biotechnology* **23**, 845-856, doi:Doi 10.1038/Nbt1117 (2005).
67 Steinhauser, M. L. & Lee, R. T. Regeneration of the heart. *Embo Mol Med* **3**, 701-712, doi:DOI 10.1002/emmm.201100175 (2011).
68 Beltrami, A. P. *et al.* Evidence that human cardiac myocytes divide after myocardial infarction. *New Engl J Med* **344**, 1750-1757, doi:Doi 10.1056/Nejm200106073442303 (2001).
69 Beltrami, A. P. *et al.* Adult cardiac stem cells are multipotent and support myocardial regeneration. *Cell* **114**, 763-776, doi:Doi 10.1016/S0092-8674(03)00687-1 (2003).
70 Mercola, M., Ruiz-Lozano, P. & Schneider, M. D. Cardiac muscle regeneration: lessons from development. *Gene Dev* **25**, 299-309, doi:Doi 10.1101/Gad.2018411 (2011).
71 Strauer, B. E. *et al.* Myocardial regeneration after intracoronary transplantation of human autologous stem cells following acute myocardial infarction. *Dtsch med Wochenschr* **126**, 932-938, doi:10.1055/s-2001-16579-2 (2001).
72 Stamm, C. *et al.* Autologous bone-marrow stem-cell transplantation for myocardial regeneration. *The Lancet* **361**, 45-46, doi:http://dx.doi.org/10.1016/S0140-6736(03)12110-1 (2003).
73 Jackson, K. A. *et al.* Regeneration of ischemic cardiac muscle and vascular endothelium by adult stem cells. *J Clin Invest* **107**, 1395-1402, doi:Doi 10.1172/Jci12150 (2001).
74 Leri, A., Kajstura, J. & Anversa, P. Cardiac stem cells and mechanisms of myocardial regeneration. *Physiol Rev* **85**, 1373-1416, doi:DOI 10.1152/physrev.00013.2005 (2005).
75 Mollmann, H. *et al.* Haematopoietic stem cells do not contribute to myocardial repair after myocardial infarction. *Circulation* **112**, U282-U282 (2005).
76 Stuckey, D. J. *et al.* Iron particles for noninvasive monitoring of bone marrow stromal cell engraftment into, and isolation of viable engrafted donor cells from, the heart. *Stem Cells* **24**, 1968-1975, doi:DOI 10.1634/stemcells.2006-0074 (2006).
77 Wollert, K. C. & Drexler, H. Clinical applications of stem cells for the heart. *Circ Res* **96**, 151-163, doi:Doi 10.1161/01.Res.0000155333.69009.63 (2005).
78 Dimmeler, S., Zeiher, A. M. & Schneider, M. D. Unchain my heart: the scientific foundations of cardiac repair. *J Clin Invest* **115**, 572-583, doi:Doi 10.1172/Jci200524283 (2005).
79 Strauer, B. E. *et al.* Repair of infarcted myocardium by autologous intracoronary mononuclear bone marrow cell transplantation in humans. *Circulation* **106**, 1913-1918, doi:Doi 10.1161/01.Cir.0000034046.87607.1c (2002).

80 Meyer, G. P. *et al.* Intracoronary bone marrow cell transfer after myocardial infarction - Eighteen months' follow-up data from the randomized, controlled BOOST (BOne marrOw transfer to enhance ST-elevation infarct regeneration) trial. *Circulation* **113**, 1287-1294, doi:Doi 10.1161/Circulationaha.105.575118 (2006).

81 Oh, H. *et al.* Cardiac muscle plasticity in adult and embryo by heart-derived progenitor cells. *Cardiac Engineering: From Genes and Cells to Structure and Function* **1015**, 182-189, doi:DOI 10.1196/annals.1302.015 (2004).

82 Dawn, B. *et al.* Cardiac stem cells delivered intravascularly traverse the vessel barrier, regenerate infarcted myocardium, and improve cardiac function. *Proceedings of the National Academy of Sciences of the United States of America* **102**, 3766-3771, doi:DOI 10.1073/pnas.0405957102 (2005).

83 Oh, H. *et al.* Cardiac progenitor cells from adult myocardium: Homing, differentiation, and fusion after infarction. *Proceedings of the National Academy of Sciences of the United States of America* **100**, 12313-12318, doi:DOI 10.1073/pnas.2132126100 (2003).

84 Leor, J., Amsalem, Y. & Cohen, S. Cells, scaffolds, and molecules for myocardial tissue engineering. *Pharmacol Therapeut* **105**, 151-163, doi:DOI 10.1016/j.pharmthera.2004.10.003 (2005).

85 Chiu, L. L. Y., Iyer, R. K., Reis, L. A., Nunes, S. S. & Radisic, M. Cardiac tissue engineering: current state and perspectives. *Front Biosci-Landmrk* **17**, 1533-1550, doi:Doi 10.2741/4002 (2012).

86 Zhang, D. H. *et al.* Tissue-engineered cardiac patch for advanced functional maturation of human ESC-derived cardiomyocytes. *Biomaterials* **34**, 5813-5820, doi:DOI 10.1016/j.biomaterials.2013.04.026 (2013).

87 Zimmermann, W. H., Melnychenko, I. & Eschenhagen, T. Engineered heart tissue for regeneration of diseased hearts. *Biomaterials* **25**, 1639-1647, doi:Doi 10.1016/S0142-9612(03)00521-0 (2004).

88 Dar, A., Shachar, M., Leor, J. & Cohen, S. Cardiac tissue engineering - Optimization of cardiac cell seeding and distribution in 3D porous alginate scaffolds. *Biotechnology and Bioengineering* **80**, 305-312, doi:Doi 10.1002/Bit.10372 (2002).

89 Patel, Z. S. & Mikos, A. G. Angiogenesis with biomaterial-based drug- and cell-delivery systems. *J Biomat Sci-Polym E* **15**, 701-726, doi:Doi 10.1163/156856204774196117 (2004).

90 Iyer, R. K., Chiu, L. L. Y., Reis, L. A. & Radisic, M. Engineered cardiac tissues. *Curr Opin Biotech* **22**, 706-714, doi:DOI 10.1016/j.copbio.2011.04.004 (2011).

91 Xiang, Z., Liao, R. L., Kelly, M. S. & Spector, M. Collagen-GAG scaffolds grafted onto myocardial infarcts in a rat model: A delivery vehicle for mesenchymal stem cells. *Tissue Eng* **12**, 2467-2478, doi:DOI 10.1089/ten.2006.12.2467 (2006).

92 Leor, J. *et al.* Bioengineered cardiac grafts - A new approach to repair the infarcted myocardium? *Circulation* **102**, 56-61 (2000).

93 Chiu, L. L. Y. & Radisic, M. Controlled release of thymosin beta 4 using collagen-chitosan composite hydrogels promotes epicardial cell migration and angiogenesis. *J Control Release* **155**, 376-385, doi:DOI 10.1016/j.jconrel.2011.05.026 (2011).

94 Perets, A. *et al.* Enhancing the vascularization of three-dimensional porous alginate scaffolds by incorporating controlled release basic fibroblast growth factor microspheres. *J Biomed Mater Res A* **65A**, 489-497, doi:10.1002/jbm.a.10542 (2003).
95 Madden, L. R. *et al.* Proangiogenic scaffolds as functional templates for cardiac tissue engineering. *Proceedings of the National Academy of Sciences of the United States of America* **107**, 15211-15216, doi:DOI 10.1073/pnas.1006442107 (2010).
96 Narmoneva, D. A., Vukmirovic, R., Davis, M. E., Kamm, R. D. & Lee, R. T. Endothelial cells promote cardiac myocyte survival and spatial reorganization - Implications for cardiac regeneration. *Circulation* **110**, 962-968, doi:Doi 10.1161/01.Cir.0000140667.37070.07 (2004).
97 Webber, M. J. *et al.* Supramolecular nanostructures that mimic VEGF as a strategy for ischemic tissue repair. *Proceedings of the National Academy of Sciences of the United States of America* **108**, 13438-13443, doi:DOI 10.1073/pnas.1016546108 (2011).
98 Mammadov, R. *et al.* Heparin Mimetic Peptide Nanofibers Promote Angiogenesis. *Biomacromolecules* **12**, 3508-3519, doi:Doi 10.1021/Bm200957s (2011).
99 Huard, J. *et al.* Muscle-derived cell-mediated ex vivo gene therapy for urological dysfunction. *Gene Ther* **9**, 1617-1626, doi:DOI 10.1038/sj.gt.3301816 (2002).
100 Bach, A. D. *et al.* A new approach to tissue engineering of vascularized skeletal muscle. *J Cell Mol Med* **10**, 716-726, doi:DOI 10.2755/jcmm010.003.14 (2006).
101 Montarras, D. *et al.* Direct isolation of satellite cells for skeletal muscle regeneration. *Science* **309**, 2064-2067, doi:DOI 10.1126/science.1114758 (2005).
102 Cerletti, M. *et al.* Highly efficient, functional engraftment of skeletal muscle stem cells in dystrophic muscles. *Cell* **134**, 37-47, doi:DOI 10.1016/j.cell.2008.05.049 (2008).
103 Sakar, M. S. *et al.* Formation and optogenetic control of engineered 3D skeletal muscle bioactuators. *Lab on a Chip* **12**, 4976-4985, doi:Doi 10.1039/C2lc40338b (2012).
104 Aviss, K. J., Gough, J. E. & Downes, S. Aligned Electrospun Polymer Fibres for Skeletal Muscle Regeneration. *Eur Cells Mater* **19**, 193-204 (2010).
105 Guo, X. *et al.* In vitro Differentiation of Functional Human Skeletal Myotubes in a Defined System. *Biomater Sci* **2**, 131-138, doi:10.1039/C3BM60166H (2014).
106 Huang, N. F. *et al.* Myotube assembly on nanofibrous and micropatterned polymers. *Nano Letters* **6**, 537-542, doi:Doi 10.1021/Nl060060o (2006).
107 Ashammakhi, N. *et al.* Biodegradable nanomats produced by electrospinning: Expanding multifunctionality and potential for tissue engineering. *J Nanosci Nanotechno* **7**, 862-882, doi:Doi 10.1166/Jnn.2007.485 (2007).
108 Tsai, W. B. & Lin, J. H. Modulation of morphology and functions of human hepatoblastoma cells by nano-grooved substrata. *Acta Biomaterialia* **5**, 1442-1454, doi:DOI 10.1016/j.actbio.2009.01.002 (2009).
109 Cooper, A., Jana, S., Bhattarai, N. & Zhang, M. Q. Aligned chitosan-based nanofibers for enhanced myogenesis. *J Mater Chem* **20**, 8904-8911, doi:Doi 10.1039/C0jm01841d (2010).

110 Bian, W. N. & Bursac, N. Engineered skeletal muscle tissue networks with controllable architecture. *Biomaterials* **30**, 1401-1412, doi:DOI 10.1016/j.biomaterials.2008.11.015 (2009).
111 Gribova, V., Gauthier-Rouviere, C., Albiges-Rizo, C., Auzely-Velty, R. & Picart, C. Effect of RGD functionalization and stiffness modulation of polyelectrolyte multilayer films on muscle cell differentiation. *Acta Biomaterialia* **9**, 6468-6480, doi:DOI 10.1016/j.actbio.2012.12.015 (2013).
112 Gunn, J. W., Turner, S. D. & Mann, B. K. Adhesive and mechanical properties of hydrogels influence neurite extension. *J Biomed Mater Res A* **72A**, 91-97, doi:Doi 10.1002/Jbm.A.30203 (2005).
113 Foster, R. F., Thompson, J. M. & Kaufman, S. J. A Laminin Substrate Promotes Myogenesis in Rat Skeletal-Muscle Cultures - Analysis of Replication and Development Using Antidesmin and Anti-Brdurd Monoclonal-Antibodies. *Developmental Biology* **122**, 11-20, doi:Doi 10.1016/0012-1606(87)90327-7 (1987).
114 Massia, S. P. & Hubbell, J. A. Covalent Surface Immobilization of Arg-Gly-Asp-Containing and Tyr-Ile-Gly-Ser-Arg-Containing Peptides to Obtain Well-Defined Cell-Adhesive Substrates. *Anal Biochem* **187**, 292-301, doi:Doi 10.1016/0003-2697(90)90459-M (1990).
115 Hartgerink, J. D., Beniash, E. & Stupp, S. I. Peptide-amphiphile nanofibers: a versatile scaffold for the preparation of self-assembling materials. *Proc Natl Acad Sci U S A* **99**, 5133-5138, doi:10.1073/pnas.072699999
072699999 [pii] (2002).
116 Burdick, J. A., Mauck, R. L., Gorman, J. H. & Gorman, R. C. Acellular Biomaterials: An Evolving Alternative to Cell-Based Therapies. *Sci Transl Med* **5**, doi:ARTN 176ps4
DOI 10.1126/scitranslmed.3003997 (2013).
117 Plotkin, M. *et al.* The effect of matrix stiffness of injectable hydrogels on the preservation of cardiac function after a heart attack. *Biomaterials* **35**, 1429-1438, doi:DOI 10.1016/j.biomaterials.2013.10.058 (2014).
118 Laflamme, M. A., Zbinden, S., Epstein, S. E. & Murry, C. E. Cell-based therapy for myocardial ischemia and infarction: Pathophysiological mechanisms. *Annu Rev Pathol-Mech* **2**, 307-339, doi:DOI 10.1146/annurev.pathol.2.010506.092038 (2007).
119 Simons, M. & Ware, J. A. Therapeutic angiogenesis in cardiovascular disease. *Nat Rev Drug Discov* **2**, 863-871, doi:Doi 10.1038/Nrd1226 (2003).
120 Lindahl, U. Heparan sulfate-protein interactions - A concept for drug design? *Thromb Haemostasis* **98**, 109-115, doi:Doi 10.1160/Th07-04-0310 (2007).
121 Houck, K. A., Leung, D. W., Rowland, A. M., Winer, J. & Ferrara, N. Dual Regulation of Vascular Endothelial Growth-Factor Bioavailability by Genetic and Proteolytic Mechanisms. *Journal of Biological Chemistry* **267**, 26031-26037 (1992).
122 Kawamura, H. *et al.* Neuropilin-1 in regulation of VEGF-induced activation of p38MAPK and endothelial cell organization. *Blood* **112**, 3638-3649, doi:DOI 10.1182/blood-2007-12-125856 (2008).